National Library of Canada
Acquisitions and Bibliographic Services Branch
395 Wellington Street
Ottawa, Ontario
K1A 0N4

Bibliothèque nationale du Canada
Direction des acquisitions et des services bibliographiques
395, rue Wellington
Ottawa (Ontario)
K1A 0N4

Your file Votre référence

Our file Notre référence

NOTICE

The quality of this microform is heavily dependent upon the quality of the original thesis submitted for microfilming. Every effort has been made to ensure the highest quality of reproduction possible.

If pages are missing, contact the university which granted the degree.

Some pages may have indistinct print especially if the original pages were typed with a poor typewriter ribbon or if the university sent us an inferior photocopy.

AVIS

La qualité de cette microforme dépend grandement de la qualité de la thèse soumise au microfilmage. Nous avons tout fait pour assurer une qualité supérieure de reproduction.

S'il manque des pages, veuillez communiquer avec l'université qui a conféré le grade.

La qualité d'impression de certaines pages peut laisser à désirer, surtout si les pages originales ont été dactylographiées à l'aide d'un ruban usé ou si l'université nous a fait parvenir une photocopie de qualité inférieure.

Canada

NUMERICAL SIMULATION OF VISCOPLASTIC MATERIAL FLOW THROUGH EXTRUSION DIES

by

Saleh S. Abdali
B.A.Sc. Chemical Engineering

A Thesis
Submitted to the School of Graduate Studies
in Partial Fulfilment of the Requirements for
the Degree of Master of Applied Science

in

Chemical Engineering
University of Ottawa

ISBN 0-315-85815-X

Canada

UNIVERSITÉ D'OTTAWA
UNIVERSITY OF OTTAWA

Abstract

Various flows through extrusion dies have been studied for viscoplastic materials exhibiting a yield stress (Bingham fluids). These include entry flows from a reservoir into a die and exit flows from a die into the atmosphere under the influence of a pressure gradient. The materials are modelled by a constitutive equation of Bingham fluids with yield stress, as modified by Papanastasiou to include an exponential term for low strain rates and to avoid discontinuities. This equation applies everywhere in the flow field in both yielded and practically unyielded regions. The Finite Element method (FEM) is used to discretize the domain and solve the set of conservation and constitutive equations along with the proper boundary conditions.

The results are given as a function of a dimensionless Bingham number (Bi) or yield stress (τ_y^*). The emphasis is on determining the extent and shape of unyielded/yielded regions as well as the extrudate swell (contraction) for planar and axisymmetric geometries (slit and capillary dies). It is found that reduction in swelling occurs as the amount of yield increases (or correspondingly as Bi increases), which becomes contraction (swell ratio below 1) and then it asymptotically increases to reach 1 as Bi$\rightarrow \infty$. The results for the pressure necessary to push the material through are used to determine the excess pressure losses over and above the Newtonian values, giving rise to entrance, exit and the total end (or Bagley) correction. These are found to

be substantially higher than the Newtonian values as Bi increases, reaching values close to 4 times their Newtonian counterparts. Furthermore, the results correctly capture the location and extent of solid (unyielded) and fluid (yielded) regions in such flows, which is of considerable interest for industrial purposes.

The combined effect of entry and exit flow under non-isothermal conditions has been also studied in an effort to simulate a visco-elastico-plastic material for which experimental data are available in the literature. The extrudate swell results show a maximum also observed experimentally but are always underpredicting the experimental values. This is also the case for pressure drops and temperature rises due to viscous dissipation. However, the results show that the non-isothermal, inelastic, viscoplastic simulations are capable of good predictions for low to moderate shear rates, before the elasticity of the material becomes dominant.

Acknowledgements

In presenting this thesis, I wish to express my appreciation to Dr. E. Mitsoulis, my supervisor, I am also grateful to Ras Lanuf Co. for their financial support.

I would also like to express my thanks to my colleagues Ahmed Hannachi and Dr. D. Kiriakidis for their assistance.

Finally I would like to thank my wife for her patience and support and my sons Mohamed and Mohaned.

Contents

List of Figures

List of Tables

Nomenclature

b	temperature shift factor, $1/K$
C_p	specific heat capacity, $J/kg.K$
d	extrudate diameter, m
D	capillary die diameter, m
$\bar{\bar{D}}$	half the rate-of-strain tensor, s^{-1}
e	error vector, dimensionless
$\{F\}$	global load vector
g	acceleration due to gravity, m/s^2
h	free surface height, m
h_T	heat transfer coefficient, $J/m^2.s.K$
H	characteristic length in y-direction, m
	channel half gap, m
H_{res}	reservoir half gap, m
$II_{\dot{\gamma}}$	second invariant of the rate-of-strain tensor, s^{-2}
II_τ	second invariant of the stress tensor, Pa^2

k	consistency index, $Pa.s^n$
k_T	thermal conductivity, $J/m.s.K$
$[K]$	global stiffness matrix
l	free surface length, m
L	die length, m
L_{res}	reservoir length, m
L_v	vortex detachment length, m
L_∞	extrudate length, m
m	stress growth exponent in Papanastasiou model, s
n	power-law index, dimensionless
$\bar{n}$	unit outward normal vector
n_B	end (Bagley) correction, dimensionless
n_{en}	entrance correction, dimensionless
n_{ex}	exit correction, dimensionless
N	iteration number, dimensionless
P	pressure, Pa
q	heat flux, $J/m^2.s$
Q	volumetric flow rate, m^3/s
r	radial global coordinate, m

R	radius, m
Sw	swell ratio, dimensionless
t	time, s
$\bar{t}$	unit tangential vector
T	temperature, $^{\circ}C$ or K
$\bar{T}$	surface traction, Pa/m
u	velocity in the r-direction, m/s
v	velocity, m/s
V	characteristic velocity, m/s
V_B	average Bingham velocity, m/s
V_N	average Newtonian velocity, m/s
W	width in 3rd-direction, m
x	axial global coordinate, m
X	vortex length, dimensionless
$\{X\}$	vector of nodal unknowns
y	transverse global coordinate, m
	vertical distance, m
y_o	yield surface, m
z	axial distance, m
	axial global coordinate, m

Greek Letters

$\dot{\gamma}$	rate-of-strain, s^{-1}
	shear rate, s^{-1}
$\bar{\dot{\gamma}}$	characteristic shear rate s^{-1}
$\dot{\gamma}_a$	apparent shear rate, s^{-1}
$\dot{\gamma}_c$	critical shear rate, s^{-1}
ΔP	pressure drop, Pa
ΔP_{en}	entrance pressure drop, Pa
ΔP_{ex}	exit pressure drop, Pa
ΔP_{res}	reservoir pressure drop, Pa
ΔP_o	die pressure drop, Pa
ΔL	length difference, m
ΔT	temperature difference, $°C$
η	apparent viscosity, $Pa.s$
$\bar{\eta}$	characteristic viscosity, $Pa.s$
θ	azimuthal global coordinate, deg
λ	relaxation factor, dimensionless
μ	Newtonian viscosity, $Pa.s$
μ_o	plastic viscosity in bi-viscosity model, $Pa.s$
ρ	density, kg/m^3

τ	extra stress, Pa
	shear stress, Pa
τ_{rz}	shear stress, Pa
τ_{xy}	shear stress, Pa
τ_y	yield stress, Pa
τ_w	wall shear stress, Pa
ψ	stream function, m^3/s
ω	vorticity, s^{-1}

Subscripts

a	apparent
	ambient
B	Bagley
	Bingham
c	critical
en	entrance
ex	exit
f	free surface
i	i^{th} node
	i^{th} coordinate

j	j^{th} coordinate
n	normal to a surface
new	new
N	Newtonian
r	r-direction
res	reservoir
sl	slit
t	tangential to a surface
T	temperature
	thermal
w	wall
y	yield
z	z-direction
o	origin/initial/reference
∞	infinite distance
12	axis directions

Superscripts

(e) element

i present iteration

T transpose of a vector or a matrix

• dimensionless quantity

Overscripts

- characteristic value

  vector

= matrix, tensor

. rate

Dimensionless Groups

Bi Bingham Number $=\frac{\tau_y D}{\mu V_B}$ (Eq. 2.57)

Bi^* Generalized Bingham Number $=\frac{\tau_y D^n}{8^{n-1} V_B^n k}\left(\frac{4n}{3n+1}\right)^n$ (Eq. 2.58)

Na Nahme Number $=\frac{b\dot{\eta}V^2}{k_T}$ (Eq. 2.62)

Pe Peclet Number $=\frac{\rho C_p V H}{k_T}$ (Eq. 2.61)

Re	Reynolds Number $=\frac{\rho V H}{\bar{\eta}}$ (Eq. 2.54)
Re^*	Generalized Reynolds Number$=\frac{\rho D^n V^{2-n}}{8^{n-1}k}\left(\frac{4n}{3n+1}\right)^n$ (Eq. 2.55)
τ_y^*	Yield Stress $=\frac{\tau_y H}{\mu V_N}$ (Eq. 2.56)
ΔP^*	Pressure Gradient *(planar)* $=\left(\frac{\Delta P}{\Delta L}\right)\frac{H^2}{\mu V_N}$ (Eq. 2.59)
	Pressure Gradient *(axisymmetric)* $=\frac{1}{2}\left(\frac{\Delta P}{\Delta L}\right)\frac{R^2}{\mu V_N}$ (Eq. 2.60)

Mathematical Symbols

Δ	increment
∂	differential operator
∇	vector differential operator
∇^2	Laplace operator
$\frac{D}{D_t}$	substantial derivative
$\sum_i$	summation over i
$\{\ \}$	column vector
$[\ ]$	matrix
$\|\ \|$	magnitude
$\|\|\ \|\|$	norm of a vector

Chapter 1

Introduction

1.1 Viscoplastic Material Flow in Extrusion Dies

During the past several decades the emphasis in rheology and continuum mechanics has been on one-phase materials, with particular attention to polymer solutions and polymer melts. Slurries, pastes and suspensions, frequently encountered in industrial problems, have received less attention than they deserve. Many of these materials exhibit a **yield stress**, a critical value of stress below which they do not flow. They are sometimes called **viscoplastic materials** or **Bingham plastics** after Bingham (1922), who first described paint in this way in 1919. Also food substances, like margarine, mayonnaise

and ketchup, are good examples of Bingham plastics. Production of composite materials usually involves processing of fiber suspensions that often exhibit yield behaviour (Metzner, 1985). Concentrated suspensions of solid particles in Newtonian liquids show a yield stress followed by nearly Newtonian behaviour after yielding and flow. A list of several materials exhibiting yield was given in a seminal paper by Bird et al. (1983), who have also made a thorough effort to provide all pertinent work on viscoplastic materials up to 1980. A schematic response of Bingham plastics in simple shear flow is given in Figure 1.1 together with the response of a Newtonian fluid.

From the processing point of view, it is understood that a variety of shaping processes that exist for polymer melts (plastics) also exists for viscoplastic materials. Such shaping processes for plastics include extrusion, injection molding, blow molding, film blowing, fiber spinning, calendering, wire coating, to name just a few. Although each process is suited for different products, almost all plastics (about 95%) pass at some point through an extruder to be compressed, conveyed down the screw channel and then melted before being shaped into the desired form or product. A typical schematic diagram of a plasticating extruder is shown in Figure 1.2, along with the various zones encountered (from Agur and Vlachopoulos, 1982).

For viscoplastic materials, extruders are also the commonest shaping device, e.g. for the continuous production of foodstuff and pastes. However,

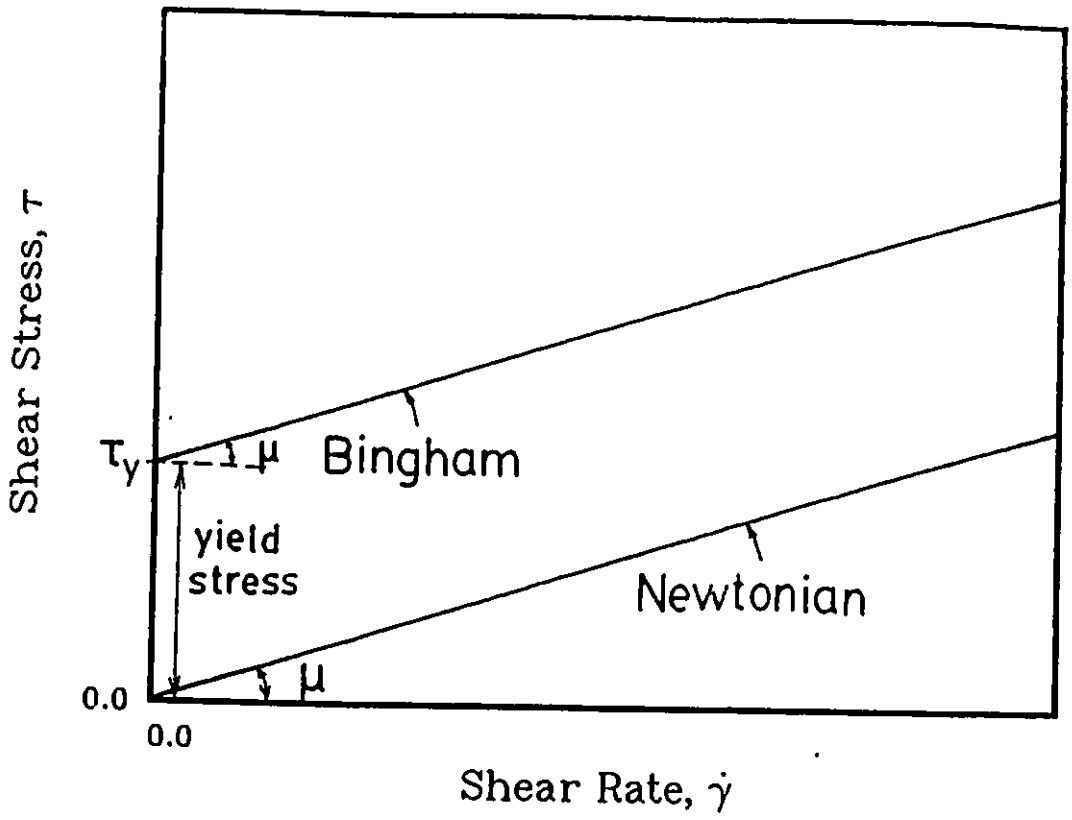

Figure 1.1: Bingham plastic behaviour in simple shear flow and definition of yield stress.

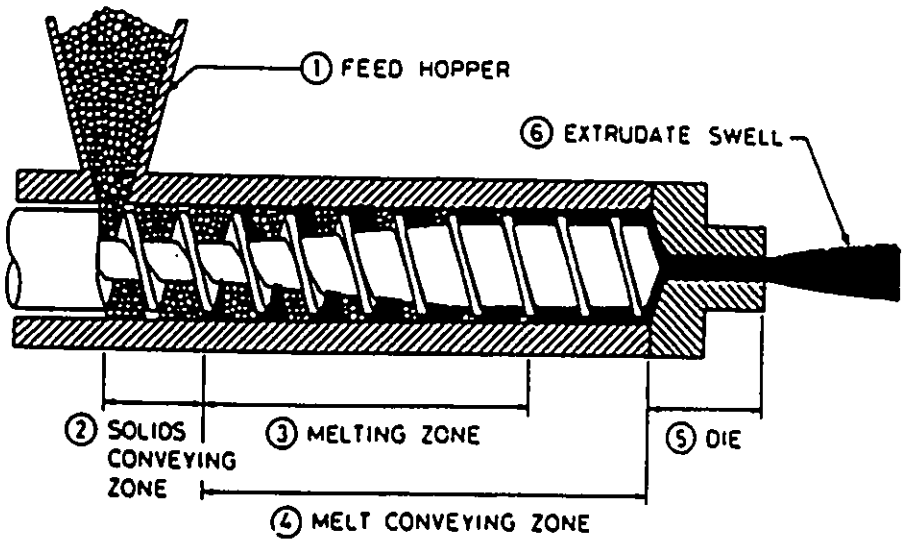

Figure 1.2: Schematic diagram of a plasticating extruder.

an extruder for viscoplastic material processing may not necessarily have the same sections as a plasticating extruder for the processing of plastics. Nevertheless, the last section of the extruder, the extrusion die, is omnipresent in all extruders and constitutes a most important part, especially for the designer. Pressure drops, flow patterns and material behaviour in extrusion dies are very important and the object of many research works. Dies come in a variety of shapes and sizes, from the simplest circular hole for the production of rods to sophisticated three-dimensional dies for shaping different materials to many configurations.

Until recently, the design of extrusion dies has been mainly based on the empirical approach of a series of experiments under varying conditions to determine the optimum geometry needed. Extensive and expensive experiments have been the norm for a variety of materials to determine such quantities as the length and opening gap for a die to give certain dimensions to the product, or the pressure drop needed for a certain extrusion throughput (flow rate). Taking into account the unusual behaviour of viscoplastic materials due to their yield stress, one of the simplest but still challenging problems even for extrusion through a capillary die, is what the die diameter should be to produce a certain extrudate diameter and at what flow rate. This, of course, happens because of an interesting and important phenomenon exhibited by viscoplastic materials, called **extrudate swell,**

which accounts for a different increase or decrease in the extrudate cross-section when the material comes out of the die into the atmosphere.

Apart from the effect of the geometry on the flow, another important parameter is the viscoplastic material itself, since different materials flow differently and therefore obey different constitutive equations. This is the subject of **rheology** of the material and many efforts have been directed towards describing the rheological behaviour of viscoplastic materials. For example, the behaviour of viscoplastic materials in shear flow may follow different curves as evidenced in Figure 1.3. Extensive experiments have been carried out to determine their properties, as summarized by Bird et al. (1983). The data obtained called for a need to correlate their properties and establish appropriate mathematical relationships. Such relationships can be used to model these materials and understand their behaviour under processing conditions by performing numerical simulations.

In the last fifteen years, the rapid development of computers has allowed the numerical solution of many complicated problems with a variety of sophisticated methods such as the numerical method of finite elements (FEM). The main advantages of this method are:

(a) its ability to easily handle complex geometries and boundary conditions;

(b) its flexibility to solve many different types of problems with only slight

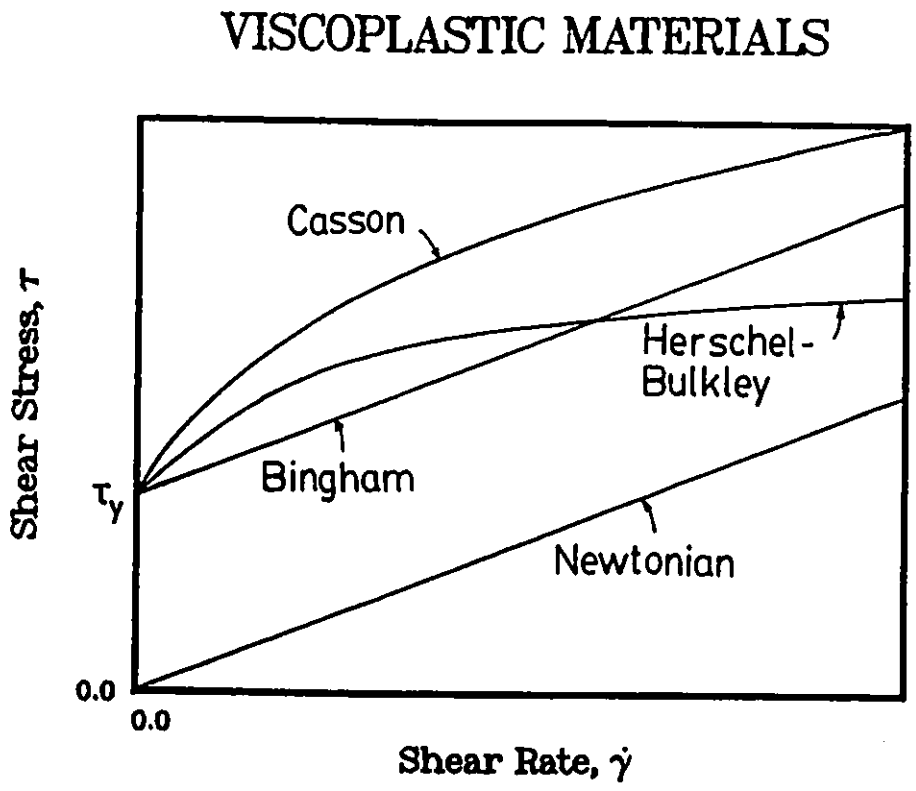

Figure 1.3: Typical shear stress vs. shear rate curves for Newtonian and viscoplastic fluids.

modifications of the same computer program.

The question of a powerful numerical method seems more or less to have been settled with the application of FEM in flow problems. One shortcoming of the method seems to be its rather involved formulation which requires a good understanding of variational principles, matrix algebra and computer programming skills. However, computer programs can become user-friendly with appropriate pre-processing of input data and post-processing output data, which greatly simplify the numerical simulations for a series of parametric studies. In that form then, the computer programs can be used by a non-expert on the numerical method itself.

1.2 Review of Numerical Simulation of Viscoplastic Material Flow in Extrusion Dies

The numerical simulation of viscoplastic material flows has been a rather recent undertaking lagging behind the tremendous research growth which occurred for viscoelastic polymer solutions and melts. Calculations have been performed mainly by the Finite Element Method (FEM), because of its ability to incorporate complicated geometrical boundaries. One of the first efforts to simulate the flow of viscoplastic materials was made by Gartling (1983) and Tanner and Milthorpe (1983), who used a bi-viscosity model to

describe the behaviour of viscoplastic materials, as shown in Figure 1.4. According to their model, a very high *unyielded* viscosity μ_o is assumed below a critical shear rate $\dot{\gamma}_c$ to account for the rigid (unyielded) solid. Above the $\dot{\gamma}_c$ value, the material flows like a Newtonian fluid with a viscosity μ. Tanner and Milthorpe (1983) thus examined the extrusion flow and extrudate swell of Bingham and Herschel-Bulkley viscoplastic materials from circular and annular dies and showed the yielded/unyielded regions in the flow domain. However, their study is neither thorough nor systematic and they showed only a couple of cases as examples.

Further work has been carried out by Tanner's group using the same approach (bi-viscosity model). O'Donovan and Tanner (1984) studied the squeeze-film flow of a Bingham fluid and Beverly and Tanner (1989) the extrusion flow and extrudate swell of a visco-elastico-plastic material for which experimental data had appeared in the literature by Carter and Warren (1987). The bi-viscosity model was also used by Lipscomb and Denn (1984) to study lubrication flows analytically, by Gartling and Phan-Thien (1984) to study the flow in a parallel-plate plastometer, by Keentok et al. (1985) to study the flow around a rotating vane in a Bingham liquid, and by Scott et al. (1988) to study the effect of inertia and yield stress in flows through expansions and stenoses for Bingham and Casson fluids. Further numerical simulations have been undertaken by Beris et al. (1985) for a sphere moving

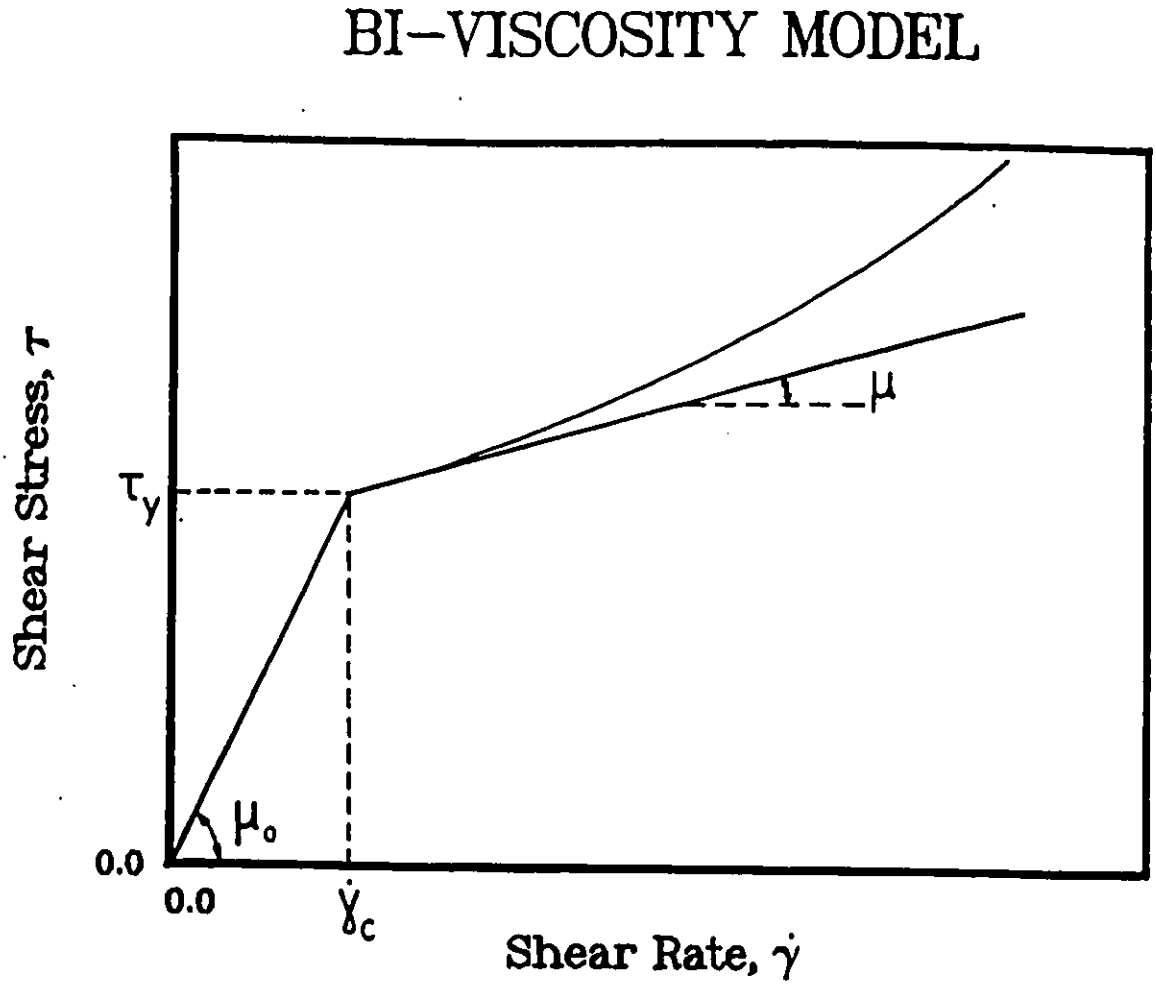

Figure 1.4: Shear stress vs. shear rate response for modified Bingham and Herschel-Bulkley fluids according to the bi-viscosity model proposed by Tanner and Milthorpe (1983).

in a Bingham liquid, but they used the von Mises criterion for solids in the unyielded zone and the Bingham model in the yielded zone to track down solid/fluid surfaces.

Papanastasiou (1987) in a pioneering paper introduced a modified Bingham model valid both in the unyielded and yielded regions, thus eliminating the need to track down solid regions via a different equation. With this model, he studied one-dimensional channel shear flow (Poiseuille flow), a two-dimensional boundary-layer flow in a bell sprayer, and finally extrusion flow thus determining extrudate swell from slit dies. However, his results are limited to some example cases and he has not undertaken a full and thorough parametric study of the flows in question. Further work by Ellwood et al. (1990) using Papanastasiou's model was extended to unsteady-state jet break-up and also included capillary and inertia effects.

Despite the growth and diversity of numerical simulations for viscoplastic materials in the 1980's, it appears that it does not exist a thorough and systematic approach to study these materials in the range of total solid (unyielded) to total liquid (yielded). This must be done for the whole range of a dimensionless number appropriate for these materials (either a dimensionless yield stress or a Bingham number). Also some discrepancies and conflicts exist in the literature with regard to the shape and extent of unyielded/yielded zones and to the use of an appropriate criterion for determining these regions.

Furthermore, although exit flows from extrusion dies and the determination of extrudate swell have been carried out by some investigators (notably Tanner's and Papanastasiou's groups), no attempt has been made whatsoever to study the entry flow from a reservoir into a die and the determination of excess pressure losses that may be present in extrusion of viscoplastic materials. This is rather surprising since this subject has been of utmost importance in the numerical simulation of viscoelastic fluids (see review by Mitsoulis, 1990).

1.3 Objectives

The objectives of this work are to study the behaviour of viscoplastic (Bingham) materials by solving the appropriate governing conservation and constitutive equations for flows inside extrusion dies using the MACVIP finite element program (Mitsoulis et al., 1983). We shall use a constitutive equation proposed by Papanastasiou (1987) to examine the entry and exit flows of viscoplastic materials through extrusion dies. The emphasis will be on finding the extent and shape of the yielded/unyielded regions by using the criterion that the material flows and deforms significantly only when the magnitude of the extra stress tensor exceeds the yield stress. The determination of the extrudate shape will also be carried out for planar and circular dies. The

excess pressure losses will be determined as a function of a dimensionless yield stress or Bingham number.

The flow of viscoplastic materials in extrusion dies will be considered as steady-state, incompressible, creeping flow (inertia forces negligible). Constitutive models considered in this study will be purely viscous (inelastic) and will include:

(a) Newtonian fluid

(b) Bingham fluid (modified according to Papanastasiou's model)

(c) Herschel-Bulkley fluid (modified according to Papanastasiou's model).

Our results will be tested against known analytical and previous numerical solutions and thus their accuracy will be established. Then the programs will be used for parametric studies in extrusion flows and finally to simulate experimental results available in the literature (Carter and Warren, 1987).

1.4 Outline of Thesis

Chapter (2): The equations of conservation of mass, momentum and energy are introduced and simplified using the appropriate assumptions. The models and the constitutive equations available for the description of flow of viscoplastic materials in extrusion dies are also presented. The relevant dimensionless groups are discussed and the appropriate boundary conditions

are outlined. The method of solution is also presented. The Finite Element formulation (FEM) of continuity and momentum equations (velocities-pressure or $u - v - p$ formulation) is briefly discussed together with the stream function formulation and a method of handling problems with free surfaces.

Chapter (3): Results from pressure-driven Poiseuille flows and entry flows in a 4:1 contraction are presented for planar and axisymmetric geometries. The validity and accuracy of the results is checked against analytical and other numerical works. The shape and extent of yielded/unyielded regions are determined and the pressures are used to calculate the entrance correction as a function of the dimensionless yield stress and Bingham number.

Chapter (4): Results from exit flows are presented for slit and capillary dies. The extrudate swell is determined as well as the shape and extent of yielded/unyielded regions. The pressures are used to calculate the exit correction as a function of the dimensionless yield stress and Bingham number. The overall end (or Bagley) corrections for entry and exit flows are also calculated.

Chapter (5): Non-isothermal calculations are undertaken for extrusion of a viscoplastic material for which experimental results are available in the literature. Comparisons are made which give rise to concluding remarks.

Chapter (6): The results of this thesis are summarized for the various problems examined. Conclusions and recommendations for future work are presented.

Chapter 2

Mathematical Modelling of Viscoplastic Materials

This chapter presents an introduction on the importance and need for analyzing and predicting the behaviour of viscoplastic materials as they flow through processing equipment. The general conservation equations for the flow analysis are presented along with the constitutive equations used. Finally the reduction of these equations for steady-state flows in planar and axisymmetric geometries is given under the appropriate assumptions.

2.1 Introduction

The determination of the velocity, pressure and temperature fields of viscoplastic materials inside extrusion dies is of considerable practical interest in the industry. The results of the above primary variables can be used to evaluate other quantities of practical importance, such as flow rates, power requirements, stresses and strains, heat dissipated, extrudate swell, the extent and shape of the yielded/unyielded regions, etc. Such information can be used in the design of processing dies.

An analysis of viscoplastic material flows through processing equipment requires simultaneous consideration of the mass, momentum and energy conservation principles. These equations must also accommodate appropriate constitutive equations that relate stresses to the velocity gradients. The geometry of the equipment enters in the specification of the boundaries. Because of the complexity of the differential equations involved and their domain of integration, nearly all problems require numerical methods for their solution. Except for highly simplified (Newtonian) constitutive equations that can describe some fluid flows in simple geometries, it is often very difficult or impossible to obtain solutions that represent adequately the behaviour of viscoplastic materials. In order to obtain a manageable and solvable form of the equations for the analysis of a very difficult problem,

some assumptions based on experience are necessary. Some of the simplifications adopted are described later in this chapter.

Extensive experiments have been carried out to determine the properties of viscoplastic materials (see Bird et al., 1983). Correlations of these properties can be used to model these materials and allow for the understanding of their behaviour under processing conditions by performing numerical simulations. To model the stress-deformation behaviour, several constitutive relations have been proposed (Fredrickson, 1964, Argon, 1975) and different yield criteria have been used (Malvern, 1969). The state of affairs is empirical and relatively undeveloped, partially due to the difficulty of obtaining accurate, reliable data on these materials at vanishingly small deformation, which is necessary to determine the existence and the level of the yield stress. The most common three-dimensional constitutive relation uses the von Mises criterion which predicts that the material flows and deforms significantly only when the magnitude of the stress tensor exceeds the yield stress; otherwise the material behaves like a strained solid. Figure 2.1 shows the behaviour of shear stress as a function of shear rate for a typical viscoplastic material through analytical expressions along with experimental data by Ellwood et al. (1990).

In practice it is often difficult to see the exact and sharp yielding embedded in von Mises theory in rheological substances. Tanner and Milthorpe

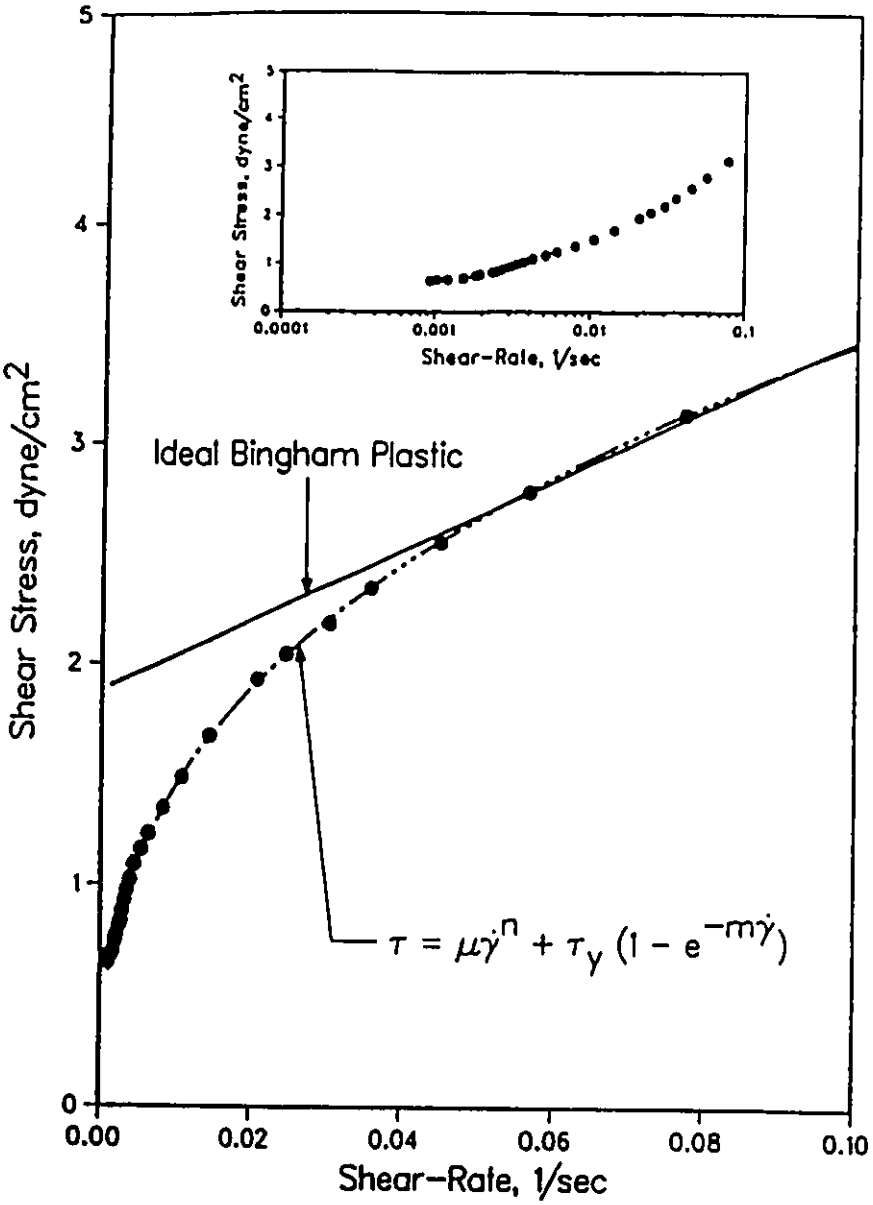

Figure 2.1: Experimental data for a sample water-borne paint and prediction by Bingham and modified Bingham models (from Ellwood et al., 1990).

(1983) suggested an alternative approach (bi-viscosity model), where it is supposed that at very low shear rates the material acts as a highly viscous liquid, and that above a critical shear rate $\dot{\gamma}_c$ a transition in behaviour occurs (yielding). In this case the criterion of yielding is that the critical shear rate $\dot{\gamma}_c$ is exceeded (Figure 1.4). The existence of a true yield stress, and therefore the accuracy of the von Mises criterion, has been questioned by several investigators. In a recent paper, Barnes and Walter (1985) concluded that *no yield stress exists*, they argue that new instruments are exploding the yield stress myth and they assert that no one has ever measured a yield stress. They state if a material flows at high stresses it will also flow, however slowly at low stresses. However this was disputed recently by Harnett and Hu (1989).

Given these engineering realities (Astarita, 1990), the material can be well approximated uniformly at all levels of stress as a liquid that exhibits infinitely high viscosity in the limit of low shear rates followed by a continuous transition to a viscous liquid. The approximation can be made more and more accurate at even vanishingly small shear rates by means of a material parameter that controls the exponential growth of stress, according to a constitutive equation proposed by Papanastasiou (1987). Experimental results (Keentok et al., 1985, Dzuy and Boger, 1985, White et al., 1986, Ellwood et al., 1990) show that in most instances the ideal Bingham model as shown in Figure 2.1 does not provide a very good approximation to real data, while

a modified Bingham equation with an exponential term gives a better fit. From the computational point of view such a model is by far superior to the von Mises criterion because it holds uniformly in both yielded and unyielded regions and so the necessity to track yield surfaces or lines is eliminated, which significantly simplifies computations in complex geometries. Such a model will also be used in the present work.

2.2 Conservation Equations

In general tensorial form the conservation equations are (Bird et al., 1960):

Mass:

$$\frac{D\rho}{Dt} + \rho(\nabla \cdot \bar{v}) = 0 \tag{2.1}$$

Momentum:

$$\rho\frac{D\bar{v}}{Dt} = -\nabla p + \nabla \cdot \bar{\bar{\tau}} + \rho\bar{g} \tag{2.2}$$

Energy:

$$\rho C_p\frac{DT}{Dt} = -\nabla \cdot \bar{q} + \bar{\bar{\tau}} : \nabla\bar{v} \tag{2.3}$$

Assuming that:

(a) the fluid is incompressible (constant density), the continuity equation for the conservation of mass (Equation 2.1) reduces to:

$$\nabla \cdot \bar{v} = 0 \tag{2.4}$$

The incompressibility assumption is not valid when large pressure gradients are present. However for most viscoplastic materials under usual processing conditions, equation (2.4) is indeed applicable.

The equation of conservation of momentum involves a balance between inertia, viscous, pressure and body forces. Because viscoplastic flows are very slow flows with extremely small Reynolds number (Re$\ll$ 1. Pearson, 1985), it may be assumed that:

(b) inertia effects are negligible in comparison with viscous and pressure forces. We also assume that:

(c) body forces (such as gravity) are negligible in comparison with viscous and pressure forces;

(d) the flow is steady ($\frac{\partial}{\partial t} = 0$), which applies to many viscoplastic processes. Thus, the conservation of momentum Equation (2.2) reduces to:

$$0 = -\nabla p + \nabla \cdot \bar{\bar{\tau}} \tag{2.5}$$

Turning to the conservation of energy (Equation 2.3), the following assumptions are usually made for viscoplastic materials:

(e) the thermal conductivity k_T is constant.

(f) the specific heat at constant pressure C_p is constant.

The resulting energy equation with convective, conductive and viscous

dissipation terms respectively, is:

$$\rho C_p \bar{v} \cdot \nabla T = k_T \nabla^2 T + \bar{\bar{\tau}} : \nabla \bar{v} \tag{2.6}$$

2.3 Constitutive Equations

To solve the above equations we also need constitutive equations that relate the extra stress tensor $\bar{\bar{\tau}}$ to the rate-of-strain tensor $\bar{\bar{\dot{\gamma}}}$:

$$\bar{\bar{\dot{\gamma}}} = \nabla \bar{v} + (\nabla \bar{v})^T \tag{2.7}$$

2.3.1 Newtonian Fluid

For Newtonian fluids we have:

$$\bar{\bar{\tau}} = \mu \bar{\bar{\dot{\gamma}}} = \mu \dot{\gamma}_{ij} \tag{2.8}$$

where μ is a constant viscosity coefficient and $\dot{\gamma}_{ij}$ are the components of $\bar{\bar{\dot{\gamma}}}$.

2.3.2 Power-Law Fluid

The most widely used model for polymer solutions and melts is the power-law fluid, for which we have:

$$\bar{\bar{\tau}} = \eta \bar{\bar{\dot{\gamma}}} = k|\dot{\gamma}|^{n-1} \bar{\bar{\dot{\gamma}}} \tag{2.9}$$

where η is the apparent viscosity, which is a function of the consistency index k, the power-law index n and the magnitude $|\dot{\gamma}|$ of the rate-of-strain tensor $\bar{\bar{\dot{\gamma}}}$ given by

$$|\dot{\gamma}| = \sqrt{\frac{1}{2} II_{\dot{\gamma}}} = \left(\frac{1}{2}\{\bar{\bar{\dot{\gamma}}} : \bar{\bar{\dot{\gamma}}}\}\right)^{\frac{1}{2}} \tag{2.10}$$

where $II_{\dot{\gamma}}$ is the second invariant of $\bar{\bar{\dot{\gamma}}}$

$$II_{\dot{\gamma}} = (\bar{\bar{\dot{\gamma}}} : \bar{\bar{\dot{\gamma}}}) = \sum_i \sum_j \dot{\gamma}_{ij}\dot{\gamma}_{ij} \tag{2.11}$$

The one-dimensional analog of equation (2.9) in simple shear flow gives:

$$\tau_{12} = k|\dot{\gamma}|^{n-1}\dot{\gamma}_{12} \tag{2.12}$$

where τ_{12} and $\dot{\gamma}_{12}$ are the shear stress and shear rate, respectively. The subscripts 1 and 2 denote the axial flow direction (x or z) and transverse flow direction (y or r), respectively.

2.3.3 Bingham Model

The simplest and most widely used model for viscoplastic fluids exhibiting a yield stress is the two-parameter model proposed by Bingham (1922):

$$\bar{\bar{\tau}} = \left(\mu + \frac{\tau_y}{|\dot{\gamma}|}\right)\bar{\bar{\dot{\gamma}}} \qquad \text{for} \quad |\tau| > \tau_y \tag{2.13a}$$

$$\bar{\bar{\dot{\gamma}}} = 0 \qquad \text{for} \quad |\tau| \leq \tau_y \tag{2.13b}$$

where μ is a constant plastic viscosity (or plasticity coefficient), τ_y is the yield stress and $|\tau|$ is the magnitude of the extra-stress tensor $\bar{\bar{\tau}}$ given by

$$|\tau| = \sqrt{\frac{1}{2} II_\tau} = \left(\frac{1}{2}\{\bar{\bar{\tau}} : \bar{\bar{\tau}}\}\right)^{1/2} \tag{2.14}$$

where II_τ is the second invariant of $\bar{\bar{\tau}}$

$$II_\tau = (\bar{\bar{\tau}} : \bar{\bar{\tau}}) = \sum_i \sum_j \tau_{ij}\tau_{ij} \tag{2.15}$$

Similarly for $|\dot{\gamma}|$, the magnitude of the rate-of-strain tensor $\bar{\bar{\dot{\gamma}}}$. Note that when $\tau_y = 0$, the Newtonian fluid is recovered. The one-dimensional analog of equation (2.13) in simple shear flow gives:

$$\tau_{12} = \left(\mu + \frac{\tau_y}{|\dot{\gamma}|}\right)\dot{\gamma}_{12} \qquad \text{for} \quad |\tau_{12}| > \tau_y \tag{2.16a}$$

$$\dot{\gamma}_{12} = 0 \qquad \text{for} \quad |\tau_{12}| \leq \tau_y \tag{2.16b}$$

2.3.4 Casson Model

Another two-constant model is that proposed by Casson (1959) for pigment oil suspension:

$$\bar{\bar{\tau}} = \eta\bar{\bar{\dot{\gamma}}} \qquad \text{for} \quad |\tau| > \tau_y \tag{2.17a}$$

$$\bar{\bar{\dot{\gamma}}} = 0 \qquad \text{for} \quad |\tau| \leq \tau_y \tag{2.17b}$$

where the apparent viscosity η is given by:

$$\eta = \left(\sqrt{\frac{\tau_y}{|\dot{\gamma}|}} + \sqrt{\mu}\right)^2 \tag{2.18}$$

The one-dimensional analog of equation (2.17) in simple shear flow gives:

$$\sqrt{\tau_{12}} = \sqrt{\tau_y} + \sqrt{\mu}\sqrt{\dot{\gamma}_{12}} \qquad \text{for } |\tau_{12}| > \tau_y \qquad (2.19a)$$

$$\dot{\gamma}_{12} = 0 \qquad \text{for } |\tau_{12}| \leq \tau_y \qquad (2.19b)$$

This model has often been used for describing blood.

2.3.5 Herschel-Bulkley Model

Numerous attempts have been made to modify the Bingham equation to account for the more complex behaviour of viscoplastic materials. The Herschel-Bulkley model (1926) is a combination of the Bingham and power-law models, proposed to account for the non-Newtonian nature of the fluid after yielding, while retaining the rigid solid-like behaviour of the Bingham model below the yield stress. This model has the form :

$$\bar{\bar{\tau}} = \left(\frac{\tau_y}{|\dot{\gamma}|} + k|\dot{\gamma}|^{n-1}\right)\bar{\bar{\dot{\gamma}}} \qquad \text{for } |\tau| > \tau_y \qquad (2.20a)$$

$$\bar{\bar{\dot{\gamma}}} = 0 \qquad \text{for } |\tau| \leq \tau_y \qquad (2.20b)$$

The one-dimensional analog of equation (2.20) in simple shear flow gives:

$$\tau_{12} = \left(\frac{\tau_y}{|\dot{\gamma}_{12}|} + k|\dot{\gamma}_{12}|^{n-1}\right)\dot{\gamma}_{12} \qquad \text{for } |\tau_{12}| > \tau_y \qquad (2.21a)$$

$$\dot{\gamma}_{12} = 0 \qquad \text{for } |\tau_{12}| \leq \tau_y \qquad (2.21b)$$

where n is the power-law index and k the fluid consistency index.

When the power-law index is unity and the fluid consistency index is equivalent to the viscosity, the Herschel-Bulkley model reduces to the Bingham model. Both models are inelastic. Equation (2.21) frequently describes the behaviour of concentrated suspensions over a wide range of shear rates. The parameters in the equations, to be determined experimentally, are the physical properties of the material.

In the case of materials described by the above constitutive equations, which require use of two governing equations depending on the value of stress, part of the material may flow whereas the rest behaves like a solid if the stress is not constant over the entire region being modeled. Although this does not lead to limitations on analytical solution in simple cases such as flow in tubes, it may pose significant awkwardness in complicated geometries. This arises from the need for tracking distributed yield surfaces and applying different constitutive equations on the two sides of the yield surface.

2.3.6 Papanastasiou Model

The material can be well approximated uniformly at all levels of stress as a liquid that exhibits infinitely high viscosity in the limit of low shear stress followed by a continuous transition to a viscous liquid. The approximation

can be made more and more accurate at even vanishingly small shear rates by means of a material parameter that controls the exponential growth of stress, according to the following constitutive equation proposed by Papanastasiou (1987) to describe the behaviour of viscoplastic fluids in both the yielded and unyielded regions:

$$\bar{\bar{\tau}} = \left(\mu + \frac{\tau_y}{|\dot{\gamma}|}[1 - exp(-m|\dot{\gamma}|)]\right)\bar{\bar{\dot{\gamma}}} \tag{2.22}$$

where μ is a constant viscosity, τ_y is the apparent yield stress and m is a stress growth exponent. For relatively large values of the exponent m, the behaviour predicted by this equation is in general quite close to the predictions of the Bingham model. This equation is an empirical design that mimics the ideal Bingham fluid and can represent a response of the class of nearly ideal Bingham fluids. The main advantage of this modification is that there is no yield surface and it appears to be more amenable to numerical calculations. Equation (2.22) approximates the von Mises criterion for relatively big exponent m ($m > 100$), and holds uniformly in yielded and unyielded regions. The one-dimensional analog of Equation (2.22) in simple shear flow gives:

$$\tau_{12} = \left(\mu + \frac{\tau_y[1 - exp(-m|\dot{\gamma}_{12}|)]}{|\dot{\gamma}_{12}|}\right)\dot{\gamma}_{12} \tag{2.23}$$

where τ_{12} and $\dot{\gamma}_{12}$ are the shear stress and shear rate, respectively. Figure 2.2 shows a graphical representation of Equation (2.23) for different values

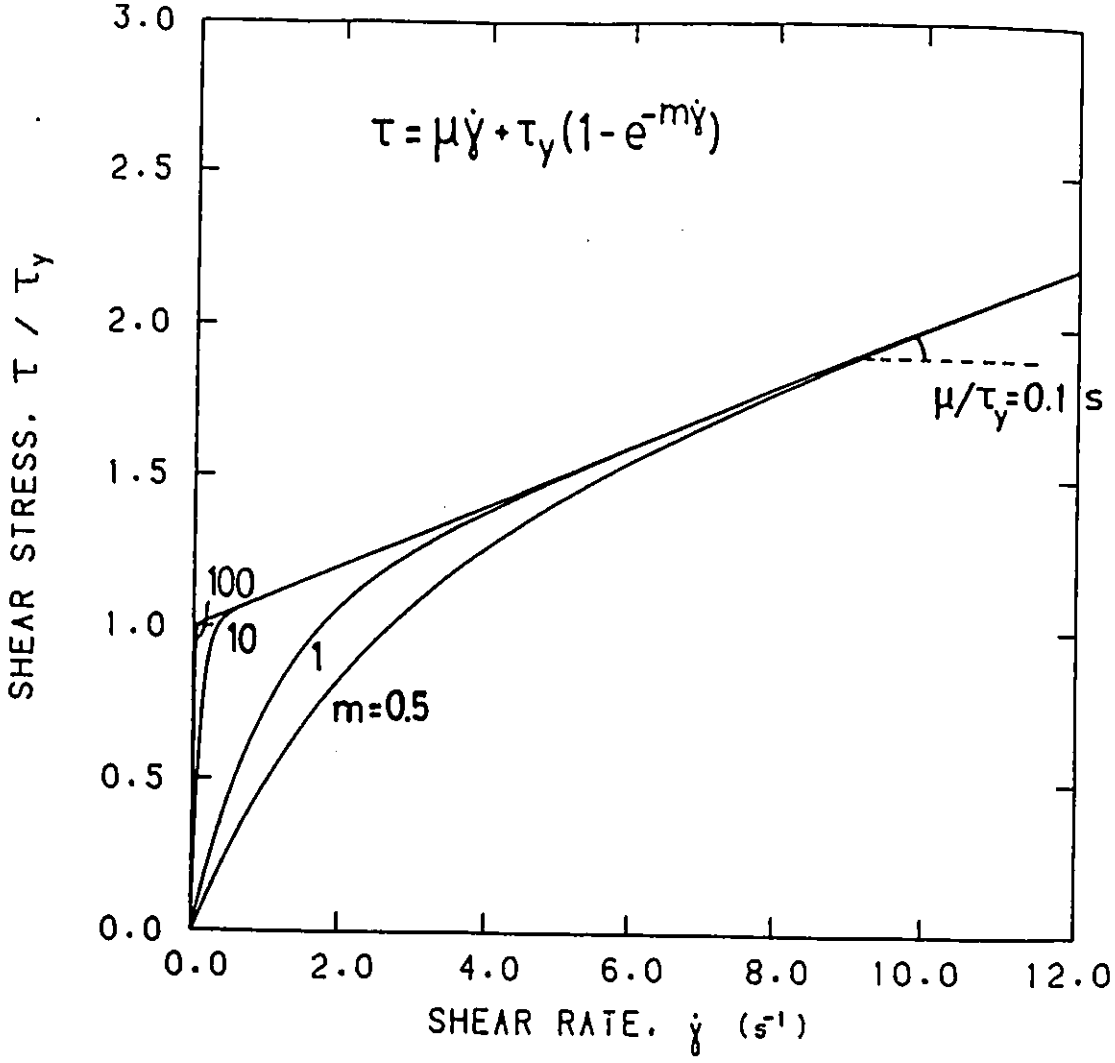

Figure 2.2: Shear stress vs. shear rate according to the modified Bingham constitutive equation (2.23) proposed by Papanastasiou (1987) for several values of the exponent m.

of the exponent m. Clearly for $m > 100$ the above equation mimics the ideal Bingham plastic.

The above model will be the working model in this thesis. To track down yielded/unyielded regions, we shall employ the criterion that the material flows (yields) only when the magnitude $|\tau|$ of the extra stress tensor exceeds the yield stress τ_y, i.e.

$$|\tau| = \sqrt{\frac{1}{2} II_{\bar{\tau}}} = \left(\frac{1}{2}\{\bar{\bar{\tau}} : \bar{\bar{\tau}}\}\right)^{1/2} > \tau_y \qquad \textit{yielded} \tag{2.24}$$

$$|\tau| \leq \tau_y \qquad \textit{unyielded} \tag{2.25}$$

Note that previous work by Papanastasiou (1987) employed the criterion of the second invariant of half the rate-of-strain tensor $\bar{\bar{D}} = \frac{1}{2}\bar{\bar{\gamma}}$ exceeding an arbitrarily small value of 0.001. This led to erroneous yielded/unyielded regions, as pointed out by Beverly and Tanner (1989), who however used very coarse grids and were not able to capture well the extent and shape of these regions. In the present work, this matter is resolved adequately. It is also believed (as was shown by numerical trials) that using as a criterion the value of yield stress, which is not arbitrary and is also a large number, reduces the uncertainty of using values very close to zero, which may be numerical noise.

2.4 Governing Equations

The flow of viscoplastic materials inside processing equipment is in general three-dimensional in nature. However, a large class of extrusion flows occurs inside tubular or annular dies (like jet nozzles), or flat dies that can be considered two-dimensional. Such geometries conveniently allow the reduction of the problem from three to two dimensions. In Cartesian coordinates we assume no change in the z-direction. In cylindrical coordinates no changes in the θ-direction could be safely assumed. Due to these assumptions the three-dimensional problem can be fully described as two-dimensional with two independent variables, namely x and y (planar case) and r and z (axisymmetric case).

2.4.1 Planar Geometries

For planar geometries (flat or slit dies), the continuity equation can be written as (Bird et al., 1960):

$$\frac{\partial v_x}{\partial x} + \frac{\partial v_y}{\partial y} = 0 \tag{2.26}$$

The equation of conservation of momentum gives:

$$(x - momentum) \qquad 0 = -\frac{\partial p}{\partial x} + \frac{\partial \tau_{xy}}{\partial y} + \frac{\partial \tau_{xx}}{\partial x} \tag{2.27}$$

$$(y - momentum) \qquad 0 = -\frac{\partial p}{\partial y} + \frac{\partial \tau_{yx}}{\partial x} + \frac{\partial \tau_{yy}}{\partial y} \tag{2.28}$$

It should be noted that because of the symmetry of the stress tensor, $\tau_{xy} = \tau_{yx}$. Thus, only three stress components are needed for planar flows. This simplifies the analysis by using a stress vector $(\tau_{xx}, \tau_{yy}, \tau_{xy})$ and a corresponding rate-of-strain vector $(\dot{\gamma}_{xx}, \dot{\gamma}_{yy}, \dot{\gamma}_{xy})$.

For planar flows, the Newtonian constitutive equation gives:

$$\tau_{xx} = 2\mu \frac{\partial v_x}{\partial x} \tag{2.29}$$

$$\tau_{yy} = 2\mu \frac{\partial v_y}{\partial y} \tag{2.30}$$

$$\tau_{xy} = \mu \left(\frac{\partial v_x}{\partial y} + \frac{\partial v_y}{\partial x} \right) \tag{2.31}$$

The modified Bingham constitutive equation (Papanastasiou model) gives:

$$\tau_{xx} = 2 \left(\mu + \frac{\tau_y}{|\dot{\gamma}|} [1 - exp(-m|\dot{\gamma}|)] \right) \frac{\partial v_x}{\partial x} \tag{2.32}$$

$$\tau_{yy} = 2 \left(\mu + \frac{\tau_y}{|\dot{\gamma}|} [1 - exp(-m|\dot{\gamma}|)] \right) \frac{\partial v_y}{\partial y} \tag{2.33}$$

$$\tau_{xy} = \left(\mu + \frac{\tau_y}{|\dot{\gamma}|} [1 - exp(-m|\dot{\gamma}|)] \right) \left(\frac{\partial v_x}{\partial y} + \frac{\partial v_y}{\partial x} \right) \tag{2.34}$$

where $|\dot{\gamma}|$ is given by:

$$|\dot{\gamma}| = \sqrt{\frac{1}{2} II_{\dot{\gamma}}} = \sqrt{\frac{1}{2} \left(\dot{\gamma}_{xx}^2 + \dot{\gamma}_{yy}^2 + 2\dot{\gamma}_{xy}^2 \right)} \tag{2.35}$$

and the components of $\bar{\bar{\dot{\gamma}}}$ are given by :

$$\dot{\gamma}_{xx} = 2 \frac{\partial v_x}{\partial x} \tag{2.36}$$

$$\dot{\gamma}_{yy} = 2 \frac{\partial v_y}{\partial y} \tag{2.37}$$

$$\dot{\gamma}_{xy} = \frac{\partial v_x}{\partial y} + \frac{\partial v_y}{\partial x} = \dot{\gamma}_{yx} \tag{2.38}$$

2.4.2 Axisymmetric Geometries

For axisymmetric geometries, the continuity equation can be written as (Bird et al., 1960):

$$\frac{\partial v_r}{\partial r} + \frac{v_r}{r} + \frac{\partial v_z}{\partial z} = 0 \tag{2.39}$$

The equation of conservation of momentum gives:

$$0 = -\frac{\partial p}{\partial r} + \frac{\partial \tau_{rr}}{\partial r} + \frac{\tau_{rr}}{r} + \frac{\partial \tau_{rz}}{\partial z} - \frac{\tau_{\theta\theta}}{r} \tag{2.40}$$

$$0 = -\frac{\partial p}{\partial z} + \frac{\partial \tau_{rz}}{\partial r} + \frac{\tau_{rz}}{r} + \frac{\partial \tau_{zz}}{\partial z} \tag{2.41}$$

It should be noted that because of the symmetry of the stress tensor, $\tau_{rz} = \tau_{zr}$. Thus, only four stress components are needed for axisymmetric flows. This simplifies the analysis by using a stress vector $(\tau_{rr}, \tau_{zz}, \tau_{rz}, \tau_{\theta\theta})$and a corresponding rate-of-strain vector $(\dot{\gamma}_{rr}, \dot{\gamma}_{zz}, \dot{\gamma}_{rz}, \dot{\gamma}_{\theta\theta})$.

For axisymmetric flows, the Newtonian constitutive equation gives:

$$\tau_{rr} = 2\mu \frac{\partial v_r}{\partial r} \tag{2.42}$$

$$\tau_{\theta\theta} = 2\mu \frac{v_r}{r} \tag{2.43}$$

$$\tau_{zz} = 2\mu \frac{\partial v_z}{\partial z} \tag{2.44}$$

$$\tau_{rz} = \mu \left(\frac{\partial v_z}{\partial r} + \frac{\partial v_r}{\partial z} \right) \tag{2.45}$$

The generalized Newtonian constitutive equation has the same form as the above, except that the constant viscosity μ is replaced by the apparent viscosity $\eta(\dot{\gamma})$. For the modified Bingham model, $\eta(\dot{\gamma})$ is given by:

$$\eta(\dot{\gamma}) = \mu + \frac{\tau_y}{|\dot{\gamma}|}(1 - exp(-m|\dot{\gamma}|)) \tag{2.46}$$

where the magnitude $|\dot{\gamma}|$ is given by:

$$|\dot{\gamma}| = \sqrt{\frac{1}{2}II_{\dot{\gamma}}} = \sqrt{\frac{1}{2}(\dot{\gamma}_{rr}^2 + \dot{\gamma}_{\theta\theta}^2 + \dot{\gamma}_{zz}^2 + 2\dot{\gamma}_{rz}^2)} \tag{2.47}$$

and the components of $\dot{\bar{\bar{\gamma}}}$ are given by:

$$\dot{\gamma}_{rr} = 2\frac{\partial v_r}{\partial r} \tag{2.48}$$

$$\dot{\gamma}_{\theta\theta} = 2\frac{v_r}{r} \tag{2.49}$$

$$\dot{\gamma}_{zz} = 2\frac{\partial v_z}{\partial z} \tag{2.50}$$

$$\dot{\gamma}_{rz} = \frac{\partial v_z}{\partial r} + \frac{\partial v_r}{\partial z} = \dot{\gamma}_{zr} \tag{2.51}$$

The above constitutive equations in the form presented here were substituted in the momentum equations (2.27,2.28 and 2.40,2.41) and used in a fully two-dimensional finite element analysis to simulate the behaviour of viscoplastic materials in several planar and axisymmetric flows.

2.5 Dimensionless Groups

Before proceeding with the boundary conditions necessary for the solution of the governing conservation and constitutive equations, it is interesting to

examine the relevant dimensionless numbers in extrusion flows. The various dimensionless groups are used to characterize the relative significance of each term in the conservation equations of momentum. The dimensionless groups are calculated at a characteristic length H and a characteristic velocity V. It is appropriate then to define a characteristic shear rate

$$\bar{\dot{\gamma}} = \frac{V}{H} \tag{2.52}$$

and a characteristic viscosity

$$\bar{\eta} = \eta(\bar{\dot{\gamma}}, T) \tag{2.53}$$

With the above definitions at hand we can now define the relevant dimensionless groups of interest in the analysis:

1. **Reynolds Number** Re

$$Re = \frac{\rho V H}{\bar{\eta}} \tag{2.54}$$

For Newtonian fluids, $\bar{\eta}$ is replaced by the Newtonian viscosity μ. For power-law fluids, a generalized Reynolds number is introduced (Boger, 1982)

$$Re^* = \frac{\rho D^n V^{2-n}}{8^{n-1} k} \left(\frac{4n}{3n+1}\right)^n \tag{2.55}$$

where V is the average velocity and D is a tube diameter or die gap. The Reynolds number is a measure of the relative importance of inertia forces

compared to viscous forces in the equation of momentum. For viscoplastic flows in general, $Re \ll 1$ (Pearson, 1985), and the creeping flow approximation is valid. As a result the inertia terms are not included in the calculations.

2. Dimensionless Yield Stress τ_y^*

For materials with yield stress it is appropriate to introduce a dimensionless yield stress τ_y^* defined by Papanastasiou (1987) as

$$\tau_y^* = \frac{\tau_y H}{\mu V_N} \tag{2.56}$$

where H is a characteristic length (half the channel width or radius R) and V_N is a characteristic velocity, taken by Papanastasiou as the average velocity of a corresponding Newtonian liquid with viscosity μ at the same pressure gradient. However this dimensionless number again introduces dependence on the Newtonian counterpart.

3. Bingham Number Bi

Bird et al. (1983) suggest the Bingham number

$$Bi = \frac{\tau_y D}{\mu V_B} \tag{2.57}$$

where D is the diameter or channel width (2H) and V_B is the average velocity of the Bingham fluid. In the case of Herschel-Bulkley fluids and in accordance with the definition of a generalized Re for power-law fluids, we can define a

generalized Bi as:

$$Bi^* = \frac{\tau_y D^n}{8^{n-1} V_B^n k} \left(\frac{4n}{3n+1}\right)^n \tag{2.58}$$

In both cases, the Newtonian or power-law fluid corresponds to τ_y^*=Bi=0. However, at the other extreme of an unyielded solid, Bi$\rightarrow \infty$ while τ_y^* reaches a dimensionless pressure gradient.

4. Dimensionless Pressure Gradient ΔP^*

$$\Delta P^* = (\frac{\Delta P}{\Delta L})\frac{H^2}{\mu V_N} \qquad (planar) \tag{2.59}$$

$$\Delta P^* = \frac{1}{2}(\frac{\Delta P}{\Delta L})\frac{R^2}{\mu V_N} \qquad (axisymmetric) \tag{2.60}$$

where $\left(\frac{\Delta P}{\Delta L}\right)$ is the pressure drop. Note that by substituting the formula for the average velocity of a Newtonian fluid, it follows that ΔP^* is equal to 3 in planar and 4 in axisymmetric geometries.

For a non-isothermal analysis, consideration of the energy equation (2.6) gives rise to the following dimensionless numbers (Heng, 1987):

5. Peclet Number Pe

$$Pe = \frac{\rho C_p V H}{k_T} \tag{2.61}$$

The Peclet number is a measure of convective heat transfer with regard to conductive heat transfer. High Pe values indicate a flow dominated by

convection. An example of such flows is high-speed wire-coating (Pe up to 100,000).

6. **Nahme Number** Na

$$Na = \frac{b\bar{\eta}V^2}{k_T} \tag{2.62}$$

where b is a temperature shift factor for the viscosity. The Nahme number is a measure of viscous dissipation effects compared to conduction, hence an indicator of coupling of the energy and momentum equations. For values of $Na > 0.1 - 0.5$ (depending on geometry and thermal boundary conditions), the viscous dissipation term leads to a considerable coupling of the conservation equations and therefore a non-isothermal analysis is necessary.

2.6 Boundary Conditions

The solution of the conservation equations (2.1-2.3) can be obtained by imposition of appropriate boundary conditions. In order to solve boundary-value problems such as in material flows through processing equipment, a rather complete set of boundary conditions is necessary.

There are basically two types of boundary conditions (Huebner and Thornton, 1982):

1 - Essential boundary conditions (or fixed boundary conditions);

2 - Natural boundary conditions (or flux boundary conditions).

The first type refers to the primary variable, e.g. velocities for the flow analysis, temperatures for the thermal analysis, and stream function values for a flow analysis based on stream function formulation. The second type of boundary conditions refers to the secondary variables (usually derivatives of the primary variables), e.g. surface traction for the flow analysis, heat fluxes for the thermal analysis and velocities for the stream function formulation.

More specifically, for flow problems the following set of boundary conditions is available (Ben-Sabar and Caswell, 1979):

1 - V_n, V_t pure velocity conditions; specify V_n, V_t

2 - T_n, T_t pure surface traction conditions; specify T_n, T_t

3 - T_n, V_t *or* V_n, T_t mixed conditions; specify T_n, V_t *or* V_n, T_t

where the subscripts n and t represent the components of a vector in the normal and tangential direction to a surface, respectively. In flow problems velocity conditions (type 1) are most commonly encountered. However in materials processing the appearance of free surfaces requires the specification of surface tractions (type 2). Such surface tractions can be air drag, drawdown forces, surface tension, etc.

Boundary conditions for the energy equation require the specification of either T or q_n on the entire surface. The following is available (Ben-Sabar and Caswell, 1979):

1 - temperature conditions; specify T

2 - (a) heat flux conditions; specify q_n

(b) linear radiation boundary conditions; specify $q_n = h_T(T - T_a)$

Condition 2(a) is specified on a boundary where the heat flux exchange is known exactly. A special case of 2(a) is $q_n = 0$ **(adiabatic condition)**, where no heat exchange exists at the boundary. Other cases involve specification of finite values for q_n. In reality, however, the exact heat exchange at the boundary is unknown. Condition 2(b) allows for more flexibility is this respect by introducing the general surface heat transfer coefficient h_T and the controlled temperature T_a. Generally, the temperature at the boundary T is unknown. Note that a special case for 2(b) is when the temperature at the boundary T is equal to T_a, i.e. the boundary temperature is being controlled at a known temperature T_a. This case is commonly known as the **isothermal wall condition.**

The boundary conditions for the stream function are (Huebner and Thornton , 1982):

1 - stream function conditions; specify ψ

2 - velocity conditions; specify $\frac{\partial \psi}{\partial \bar{n}}$

where $\frac{\partial \psi}{\partial \bar{n}}$ represents the tangential velocity at the surface.

2.7 Free Surface Flow

Flows with free surfaces for viscoplastics processing are encountered whenever a viscoplastic material exits from a die to the atmosphere (free surface flows). This problem is particularly difficult to solve because not only the flow characteristics (velocities, pressures, temperatures, etc.) are unknown, but also the location of the free surface that forms part of the boundary is unknown. The only condition that makes this class of problems solvable is the fact that no fluid can flow through a free surface, which is a streamline (Figure 2.3). Hence at the free surface

$$\bar{n} \cdot \bar{v} = 0 \tag{2.63}$$

where $\bar{n}$ is the unit outward normal vector to the surface and $\bar{v}$ the velocity vector.

The FEM is very attractive for free surface problems because of the ability of the elements to deform and take the shape of the flowing fluid. A simple procedure originally developed by Nickell et al. (1974) is to assume at first a location for the free surface (usually an extension of the solid boundary line that the fluid last encountered) and solve the system of conservation equations for these boundaries. Once the velocity field has been found, a streamline can be constructed based on the velocities v_x and v_y found on

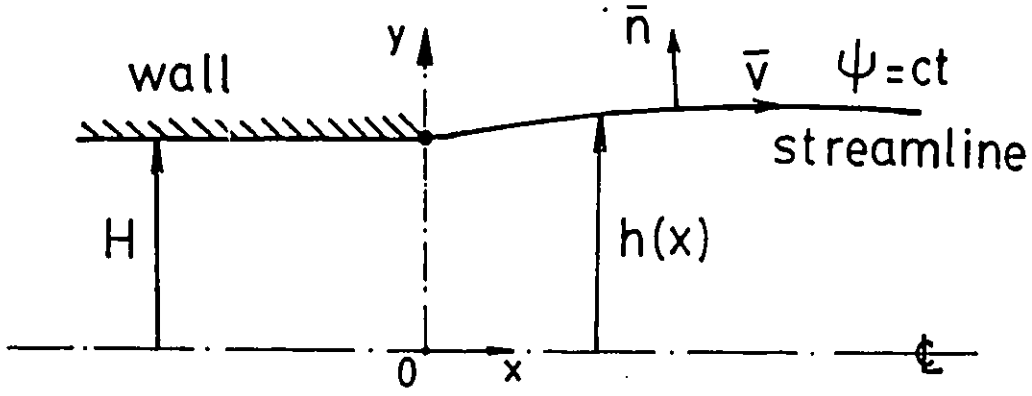

Figure 2.3: Free surface and definition of a streamline.

that surface and the equation that defines a streamline, i.e.

$$\frac{v_x}{dx} = \frac{v_y}{dy} \tag{2.64}$$

Integration of equation (2.64) can be carried out (usually numerically by applying Simpson's rule) to locate a new surface $h_{new}(x)$ which is given by

$$h_{new}(x) = h_o + \int_o^l \frac{v_y}{v_x} dx \tag{2.65}$$

where $h_0 = h_{new}(0)$ and l is the length in the x-direction. The old surface is then updated using

$$h^{i+1}(x) = h^i(x) + \lambda[h_{new}(x) - h^i(x)] \tag{2.66}$$

where $h^{i+1}(x)$ is the updated surface, $h^i(x)$ is the old surface and λ is a relaxation factor. So far the optimal range for λ has been found to be between 0.5 and 1.

With the updated boundary, the system of conservation equations is solved again in the new domain. Recent velocities are used to compute a new surface and the process is repeated until no change in the location of the free surface is observed.

Finally, a more general procedure for handling unusual free surfaces in complex flows has been developed by Kistler and Scriven (1984), and is known as $v_x - v_y - p - h$ formulation. In this mothed the coordinates h_i of the free surface are not decoupled from the system of equations, but solved for

simultaneously with the other primary variables. This method is currently applied by Hannachi (1990) for multilayer flows to locate interface and free surfaces.

2.8 Method of Solution

The numerical method used in this study is the Finite Element Method (FEM). The finite element method is a numerical analysis technique for obtaining approximate solutions to a wide variety of engineering problems. The main advantage of FEM over other numerical methods is its ability to solve problems in irregular and complex geometries with unusual boundary conditions (Vlachopoulos, 1977). According to this method, the flow domains are initially discretized into numerous, small triangular subdomains called *finite elements*. This is normally done automatically, unless a particular variation in the grid arrangement is required. The size or shape of each individual element need not be the same. Considering every element separately, a given contribution to the overall solution is determined, thus resulting in a *piecewise* approximation using the governing differential equations.

The solution of the equations along with the boundary conditions was carried out using the MACVIP finite element program developed for creeping viscoelastic flows (Mitsoulis et al., 1983). MACVIP implements a finite

element formulation using the **primitive variable approach** and the **principles of virtual work** for planar or axisymmetric geometries. The primitive variable approach involves solving for axial and radial velocities (v_x and v_y, respectively) and the pressure (p). Each triangular element contains six nodes. The velocities v_x and v_y require solution at each node and the pressure p requires solution only at the three vertex nodes, as shown in Figure 2.4. Knowledge of the nodal quantities allows interpolation over the element to determine the value of a given field variable at any point. This is accomplished using continuous functions known as *interpolation functions*. Velocities are interpolated quadratically and pressures are interpolated linearly over the element domain. Secondary variables such as stresses, rates-of-strain and stream function values can be determined from the known primitive variables. A more in-depth explanation of the principles behind the FEM can be found in the book by Huebner and Thornton (1982).

The analysis using MACVIP follows the procedure as outlined in the flowchart of Figure 2.5. A complete data file is composed of input data essential for proper simulation using the FEM. Such data includes material properties, operating and boundary conditions, information to allow construction of the finite element grid, geometric structure of the die, required number of solution and/or free surface iterations, and various flags to invoke or suppress certain capabilities of the program (such as non-isothermal or

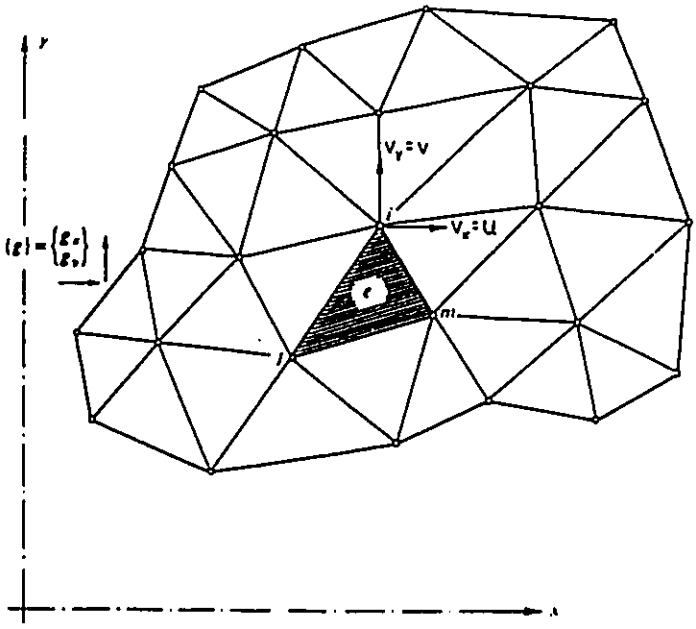

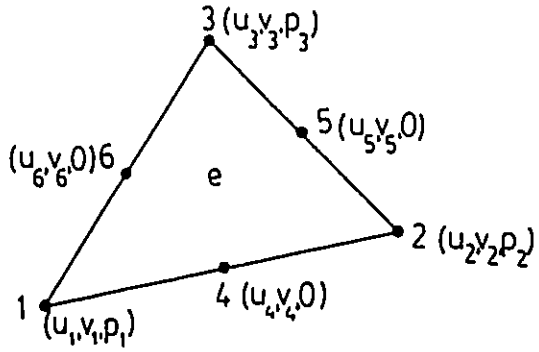

Figure 2.4: (a) Triangular finite element discretization of the flow domain; (b) Typical triangular element used in the FEM analysis (u-v-p formulation).

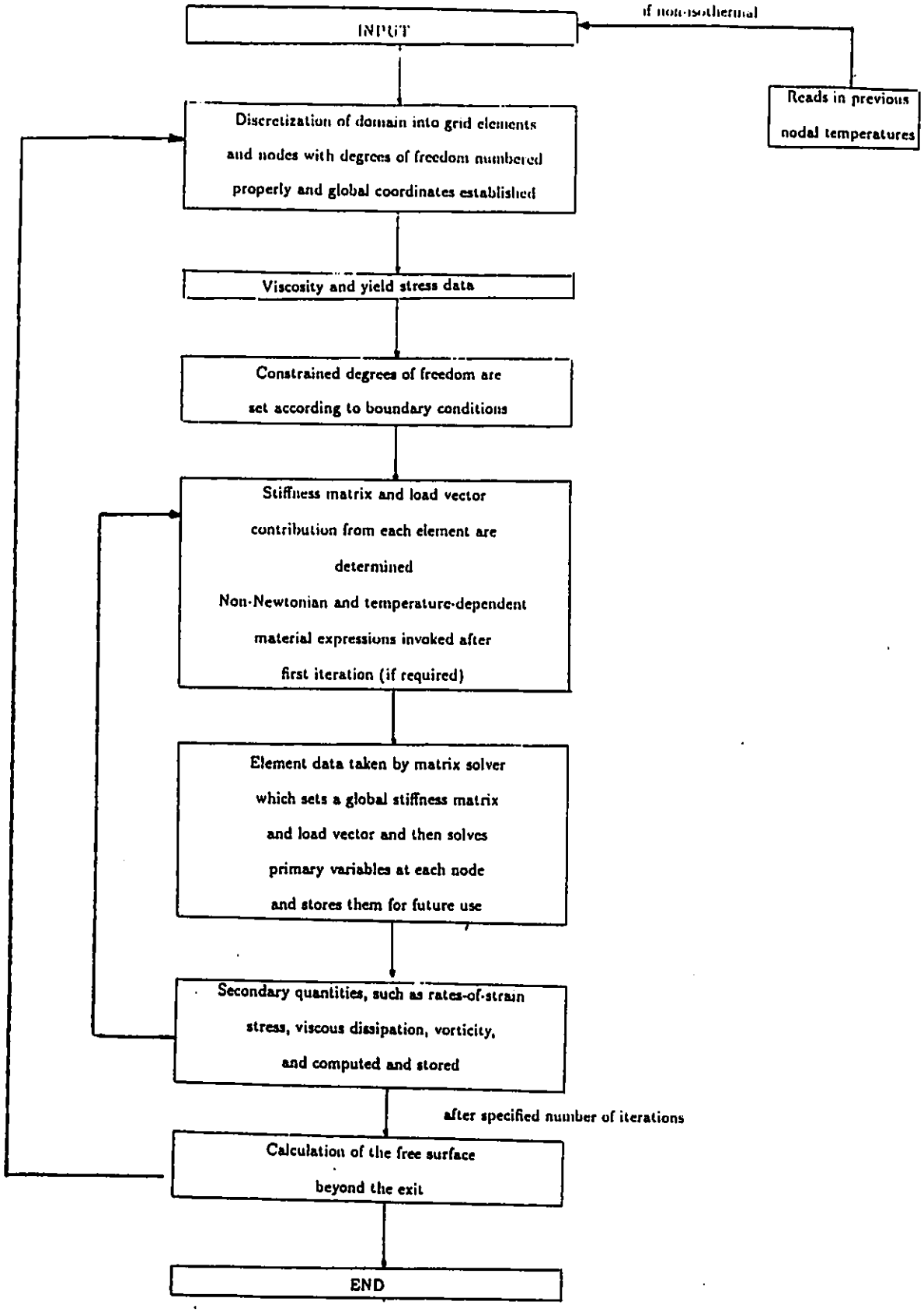

Figure 2.5: Flow sheet for the organization of main program (MACVIP).

non-Newtonian analysis). Initially the finite element grid is constructed, after which all other data is incorporated. If the analysis is non-isothermal, temperature data is read in from an external file and used to calculate new material property values.

Since this method is based on solution contributions from area domains rather than individual points, the differential equations are rewritten in approximate integral equations and having set the boundary conditions, a set of simultaneous linear algebraic equations is created. The primitive variables are then found from the following expression:

$$\begin{pmatrix} [K_v] & [K_p] \\ [K_p]^T & [0] \end{pmatrix}_n \begin{pmatrix} \begin{bmatrix} v_x \\ v_y \end{bmatrix} \\ [p] \end{pmatrix}_n = \begin{pmatrix} [F] \\ [0] \end{pmatrix}_n \tag{2.67}$$

The individual contributions from each element are found through integration of the individual terms of the FEM expressions corresponding to the conservation equations. Together they produce a symmetric **stiffness matrix**, $[K]$, for each element n, with all contributions eventually added up and equated with the **load vector**, F, that contains body forces, surface tractions and boundary conditions. These algebraic equations can be solved by using either a frontal method (subroutine FRONTS in MACVIP, Hood, 1976 and Taylor and Hughes, 1981) or a banded Choleski decomposition method

(subroutine GBAND in MACVIP, Mitsoulis, 1984). For regular grids the latter was found to be much faster in execution and was used in the present work.

Since the apparent viscosity is strain-rate and yield-stress dependent, a non-linear system of equations results which has to be solved through some iterative procedure. Although a Newton-Raphson iterative scheme would be recommended, here we have used a direct substitution scheme (Picard method). This avoids calculating the Jacobian (which can be time-consuming) and it also enjoys a wider convergence range. The solution process starts from the Newtonian field ($\tau_y = 0$), which is used to obtain a first approximation. Iterations are performed until convergence for the current yield stress is achieved (usually when the norm-of-the-error < 0.01, although we have tried runs with tolerance $< 10^{-4}$ with results virtually identical). The new solution is then used as an initial estimate for the higher yield stress value (zeroth-order continuation on the τ_y-parameter). The number of iterations increased substantially as τ_y increased (departure from the Newtonian liquid and approach to a solid plastic). From previous experience (Ellwood et al., 1990) and our own runs the value of m in Equation (2.22) was kept constant at 200, since higher values ($m = 1000$) had no effect on the results.

In cases where there is a free surface, after each iteration the free surface is determined (subroutine SWELL in MACVIP) from the computed velocity

field (more details are given later). The grid is then regenerated to account for the altered domain due to the inclusion of the free surface, and the process for $v_x - v_y - p$ solution is repeated. The iterative process stops when both the norm-of-the-error is below the prescribed tolerance and virtually no change is seen for the location of the free surface.

Computer time requirements for MACVIP vary due to various considerations such as number of iterations desired and the extent of intensity of the analysis. A denser grid will undoubtedly yield more precise data although the increase in CPU time required could make costs prohibitive. Therefore a balance must be struck between the two concerns.

Figure 2.6 shows how the main program (MACVIP) interacts with other programs which have been designed to solve for other variables by using data created by the former. The solution for nodal temperatures in a non-isothermal analysis is done by the program POISSON FORTRAN. It requires the data files produced by the main program on coordinates (COORD DATA), velocities and pressures (VEL DATA) and viscous dissipation (VDISS DATA), and it produces the nodal temperatures (TEMP DATA).

As with the pressure determination, a linear approximating function is used for evaluation of temperatures over elements. This function is substituted into an integral form of the differential equation for the conservation of energy, which accounts for thermal variations due to convection, conduc-

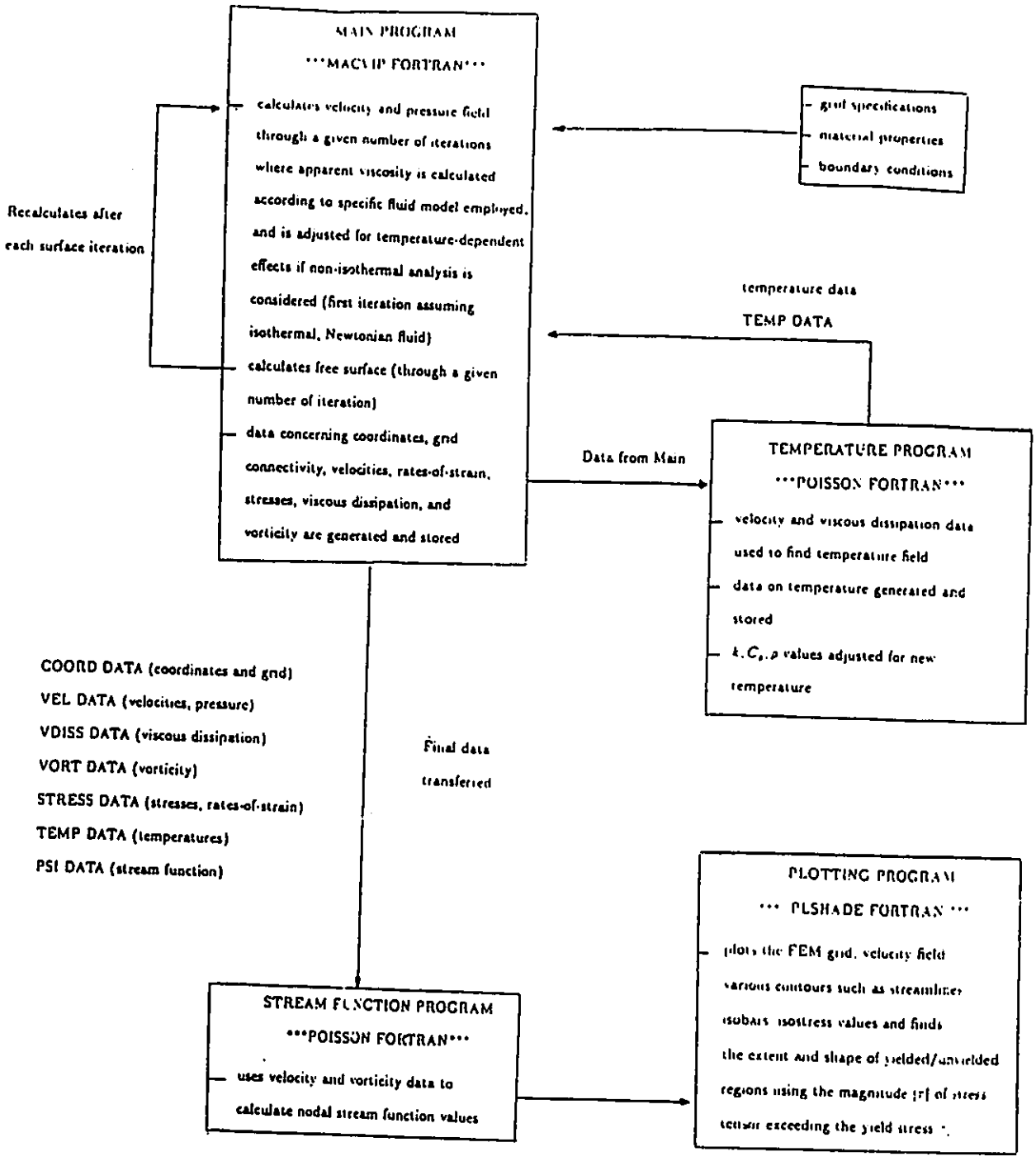

Figure 2.6: Flow sheet for the overall organization of all programs used.

tion, and viscous dissipation. From this, a linear system of finite element equations is obtained, expressed in the form

$$[K_T][T^*] = [F_T] \tag{2.68}$$

where $[K_T]$ is the global heat stiffness matrix (unsymmetric), $[F_T]$ is the heat load vector incorporating all boundary conditions, and $[T^*]$ is the column matrix of the unknown nodal temperatures. The matrix solver used is based on the Choleski decomposition method for non-symmetric matrices (GBAND). It was found that time requirements for execution were approximately in the order of 1 CPU secs.

Temperature oscillations are usually found to exist at moderate to high Peclet numbers (i.e. relatively high convection, Mitsoulis, 1984). To suppress these oscillations without making major grid density increases, a mathematical method called **upwinding** can be implemented (Heng, 1987). Basically, the contribution of the convective term is found through integration of the element matrices over the area of a linear quadrilateral. In POISSON FORTRAN every 2 parent 6-node triangles are subdivided into 4 quadrilateral elements having 4 nodes each. More details are given by Heng (1987).

After the final series of iterations has been completed by the main program, data is transferred to find the stream function values. This is accomplished by using the same program and format used to solve for temperatures, since mathematical description of the two are very similar (both

satisfy the Poisson equation). Therefore by setting the thermal conductivity, k_T, equal to 1, eliminating the convection term and replacing the viscous dissipation (VDISS DATA) with vorticity (VORT DATA), quick determination of the stream function (PSI DATA) is accomplished using the POISSON FORTRAN program. Finally, visual displays are created to illustrate the flow within the domain by using the PLSHADE FORTRAN program. The stream function values are normalized, after which streamline patterns are produced by connecting points of equal value (i.e. contours). This procedure is also carried out for temperature values to give a presentation of isotherms. Other data, such as velocities, pressures, stresses, rates-of-strain, vorticity, the magnitudes of the rate-of-strain $|\dot{\gamma}|$ and stress tensors $|\tau|$, yield stress, etc., are read in directly to quickly produce visual displays of their distributions in the flow domain. These include the velocity field, isobars, stress contours, and most importantly, the extent and shape of the yielded/unyielded regions by finding the envelope of $|\tau|$ values exceeding the yield stress τ_y.

Chapter 3

Entry Flow in a 4:1 Contraction

Before proceeding with the numerical analysis of actual extrusion processes, the finite element program was tested against some well-known analytical results for simple shear flow of Bingham fluids. The effect of the finite element mesh is examined on the results and the iterative process highlighted. The entry flow from a reservoir into a die having a contraction ratio of 4:1 is then considered for planar and axisymmetric geometries. The extent and shape of yielded/unyielded regions are determined based on the criterion that the material flows (yields) when the magnitude of the stress tensor exceeds the yield stress. The results for pressure are used to determine the excess pressure losses that give rise to the entrance correction.

3.1 Poiseuille Flow of Bingham Fluids

3.1.1 Unidirectional Flow between Parallel Plates

A Bingham material between two parallel plates of length L and width W is being driven in the x-direction by a constant pressure gradient (see Figure 3.1). In this case, the momentum Equation (2.5) reduces to a single scalar equation:

$$\tau_{xy} = \left(\frac{dp}{dx}\right) y = \left(\frac{\Delta P}{L}\right) y \tag{3.1}$$

where $\frac{dp}{dx}$ is a constant pressure gradient and the stress τ_{xy} is given by Equation (2.16). Following Bird et al. (1983), the *yield surface*, at which $\tau_{xy} = \tau_y$, is then located at $y = y_o$ given by:

$$y_o = \tau_y \left(\frac{L}{\Delta P}\right) \tag{3.2}$$

The velocity profile is given by:

$$v_x^{>} = \frac{H^2}{2\mu}\left(\frac{\Delta P}{L}\right)\left(1 - \left(\frac{y}{H}\right)^2\right) - \frac{\tau_y H}{\mu}\left(1 - \left(\frac{y}{H}\right)\right) \qquad (y_o \le y \le H) \quad (3.3a)$$

$$v_x^{<} = \frac{H^2}{2\mu}\left(\frac{\Delta P}{L}\right)\left(1 - \left(\frac{y_o}{H}\right)^2\right) - \frac{\tau_y H}{\mu}\left(1 - \left(\frac{y_o}{H}\right)\right) \qquad (0 \le y \le y_o) \quad (3.3b)$$

The superscripts $>$ and $<$ denote that the expressions are for $y \ge y_o$ or $y \le y_o$, respectively. The volume flow rate Q is then given by:

$$Q = W\int_{-H}^{H} v_x(y)dy = \frac{2WH^2\tau_w}{3\mu}\left(1 - \frac{3}{2}\left(\frac{\tau_y}{\tau_w}\right) + \frac{1}{2}\left(\frac{\tau_y}{\tau_w}\right)^3\right) \qquad (\tau_w \ge \tau_y) \tag{3.4}$$

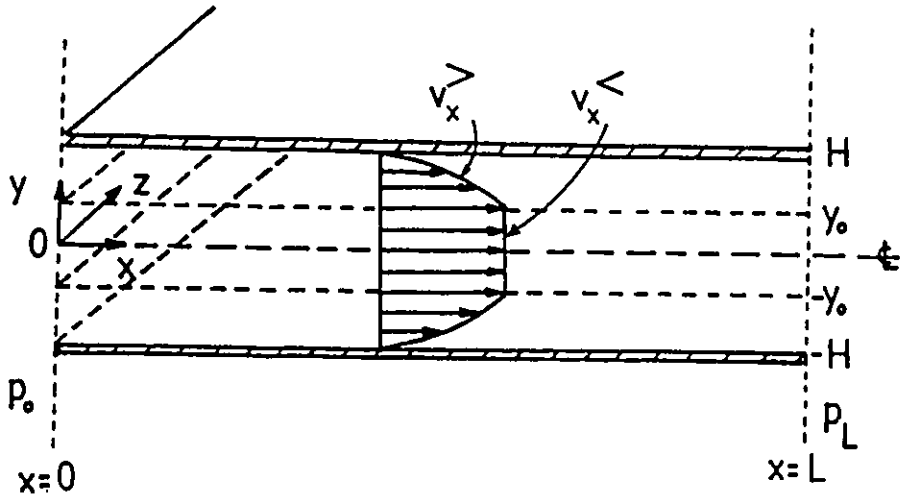

Figure 3.1: Flow in a planar slit showing the plug flow region $-y_o \leq y \leq y_o$ and the plastic flow regions $y_o \leq y \leq H$ and $-H \leq y \leq -y_o$.

where τ_w is the wall shear stress given by:

$$\tau_w = \left(\frac{\Delta P}{L}\right) H \tag{3.5}$$

For the FEM analysis, the grid used consists of 120 triangular elements, 275 nodes and 746 unknown d.o.f. (25 nodes across, 11 nodes along the domain). Figure 3.2 shows the finite element grid along with the boundary conditions. Because of the symmetry involved only half the domain need be considered. The boundary conditions are:

- on edge AD either a fully-developed profile v_x or a uniform surface traction $\bar{T}$ to account for the pressure forces acting on the material;
- on edge CD, $v_x = 0$ (no-slip condition at wall);
- on all four edges, $v_y = 0$;
- at an arbitrary point downstream (here at C), p=0.

The finite element iterative process starts from the Newtonian solution and using direct substitution (Picard method) proceeds to the Bingham solution using Papanastasiou model (Equation 2.22) with $m = 200$, which mimics very well the ideal Bingham fluid. The number of iterations increases with the yield stress in order to achieve the same tolerance of error. For the case of $\mu = 0.001\ MPa.s$, $\tau_y = 0.007\ MPa$, $\bar{T} = \frac{dp}{dx} = 0.13125\ MPa/cm$, $H = 0.1\ cm$ and $L = 0.1\ cm$, the dimensionless yield stress $\tau_y^* = 1.6$ and the Bingham number $Bi = 11.6$. It takes 24 iterations to reach a norm-of-the-error below 10^{-3} and the norm-of-the-residual below 10^{-4} (see also

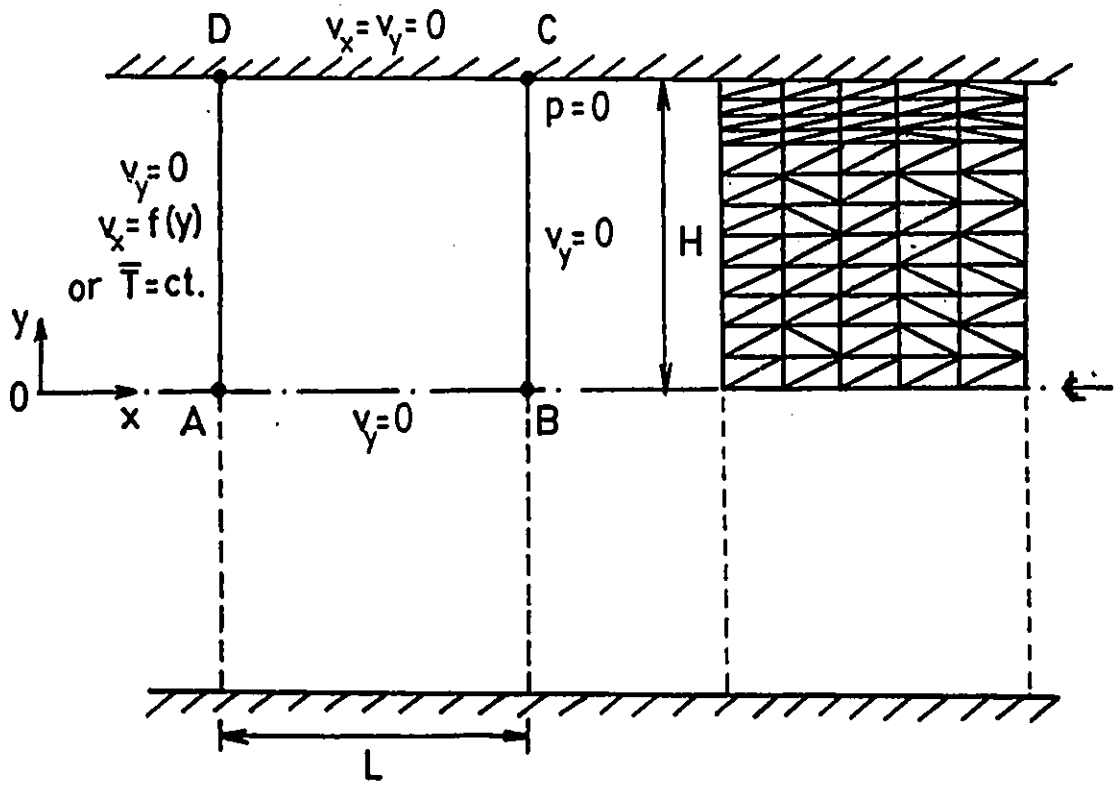

Figure 3.2: Boundary conditions in pressure-driven flow through a planar slit and finite element grid used in the computations.

Appendix A)

The solution is shown is Figure 3.3, where the velocity profile is compared to the analytical solution (Equation 3.3). The pressure is linear in the x-direction (Figure 3.4a) while the shear stress is linear in the y-direction (Figure 3.4b). The *yield surface* y_o was found to be in excellent agreement with the analytical value ($y_o = 0.5333H$) of Equation (3.2). Since the FEM solution is two-dimensional, the fully-developed flow field reproduces itself in the x-direction, giving rise to the graphs of Figure 3.5, where the velocity field, isobars, streamlines and shear stress contours are presented together with the unyielded (shaded) core. The contour values are made dimensionless between 0 and 1 with increments of 0.1. It is noteworthy that slight numerical inaccuracies appear near the entry inside the unyielded region (see e.g. the first isobar) but these quickly correct themselves downstream.

3.1.2 Axial Flow in a Circular Tube

A Bingham material flowing in a circular tube of radius R and length L is being driven in the z-direction by a constant pressure gradient (Poiseuille flow in a tube, see Figure 3.1, where H is substituted by R and y by r). In this case, the wall shear stress τ_w is given by:

$$\tau_w = \left(\frac{\Delta P}{L}\right)\frac{R}{2} \tag{3.6}$$

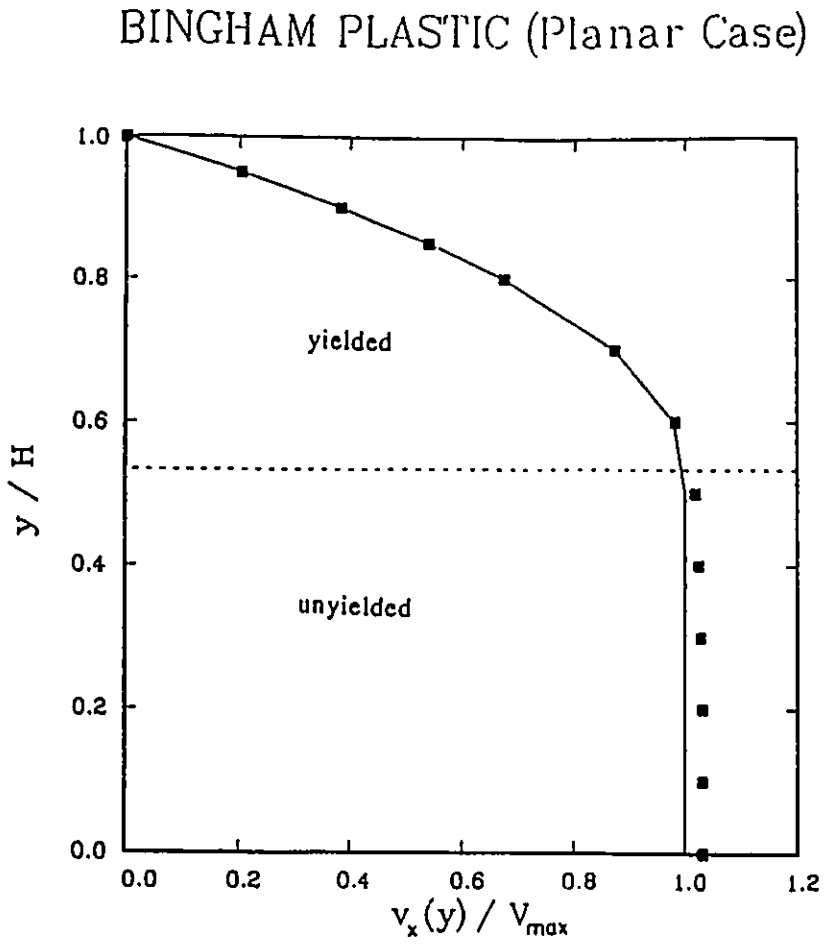

Figure 3.3: Comparison between the analytical solution (solid line) and numerical solution (symbols) for the velocity profile in fully-developed pressure-driven flow of a Bingham plastic between parallel plates (Data: μ=0.001 MPa.s, τ_y=0.007 MPa, H=0.1 cm, L=0.1 cm, dp/dx=0.13125 MPa/cm; τ_y^*=1.6, Bi=11.6).

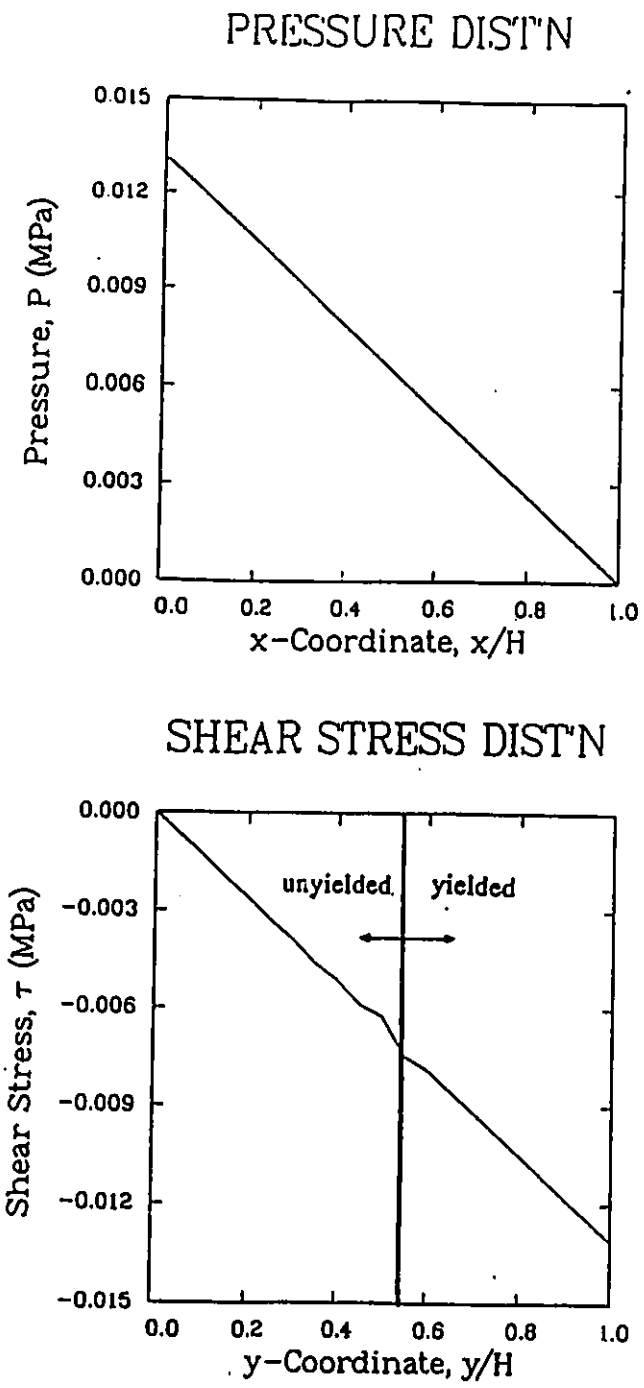

Figure 3.4: (*a*) Axial pressure distribution, (*b*) transverse shear stress distribution in pressure-driven flow of a Bingham plastic between parallel plates (same data as in Figure 3.3).

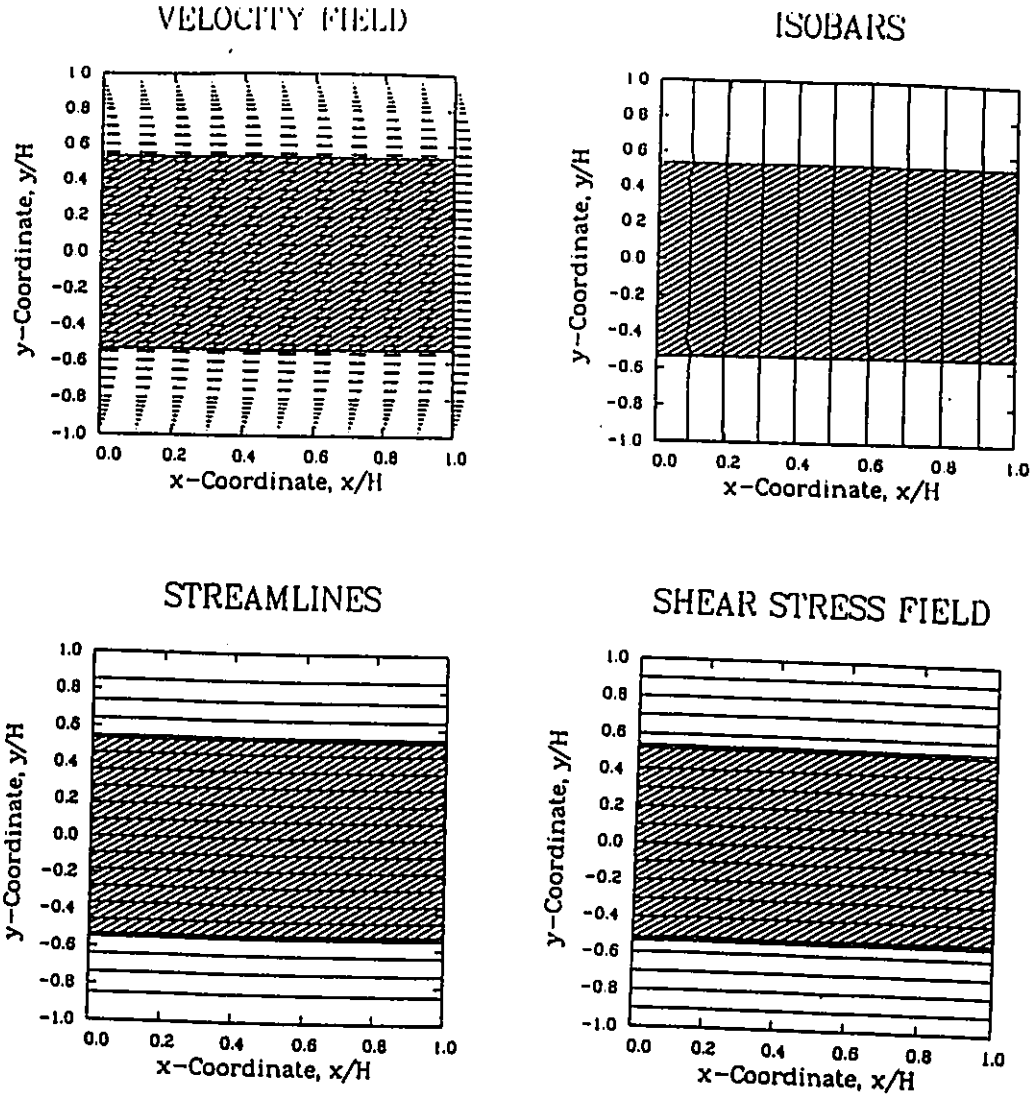

Figure 3.5: Velocity field, isobars, streamlines and shear stress field given by the FEM solution in pressure-driven flow of a Bingham plastic between parallel plates (same data as in Figure 3.3).

and the yield surface is located at

$$r_o = 2\tau_y \left(\frac{L}{\Delta P}\right) = R\left(\frac{\tau_y}{\tau_w}\right) \tag{3.7}$$

The velocity distribution is given as:

$$v_z^{>} = \frac{R^2}{4\mu}\left(\frac{\Delta P}{L}\right)\left(1-\left(\frac{r}{R}\right)^2\right) - \frac{\tau_y R}{\mu}\left(1-\left(\frac{r}{R}\right)\right) \qquad (r_o \le r \le R) \quad (3.8a)$$

$$v_z^{<} = \frac{R^2}{4\mu}\left(\frac{\Delta P}{L}\right)\left(1-\left(\frac{r_o}{R}\right)^2\right) - \frac{\tau_y R}{\mu}\left(1-\left(\frac{r_o}{R}\right)\right) \qquad (0 \le r \le r_o) \quad (3.8b)$$

where the second expression describes the plug flow region. The volume flow rate Q is then given by:

$$Q = \pi R^4 \int_0^R v_z(r) r dr = \frac{\pi R^4}{4\mu}\left(\frac{\Delta P}{L}\right)\left(1-\frac{4}{3}\left(\frac{\tau_y}{\tau_w}\right)+\frac{1}{3}\left(\frac{\tau_y}{\tau_w}\right)^4\right) \qquad (\tau_w \ge \tau_y) \tag{3.9}$$

which is known as the **Buckingham-Reiner** equation (Bird et al., 1983), corresponding to the **Hagen-Poiseuille** equation for Newtonian fluids.

For the FEM analysis, the same grid was used as before for the planar analysis. The boundary conditions are the same and the solution has been pursued for the same material data as before but with $\bar{T} = \frac{dp}{dz} = 0.3\ MPa/cm$. In this case $\tau_y^* = 1.87$ and $Bi = 9.5$. It takes 19 iterations to reach a norm-of-the-error below 10^{-3} and the norm-of-the-residual is below 10^{-6} (see also appendix A).

The solution is shown in Figure 3.6, where the velocity profile is compared to the analytical solution (Equation 3.8). The pressure is linear in

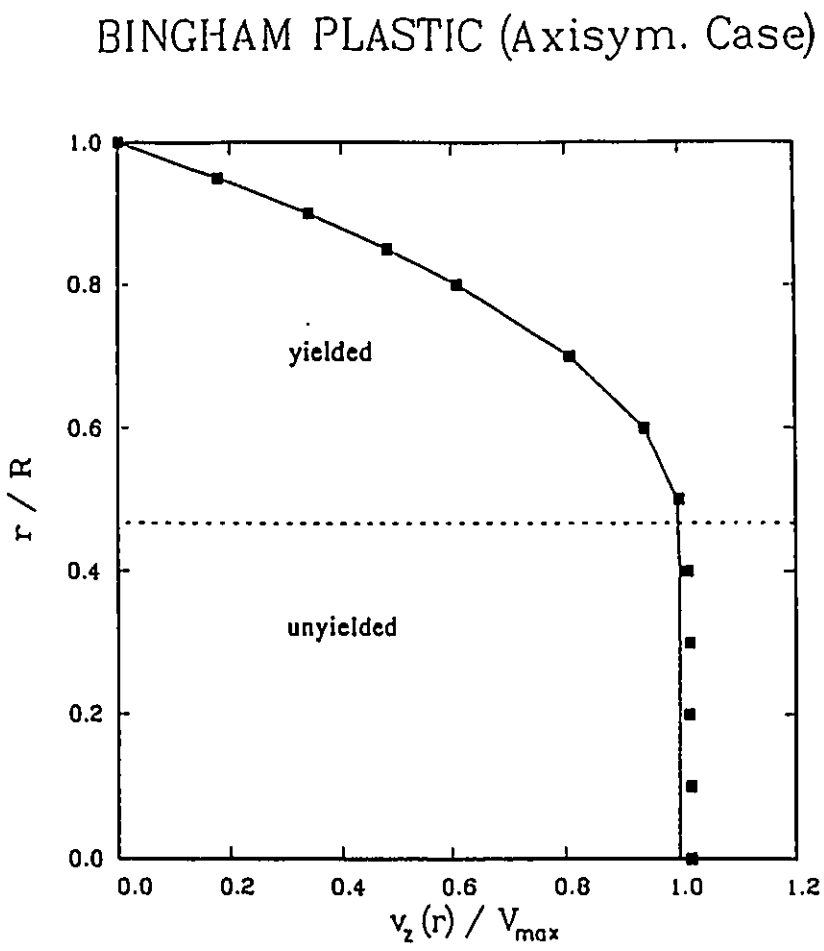

Figure 3.6: Comparison between the analytical solution (solid line) and numerical solution (symbols) for the velocity profile in fully-developed Poiseuille flow of a Bingham plastic in a tube (Data: μ=0.001 MPa.s, τ_y=0.007 MPa, R=0.1 cm, L=0.1 cm, dp/dz=0.3 MPa/cm; τ_y^*=1.87, Bi=9.5).

the z-direction (Figure 3.7a) while the shear stress is linear in the r-direction (Figure 3.7b). The yield surface r_o was found to be in excellent agreement with the analytical value ($r_o = 0.46667R$) of Equation (3.7). Since the FEM solution is two-dimensional, the fully-developed flow field reproduces itself in the z-direction, giving rise to the graphs of Figure 3.8, where the velocity field, isobars, streamlines and shear stress contours are presented together with the unyielded (shaded) core. The contour values are made dimensionless between 0 and 1 with increments of 0.1. It is noteworthy that slight numerical inaccuracies appear near the entry inside the unyielded region (see e.g. the first isobar) but these quickly correct themselves downstream. The above results provide confidence in the finite element solution before embarking on the next case of entry flow through a 4:1 abrupt contraction.

3.2 Entry Flow in a 4:1 Abrupt Contraction

3.2.1 Introduction

Almost all viscoplastic materials at some stage in their life-time are forced to flow through forming devices such as dies, from which they emerge shaped into a final product. The flow through a die involves a drastic change of geometry from a rather large reservoir to a smaller contraction (slit or capillary) through which the viscoplastic material exits to the atmosphere (see

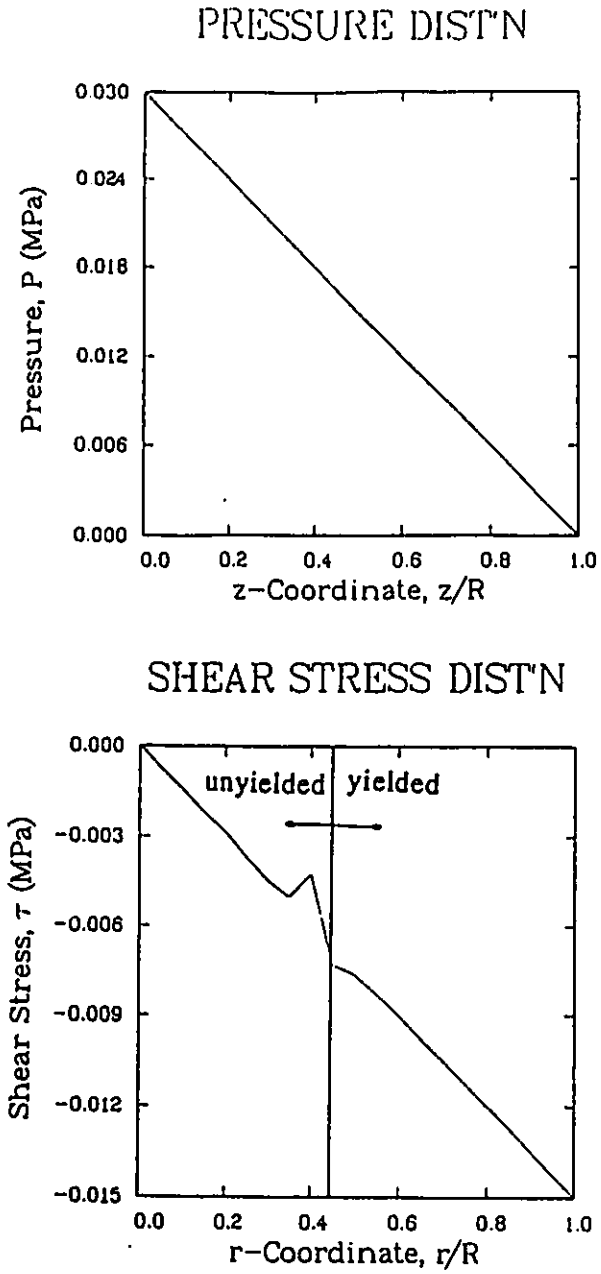

Figure 3.7: (*a*) Axial pressure distribution, (*b*) radial shear stress distribution in Poiseuille flow of a Bingham plastic in a tube (same data as in Figure 3.6).

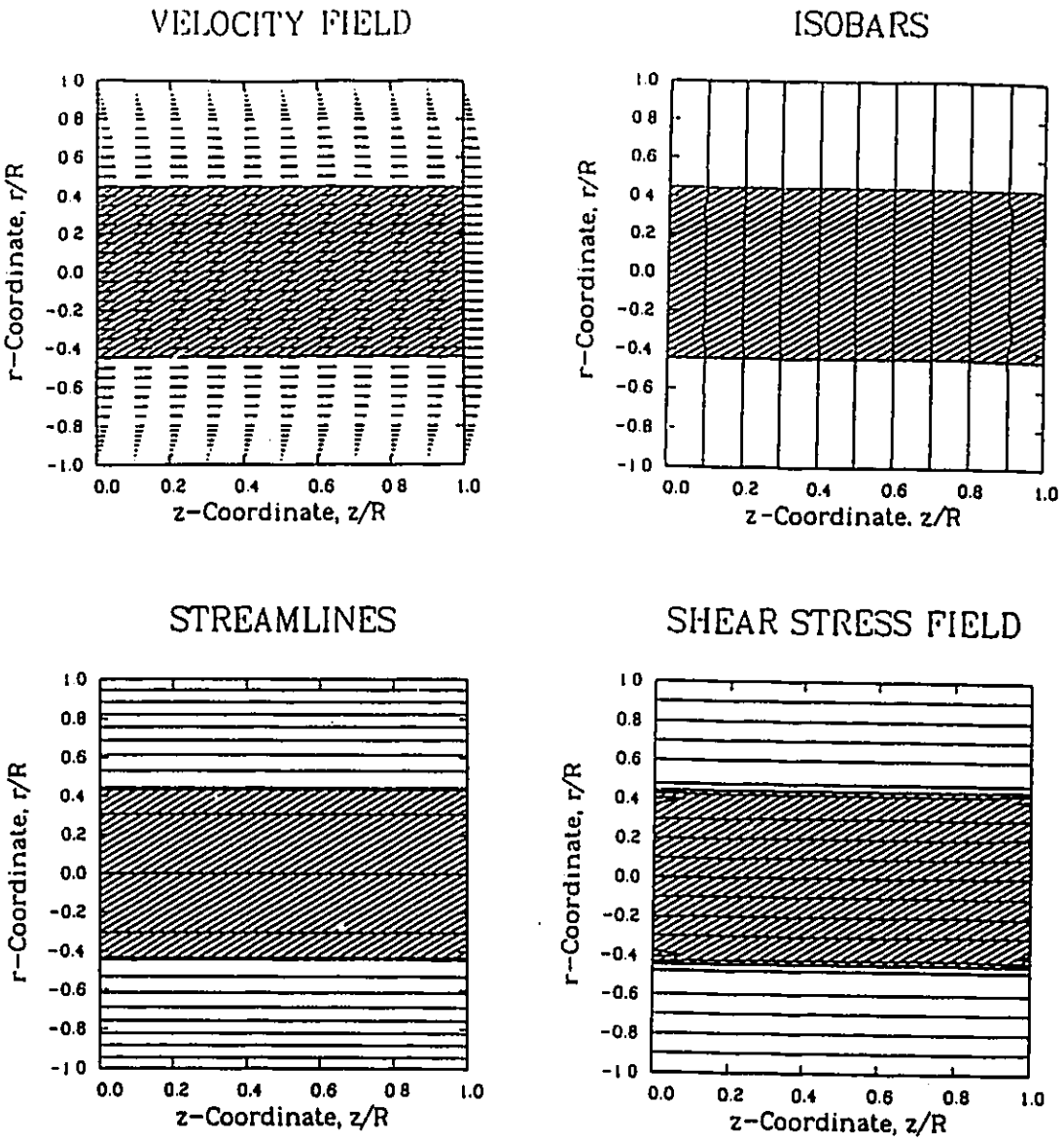

Figure 3.8: Velocity field, isobars, streamlines and shear stress field given by the FEM solution in Poiseuille flow of a Bingham plastic in a tube (same data as in Figure 3.6).

Figure 3.9a). Flow instabilities have been encountered in die entry flows especially for polymer solutions and melts (Boger, 1982), and they constitute important commercial problems. Due to the contraction present in the die entry, the flow must be treated at least as two-dimensional. Such a flow is no longer viscometric or simple shear flow and the viscoplastic nature of the material becomes evident. This involves a growth of the unyielded regions with yield stress or Bingham number and an increase in the pressure drop. The literature abounds with both theoretical and experimental attempts to understand this flow field, but mainly for Newtonian fluids and viscoelastic polymer solutions and melts (White et al., 1987). For viscoplastic materials no attempt has been made so far to study their behaviour in contractions, either within a theoretical or experimental framework. It is, therefore, a major purpose of this study to investigate the flow of viscoplastic materials through contractions and report the results as a function of the dimensionless yield stress and Bingham number.

The emphasis in the present work will be on finding the extent and shape of yielded/unyielded regions as well as the excess pressure losses to push the viscoplastic materials through the contraction. It is well-known that whenever a molten polymer enters from a reservoir into a die and then emerges from the die into the atmosphere, excess pressure drops are required over and above the fully-developed losses (see Figure 3.9b). These pressure drops

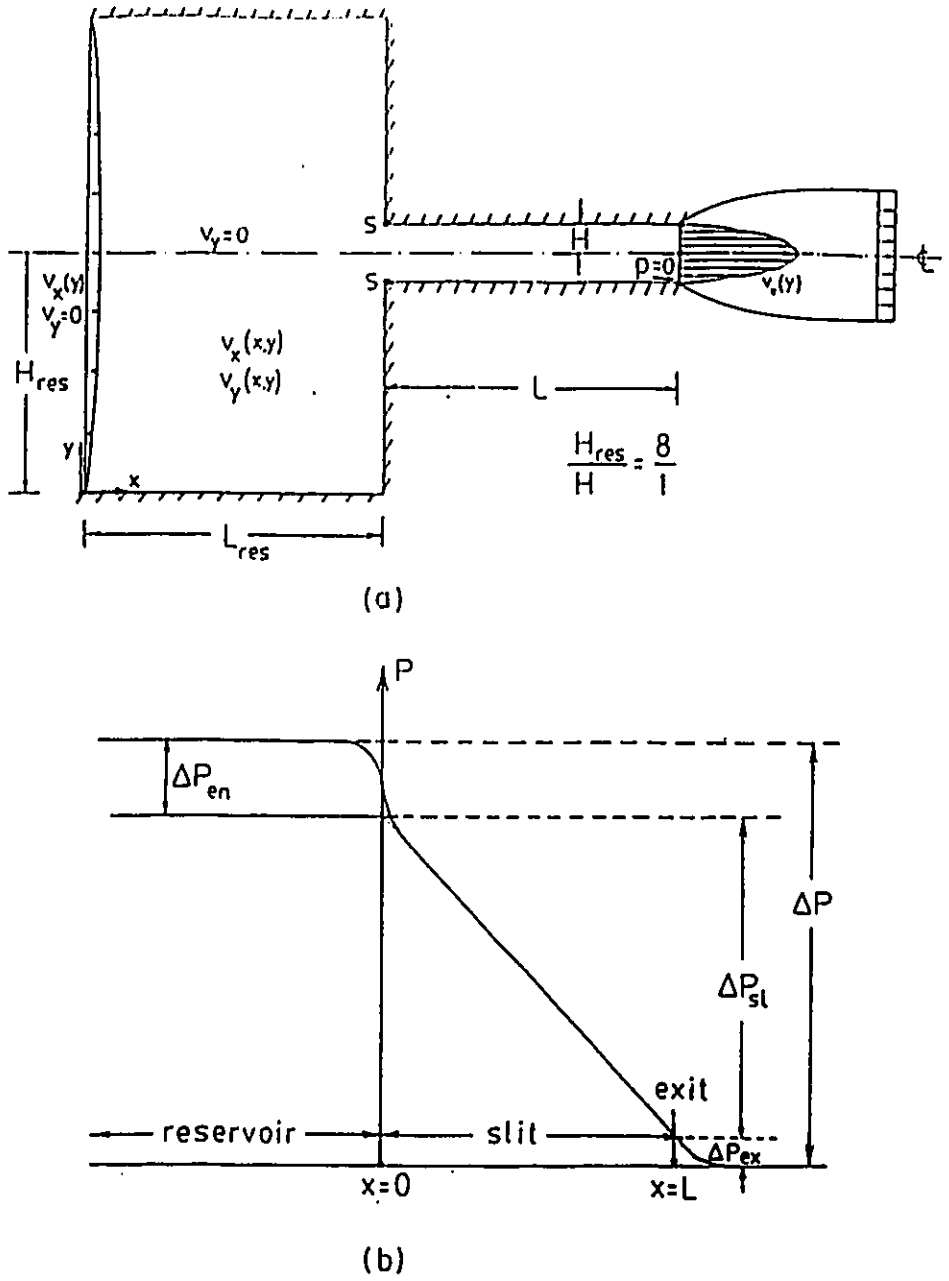

Figure 3.9: (*a*) Entry and exit flow from a slit die. (*b*) Pressure profile along the reservoir, the slit die and the extrudate.

are usually referred to as **entrance** and **exit pressure losses** and the corresponding total correction to Poiseuille flow in the die is referred to as the **end correction** (also known as **Couette correction** for Newtonian fluids and **Bagley correction** for non-Newtonian fluids). The origin and significance of end correction in dies for viscoelastic materials has been examined by many investigators and has been the object of controversy (Mitsoulis et al., 1984a, Kwag and Vlachopoulos, 1991). For flow through dies we may write:

$$\tau_w = \frac{P_{res}}{2\left(\frac{L}{2H} + n_B\right)} \tag{3.10}$$

where τ_w is the shear stress at the wall for fully-developed flow in the die, P_{res} is the gauge pressure in the reservoir, L is the die length, $2H$ is the die gap (or diameter for capillary dies) and n_B is the end (or Bagley) correction. The correction is due to excess pressure drops at the entry and exit. Thus, we have:

$$n_B = n_{en} + n_{ex} \tag{3.11}$$

where

$$n_{en} = \frac{\Delta P_{en}}{2\tau_w} \tag{3.12}$$

$$n_{ex} = \frac{\Delta P_{ex}}{2\tau_w} \tag{3.13}$$

For viscoelastic polymer solutions and melts, $1 < n_B < 100$ (Ballenger and White, 1971, Han, 1976), while for Newtonian fluids the values have been

found recently through accurate numerical calculations (FEM, Hieber, 1987), and they never exceed 1.

Another feature in die entry flows through contractions is the size and intensity of the corner vortex in the reservoir. For viscoelastic polymer solutions and melts, experimental studies (White and Kondo, 1977/1978, Nguyen and Boger, 1979) have shown an increase of size and intensity of the vortex as the flow rate increases. Quite recently, Luo and Mitsoulis (1990) have been able to theoretically predict these developments by using an integral constitutive equation capable of describing the viscoelastic memory phenomena of polymers.

For viscoplastic materials, the total lack of entry flow calculations leaves the question of entry vortices in contractions an unanswered subject. However, the problem of viscoplastic material flow through abrupt expansions and stenoses has recently been studied by Scott et al. (1988) for a range of Bingham and Reynolds numbers.

The choice of the contraction ratio β has been the object of several investigations (Hieber, 1987, Mitsoulis, 1988). These studies have shown that the results are definitely dependent on contraction ratio. However, most of the important features in entry flows are well captured in a 4:1 contraction ratio, and thus it has been agreed by workers in the field to use this as a benchmark problem. We will also use it in the course of the present study.

3.2.2 Entry Flow of Newtonian Fluids

The physical system for the analysis of a sudden entry flow is illustrated in Figure 3.10 and is representative of flow of viscoplastic materials from a reservoir into an extrusion die. The abrupt contraction shown represents a 4:1 ratio between the half width H_{res} of the inlet section (reservoir) and the half width H of the outlet section (slit die). There is a stress singularity at point S where the material enters the die. Due to symmetry, the calculation was performed on only half of the domain. The boundary conditions are:

- a fully-developed Poiseuille velocity profile for Bingham fluids at the upstream plane (Bird et al., 1983 and Equation 3.3);
- no slip conditions at the walls;
- v_y equal to zero everywhere along the domain perimeter.

The pressure is also specified to be zero at one point (here at the exit centerline).

Two FEM grids were used for the $v_x - v_y - p$ formulation as shown in Figure 3.11. The upper grid (GRID1) has 336 elements, 741 nodes and 1492 unknown degrees of freedom (13 nodes across and 57 nodes along) and it has been used in previous studies by Mitsoulis (1986a). The lower denser grid (GRID2) consists of 560 elements, 1197 nodes and 2504 degrees of freedom (21 nodes across and 57 nodes along). The lengths before and after the contraction were also chosen so that the assumption of a fully-developed

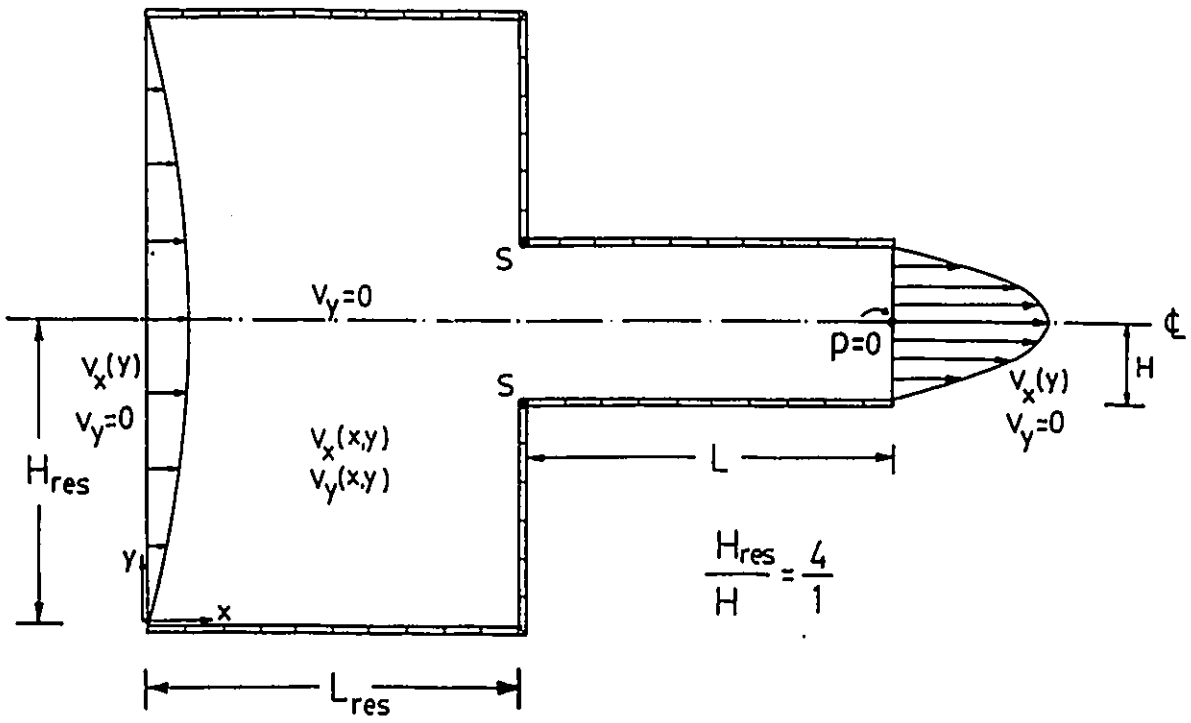

Figure 3.10: Entry flow problem and boundary conditions for a 4:1 abrupt planar contraction.

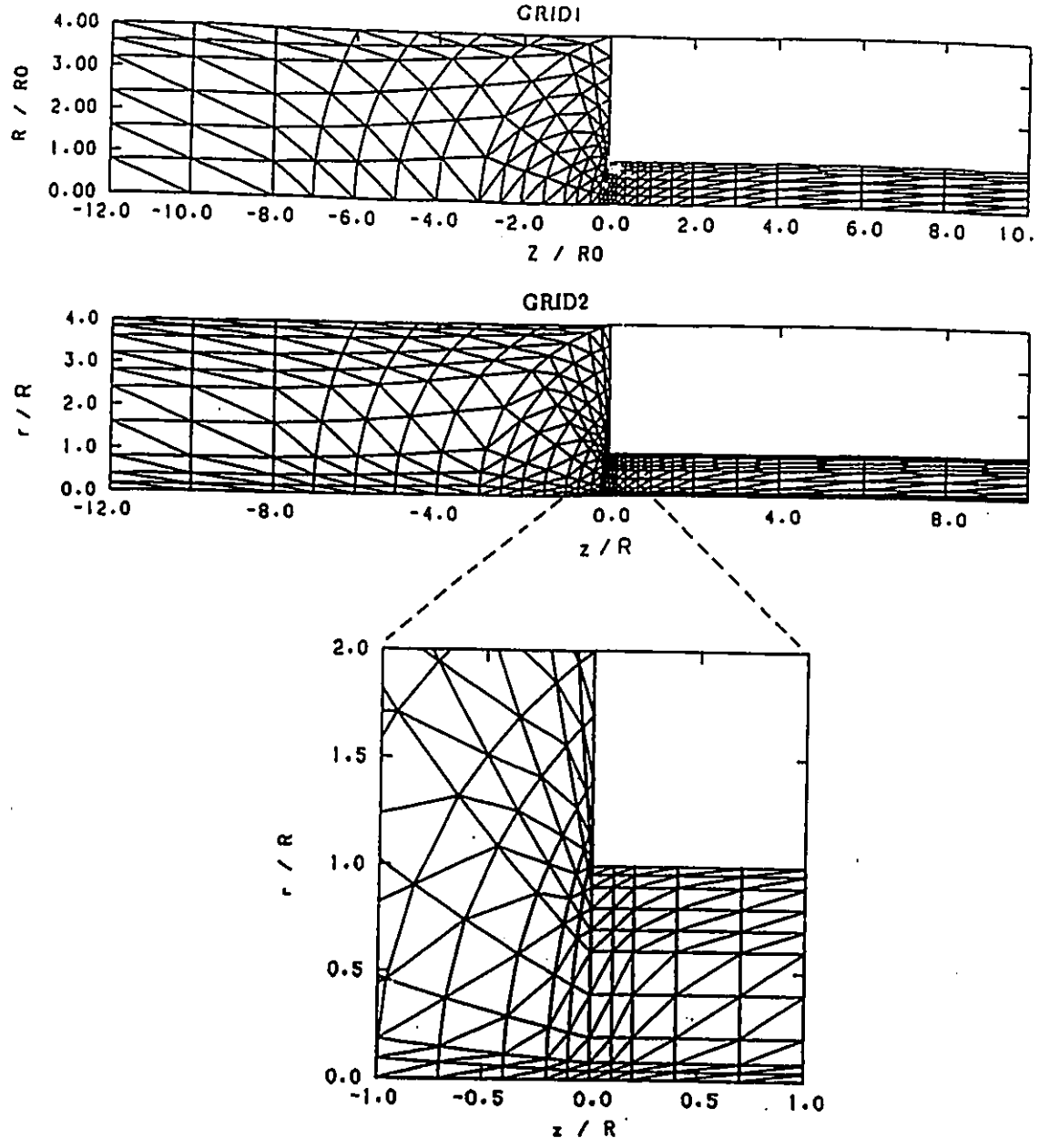

Figure 3.11: Finite element grids used for the entry flow in a 4:1 abrupt contraction.

Poiseuille velocity profile at the entrance and the exit is fully justified. A denser grid is used near the die entry to better capture the stress singularity at the entry point S (Mitsoulis, 1986a). The use of such dense grids ensures that the results are virtually free from mesh influence. The number of iterations required to attain a norm-of-error ≤ 0.001 depended on the dimensionless τ_y^* (*or* Bi). The Newtonian fluid solution (linear solution, no iterations needed) required about 7 CPU secs with GRID1 and 22 CPU secs with GRID2 in the University of Ottawa's AMDAHL-5880 mainframe computer.

The Newtonian results from the denser GRID2 are shown in Figure 3.12, for the planar case, where the flow field is visualized through velocity vectors and streamlines. The corresponding results for the axisymmetric case (circular dies) are shown in Figure 3.13 along with the experimental flow field of a Newtonian fluid (glycerine) given by Boger (1982). These results are identical with previous results obtained with GRID1 by Mitsoulis (1986a). The velocity field shows no irregularities and the fully-developed Poiseuille velocity profile for Newtonian fluids is recovered within one half width H or radius R after entrance to the die. The area near the corner of the reservoir is almost stagnant region.

The streamlines have been obtained *a posteriori* by employing the stream function formulation. Referring to Figure 3.10 the boundary conditions used

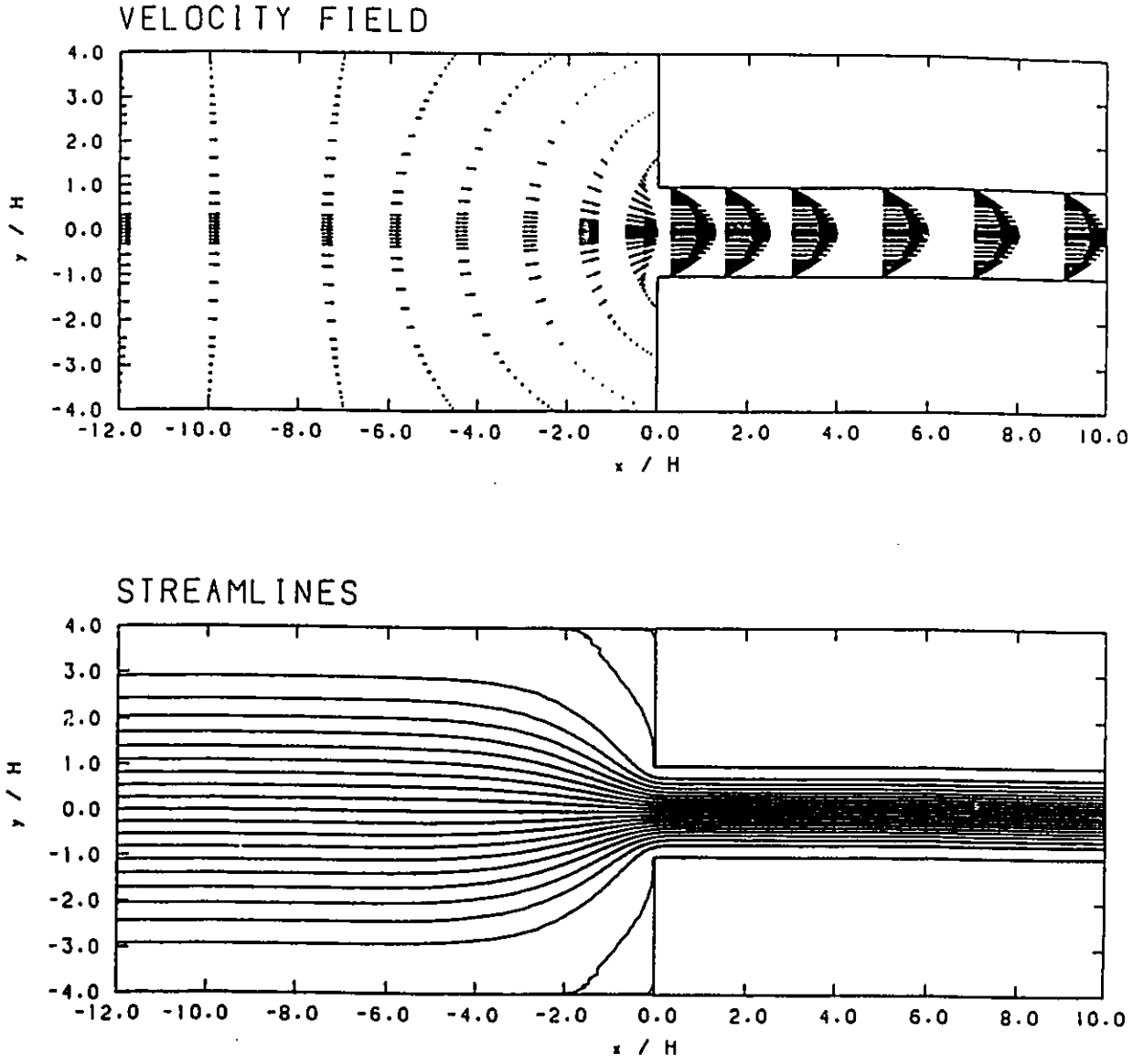

Figure 3.12: Results from the solution of a Newtonian fluid flowing through a 4:1 abrupt planar contraction.

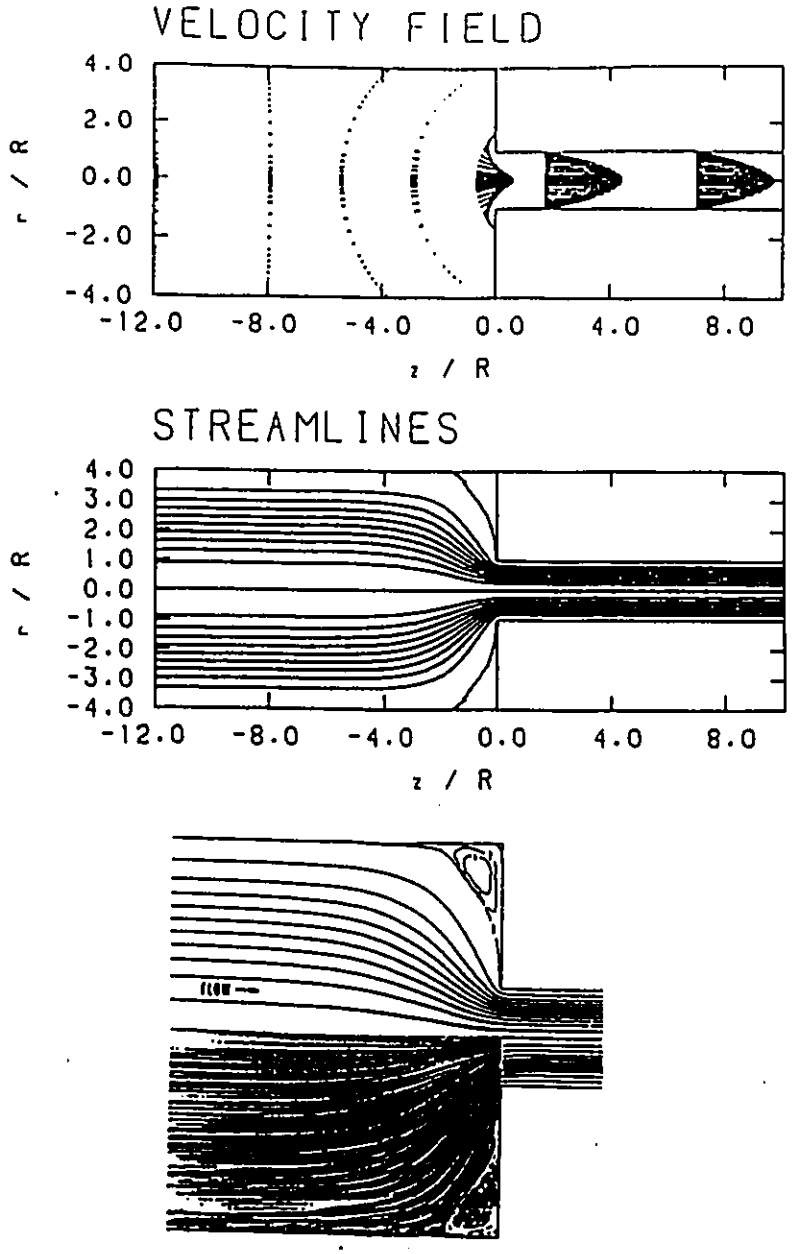

Figure 3.13: Results from the solution of a Newtonian fluid flowing through a 4:1 abrupt circular contraction and comparison with experimental flow pattern of a Newtonian fluid (glycerine) given by Boger (1982).

were:

- along the centerline, $\psi = 0$;

- along the solid wall, $\psi = Q$;

- at entry and exit planes, $\frac{\partial \psi}{\partial \hat{n}} = 0$.

The streamline patterns (Figures 3.12b and 3.13b) show smooth rearrangement from the reservoir to the capillary. A small and weak corner vortex appears having an intensity that reaches a minimum value of -0.003. The value of the ratio:

$$X = \frac{L_v}{2H_{res}} \tag{3.14}$$

where L_v is the detachment length of the vortex and $2H_{res}$ is the reservoir width (or reservoir diameter D_{res}) was found to be 0.15, in excellent agreement with previous numerical results (Mitsoulis, 1986a), and experimental values (Boger, 1982).

The entrance correction n_{en} can be calculated from

$$n_{en} = \frac{\Delta P - (\Delta P_{res} + \Delta P_o)}{2\tau_w} \tag{3.15}$$

where ΔP_{res} is the pressure drop obtained for fully-developed flow in the reservoir, ΔP_o the corresponding value obtained for the slit and τ_w the wall shear stress at the slit wall. The values for the Newtonian fluid from the two grids were found to be 0.376 (GRID1) and 0.381 (GRID2) for the planar case and compare favorably with previous results by Mitsoulis (1986a), who gives

0.376 (result with GRID1). The corresponding results for the axisymmetric case were found to be 0.566 (GRID1) and 0.579 (GRID2) and compare favorably with previous results by Mitsoulis (1986a), who gives 0.566 (result with GRID1).

3.2.3 Entry Flow of Bingham Fluids

Calculations were carried out for different τ_y values and using $m = 200$ in the constitutive Equation (2.22). Following Papanastasiou (1987), we have pursued the calculations for $0 \leq \tau_y^* < \Delta P^*$ (or respectively, $0 \leq Bi < \infty$), where the dimensionless pressure gradient ΔP^* is equal to 3 for planar and 4 for axisymmetric geometries in the downstream channel. The progressive growth of solid (unyielded) regions in the flow field is shown for the planar geometry in Figure 3.14 and for the axisymmetric geometry in Figure 3.15, for increasing values of τ_y^* (or Bi). The shaded areas correspond to unyielded regions (solid). The fully-developed conditions at entry and exit (analytical solutions available for Poiseuille flow of a Bingham fluid, Bird et al., 1983) give rise to horizontal lines in the envelope for the solid region, which is much larger in the reservoir than the downstream tube, as expected due to a much slower flow (hence stress level) in the reservoir. Also note the dead space near the corners, where the material remains unyielded. As the Bingham number increases, a bigger solid region appears closer to the die

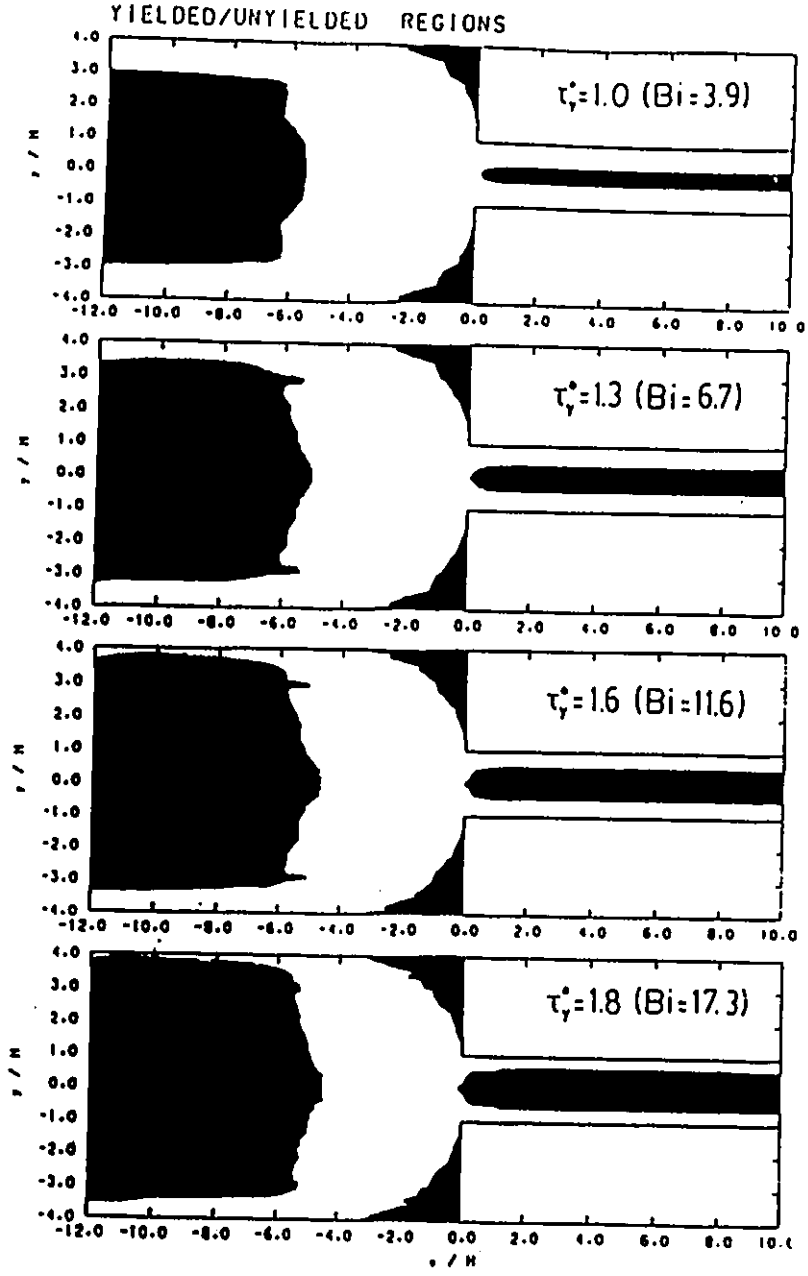

Figure 3.14: Progressive growth of the unyielded zone (shaded) for entry flow of Bingham fluids in a 4:1 abrupt contraction (planar case).

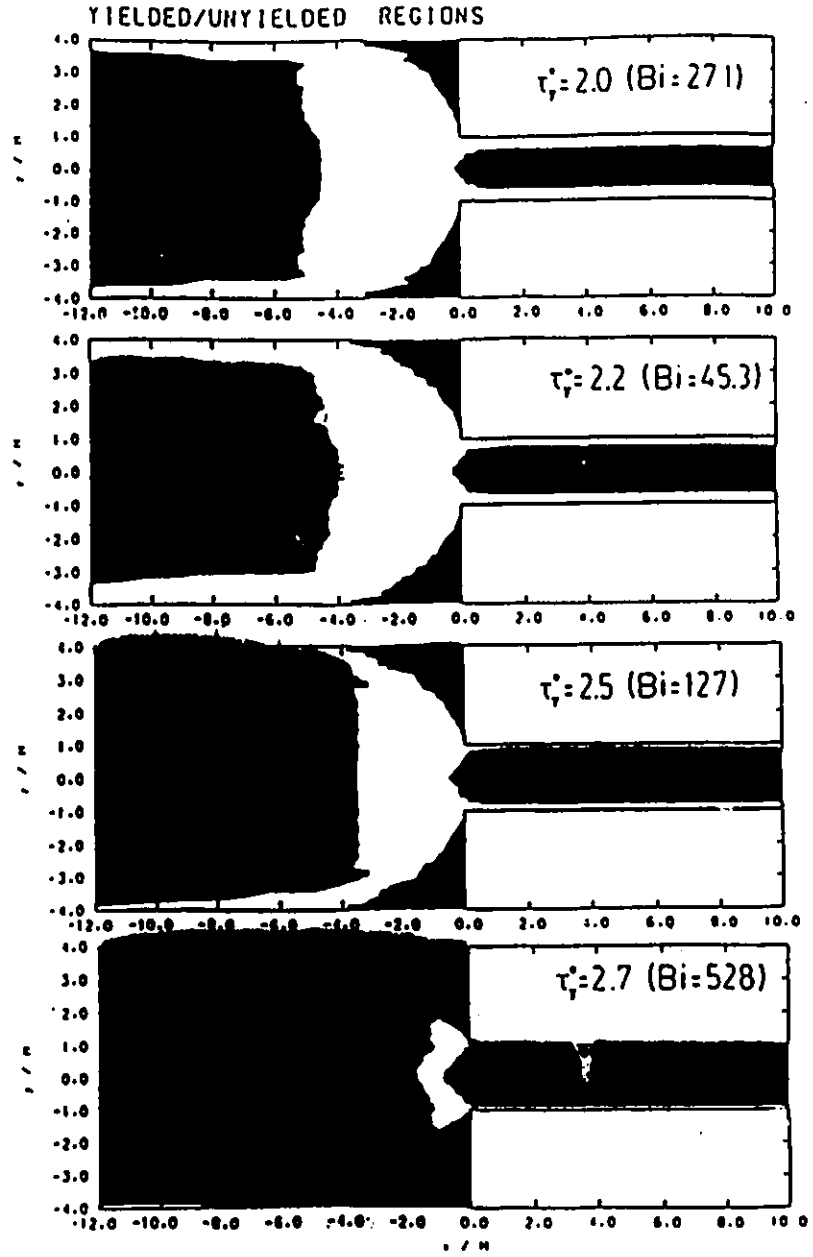

Figure 3.14 (cont'd).

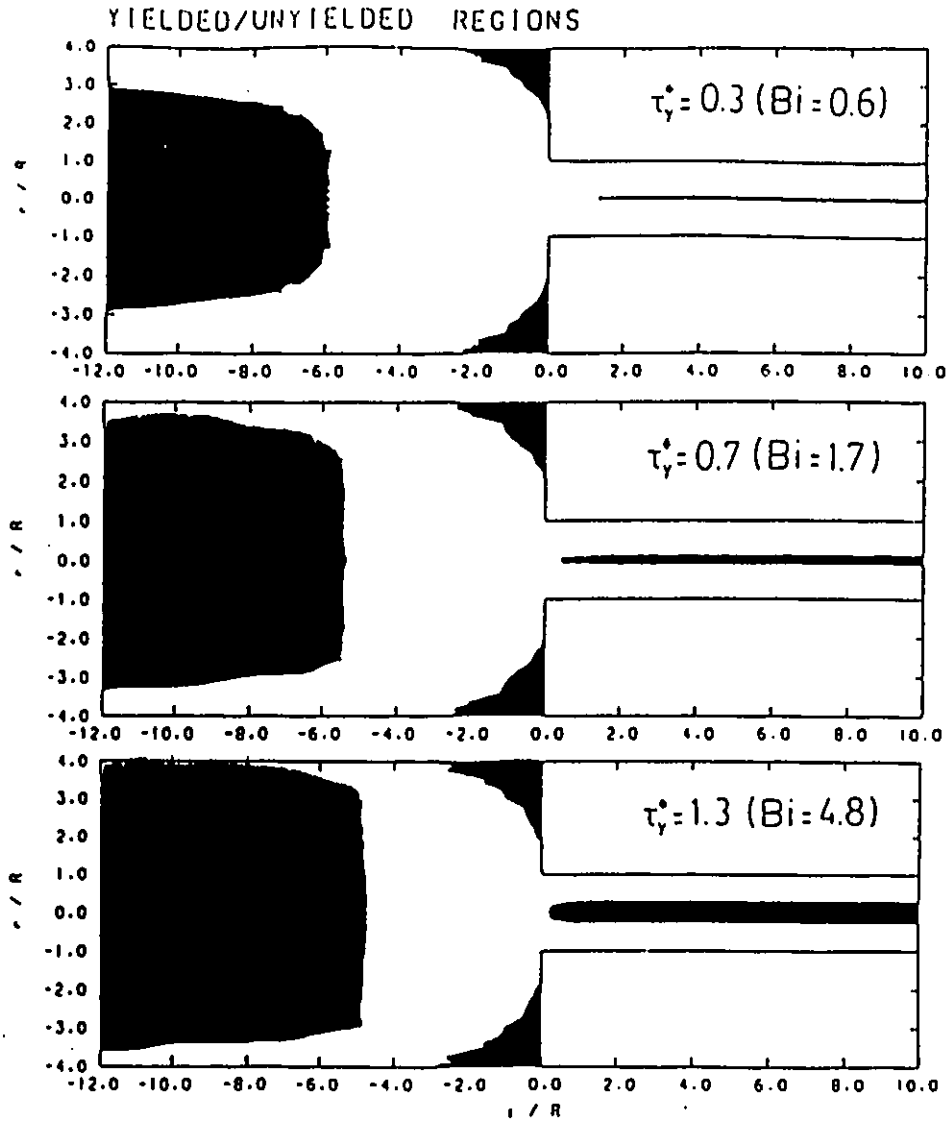

Figure 3.15: Progressive growth of the unyielded zone (shaded) for entry flow of Bingham fluids in a 4:1 abrupt contraction (axisymmetric case).

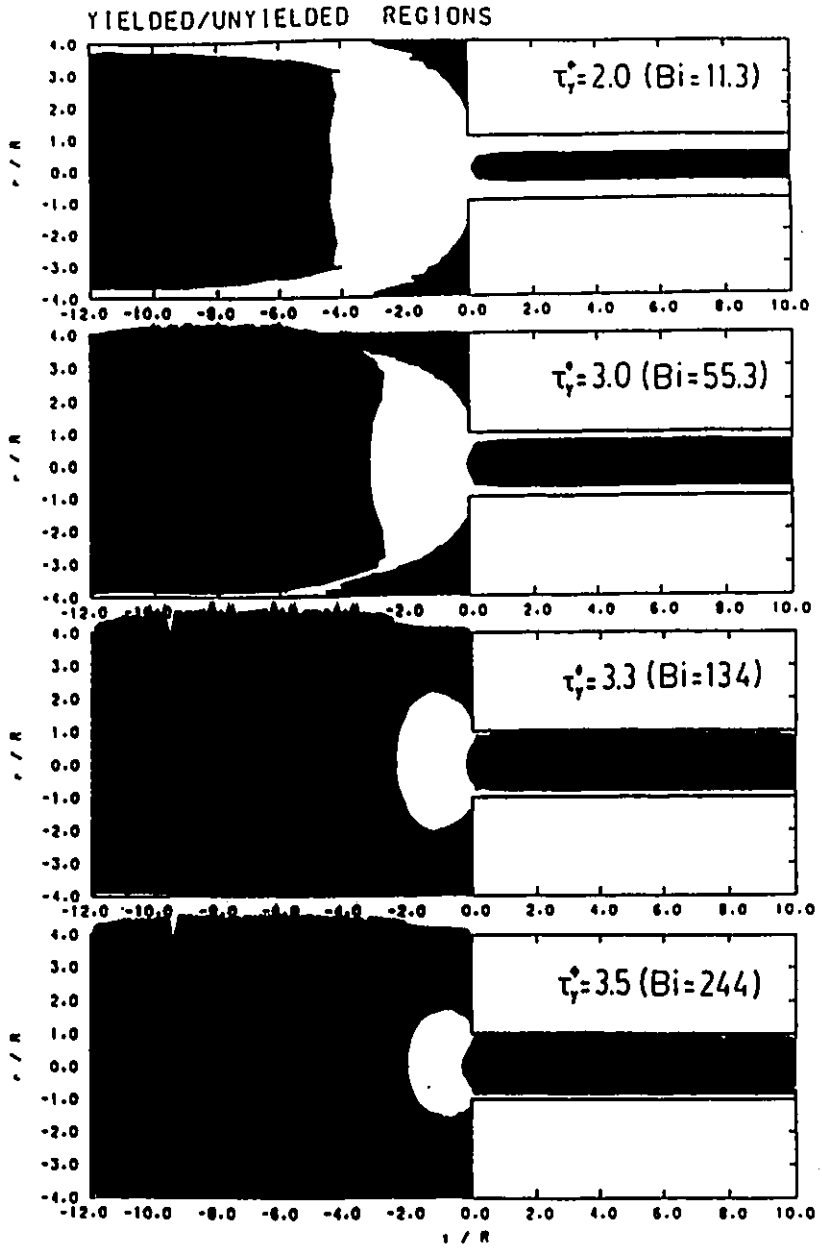

Figure 3.15 (Cont'd)

entrance. Finally for very high Bi values only the high gradient areas near the entrance corners remain yielded. In a physical situation and for a given Bingham material, we expect the process to be reversed from the one shown, i.e. at very low extrusion rates (or shear rates) the material will be mostly unyielded; as the throughput increases and the shear rates get higher, the material behaves more like a fluid having reduced solid regions until finally it flows as a Newtonian fluid ($\tau_y^* = Bi = 0$).

With regard to the well-known small Newtonian vortex in the reservoir, it was found that this space always remains about the same size and becomes an unyielded region even for small Bi numbers.

The overall pressure drop ΔP in the system obtained from each run can be used to evaluate the entrance correction n_{en} as defined in Equation (3.8).

The results for the two geometries are shown in Figure 3.16 as a function of τ_y^* and in Figure 3.17 as a function of Bi. Note the virtually linear relationship with τ_y^* and sigmoidal behaviour with Bi. The linear relationship follows the equations:

$$(planar) \qquad n_{en} = 0.552\tau_y^* + 0.381 \qquad (3.16a)$$

$$(axisymmetric) \qquad n_{en} = 0.562\tau_y^* + 0.579 \qquad (3.16b)$$

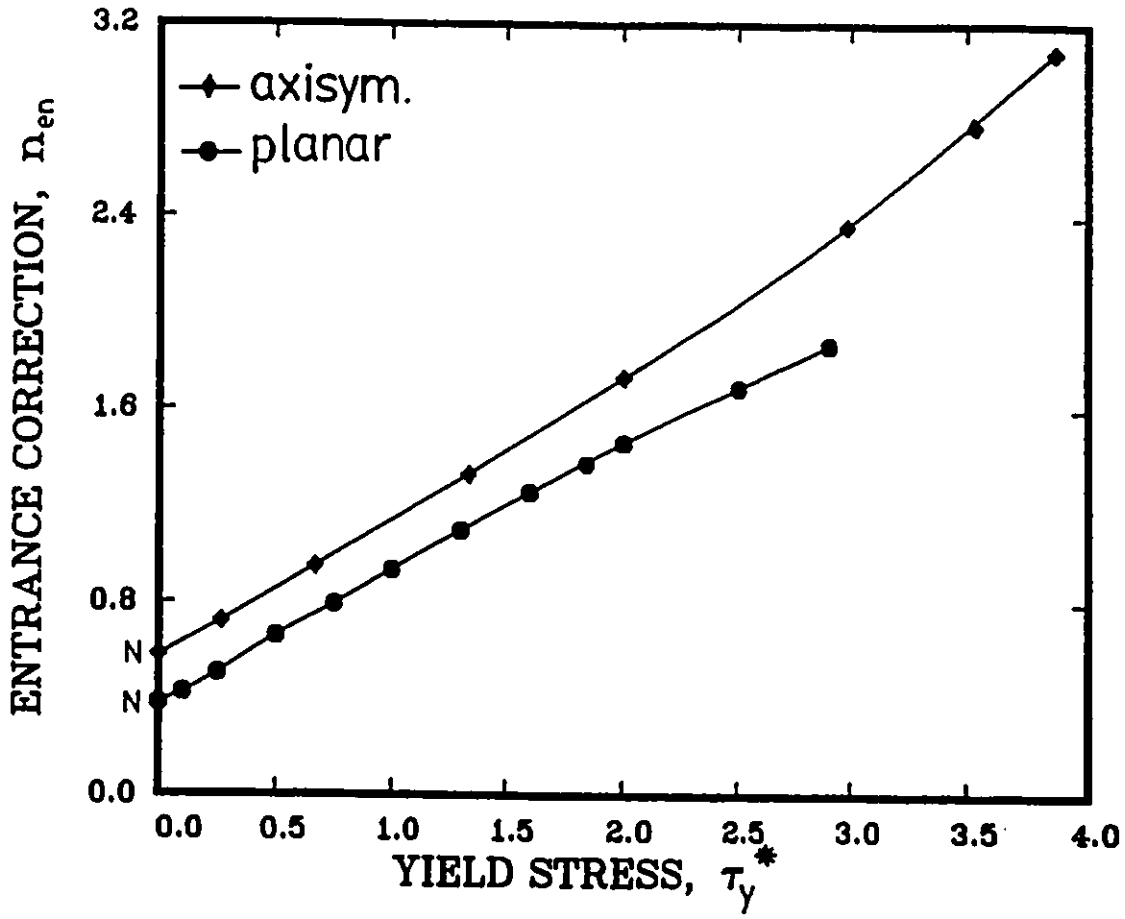

Figure 3.16: Entrance correction vs. dimensionless yield stress τ_y^* for Bingham fluids flowing in a 4:1 abrupt contraction.

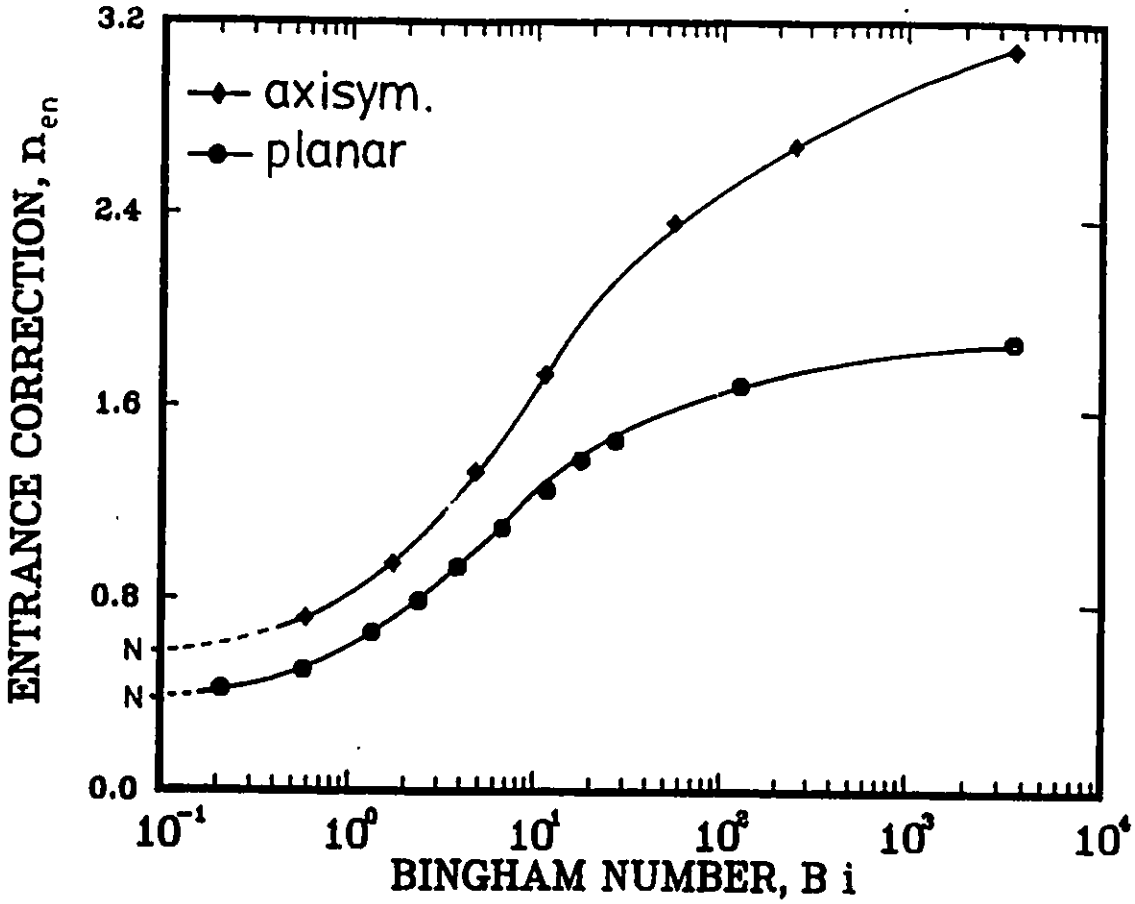

Figure 3.17: Entrance correction vs. Bi for Bingham fluids flowing in 4:1 abrupt contraction.

These results indicate that increasing the yield stress increases substantially the excess pressure losses and thus the entrance correction. Similar results have been found for power-law fluids for decreasing power-law index (Boger et al., 1978, Mitsoulis et al., 1984a). The numerical values of all results are given in Appendix B in form of tables.

3.3 Concluding Remarks

This chapter has presented a finite element analysis of Bingham viscoplastic materials for fully developed pressure-driven (Poiseuille) flow between parallel plates and in tubes and for entry flow in 4:1 abrupt planar and axisymmetric contractions. The constitutive equation used incorporated Papanastasiou's modification to the Bingham model, which is valid for both yielded and unyielded zones. The present analysis accurately captures the extent and shape of yielded/unyielded regions and for the first time it shows the progressive growth of solid regions in die entry flows from total fluid (Newtonian case) to total solid, as the dimensionless Bingham number increases approaching infinity. New results also include the determination of the excess pressure losses over and above the Newtonian values (entrance correction), necessary to push Bingham plastics through the contraction. It has been found that these losses are appreciable, reaching up to 5 times higher

values than their Newtonian counterparts for the case of high Bi values.

Chapter 4

Exit Flow and Extrudate Swell

This chapter presents a finite element study of exit flows from slit and capillary dies. A full two-dimensional analysis of the flow field is carried out for viscoplastic materials modelled as Bingham plastics according to Papanastasiou model, and the degree of the extrudate swell (or contraction in this case) is determined and compared with previous results available in the literature. A thorough parametric study is undertaken for the whole range of a dimensionless yield stress or Bingham number. The extent and shape of yielded/unyielded regions are determined based on the criterion that the material flows when the magnitude of the stress tensor exceeds the yield stress. The results for pressure are used to determine the excess pressure losses that give rise to the exit correction. The combined effects of entrance and exit losses are used to determine the end (or Bagley) correction for viscoplastic

material flow through extrusion dies.

4.1 Introduction

It is well-known that die exit flow of polymeric liquids is accompanied by a considerable increase in the cross-sectional area of the emerging jet. This phenomenon is usually called **extrudate swell (die swell)**. It occurs for both Newtonian and non-Newtonian fluids but it is much more important for highly elastic fluids such as solutions or melts of commercial polymers (Vlachopoulos, 1981). The swelling ratio of extrudate diameter (width) to die diameter (width) may range from 1 to 4 (see Figure 4.1).

Newtonian round jets swell at low Reynolds numbers with the maximum value being about 13%. This is due to streamline adjustments as the fluid emerges from an orifice into the atmosphere and acquires a free surface. Using a finite element program, Tanner (1973) solved the conservation of mass and momentum equations for slow flow and constructed the streamline of the free jet through an iterative procedure. Thus, he was able to predict a swelling of 13% for capillary dies, which agrees with earlier experimental observations (Middleman and Gavis, 1961). For large values of Re it is easy to show by performing an overall mass and momentum balance that the emerging jet exhibits a 13% diameter contraction. Thus, for Newtonian round jets the

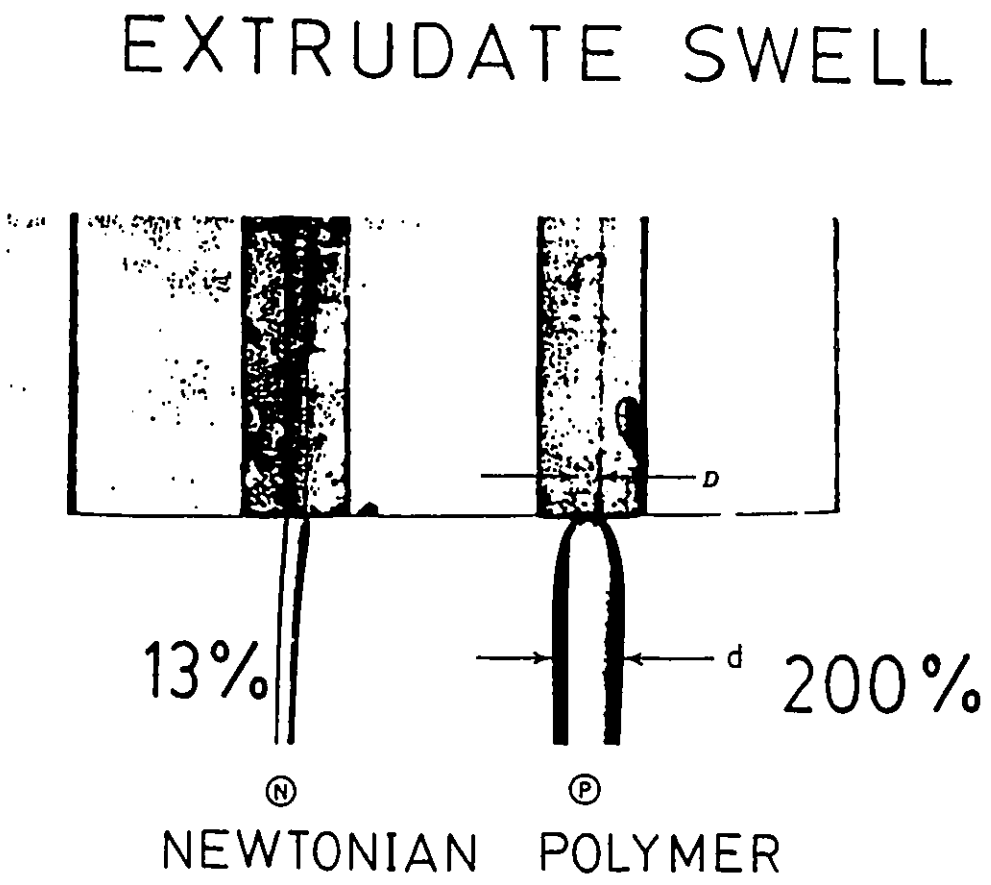

Figure 4.1: Extrudate swell of a Newtonian fluid N and a polymer solution P emerging from a capillary tube (from Bird at al., 1977).

swelling ratio varies from 1.13 to 0.87.

The swelling from planar slit dies and for slow flows (low Re) was found to be about 19% (FEM, Reddy and Tanner, 1978, Coleman, 1980, Coleman, 1981, Crochet and Keunings, 1982a, Mitsoulis, 1986a). For large values of Re it is easy to show a 17% contraction of the emerging plane sheet. Thus for Newtonian planar sheets the extrudate swell varies from 1.19 to 0.83.

With the single exception of a finite-difference solution (Ryan and Dutta, 1981), all numerical work has been done using the finite element method. This is due to the flexibility of the finite element grid to take the shape of the extrudate. The unknown *a priori* free surface of the extrudate and the presence of a stress singularity at the point where the fluid leaves the solid wall make the solution process a delicate but attainable task.

In the extrusion of non-Newtonian viscoplastic fluids a reduction of extrudate swell has been found as the Bingham number increases from the Newtonian values of 19% for planar and 13% for axisymmetric dies to 0% as expected for extrusion of solids (Papanastasiou, 1987, Tanner and Milthorpe, 1983, Ellwood et al., 1990).

Another characteristic of the solution in exit flows is the determination of the exit correction n_{ex}, which is defined as the pressure drop in excess to that found for a fully-developed Poiseuille flow in the die without considering

the extrudate,

$$n_{ex} = \frac{\Delta P - \Delta P_o}{2\tau_w} \tag{4.1}$$

where τ_w is the shear stress at the wall for fully-developed flow in the die, ΔP_o is the corresponding pressure drop, and ΔP is the overall pressure drop in the system. While the values for Newtonian fluids have been long established (Boger et al., 1978), no results have appeared in the literature for the exit correction of Bingham plastics.

4.2 Exit Flow of Newtonian Fluids

The physical system for the analysis of the exit flow problem is illustrated in Figure 4.2 and is representative of flow from a slit die into the atmosphere. A stress singularity appears at the exit point S where the fluid leaves the die wall because of a change in the velocity from zero at the wall to a finite value at the free surface. The boundary conditions include a fully-developed Poiseuille velocity profile at the upstream plane, no-slip conditions at the wall, and $v_y = 0$ at the plane of symmetry and the downstream plane. The pressure is also specified at zero at one point (here at the center-line of the downstream plane). Because of the symmetry involved only half the domain need be considered.

The size and the dimensions of the system were chosen to represent a

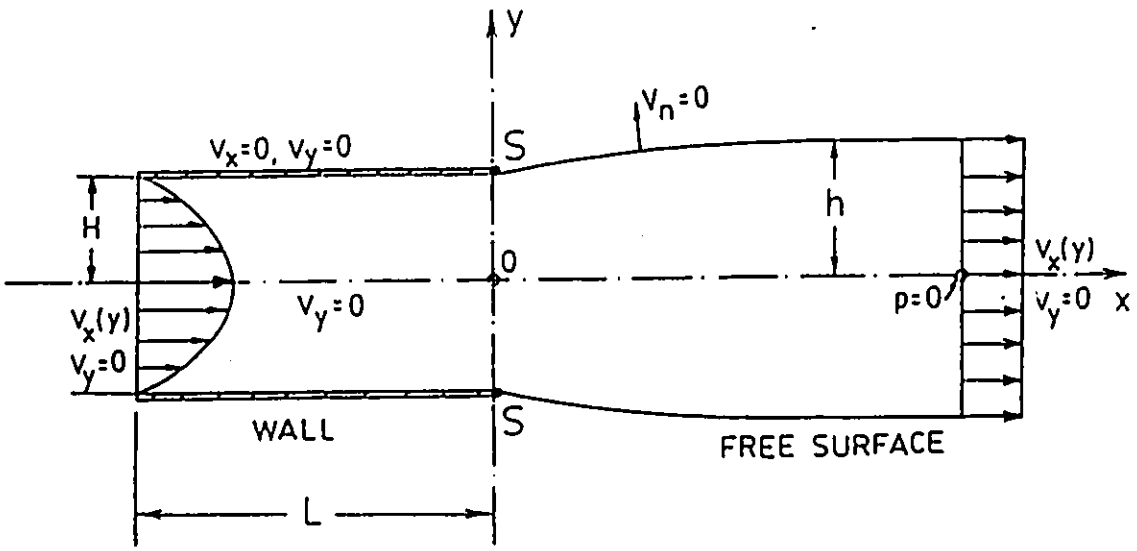

Figure 4.2: Exit flow from a slit die accompanied by extrudate swell along with the boundary conditions.

typical die in accordance with the size and the dimensions of the dies considered in the analysis of entry flows (see Figure 3.11). The length was chosen such that the assumption of a fully-developed Poiseuille flow at the upstream plane is justified. Note that the die of Figure 3.11 has a $L/R = 10:1$. Here we have considered a $8:1$ ratio, assuming that the flow has fully developed within a length of $4R$ after entrance to the die. This assumption is generally true for inelastic and viscoplastic materials. The extrudate length was taken to be $8R$.

Calculations were performed with two grids, GRID1 having 276 elements, 611 nodes and 1274 unknown d.o.f. (13 nodes across and 47 nodes along, Mitsoulis, 1986a) and another denser GRID2 having 460 elements, 987 nodes and 2106 d.o.f. (21 nodes across and 47 nodes along). The Newtonian problem requires about 5 CPU secs/iteration with GRID1 and 15 CPU secs/iteration with GRID2 in the University of Ottawa's AMDAHL-5850 mainframe computer. Four iterations are sufficient for the Newtonian fluid solution, i.e. requiring about 20 CPU secs with GRID1 and 60 CPU secs with GRID2 for the final solution. Figure 4.3 presents in dimensionless coordinates the two grids used in the computations. Each quadrilateral is further subdivided into 2 triangles for the velocity-pressure formulation and 4 quadrilaterals for the stream function/temperature formulation. Many elements are concentrated near the exit where a stress singularity exists. It should be noted that such

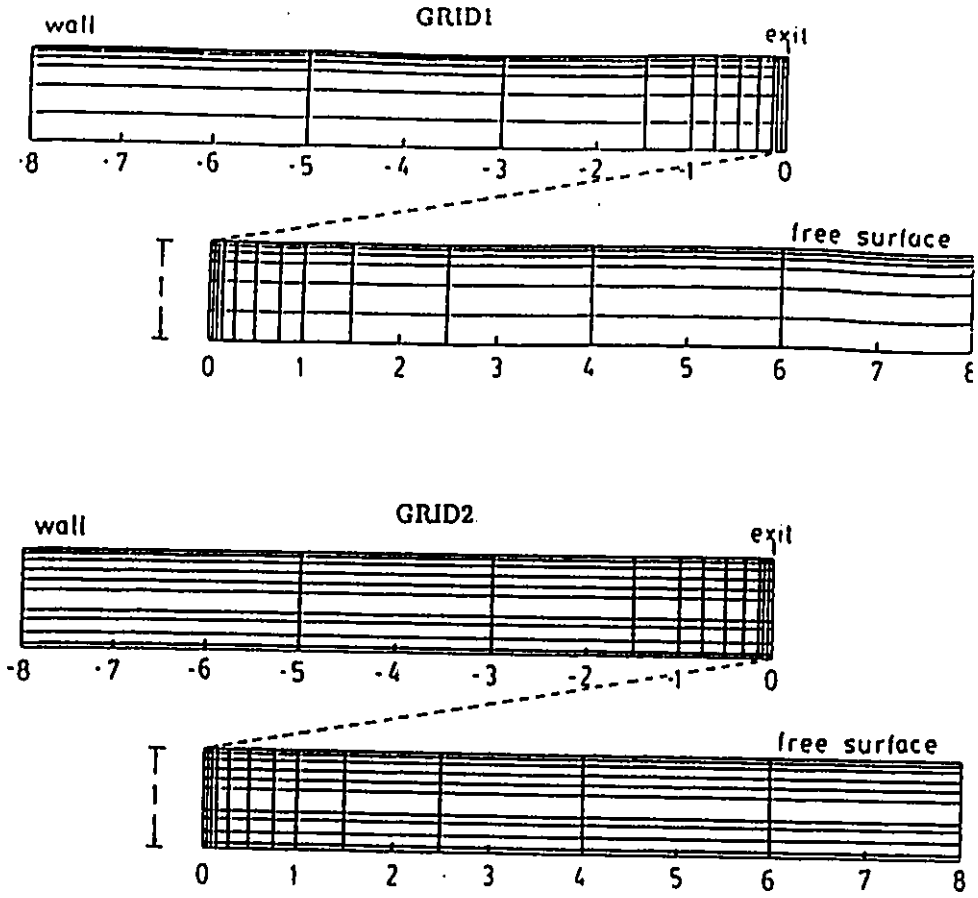

Figure 4.3: Finite element grids used for the exit flow problem and the determination of extrudate swell. Each quadrilateral element is further subdivided into 2 triangular elements for the u-v-p formulation.

refined grids must be used in order to better approximate the steep stress and pressure changes near the exit. As in the case of entry flow, it was found that although the flow field was rather robust to grid changes, the pressure drop, and hence the exit correction, were very sensitive to the number of elements near the exit plane (Mitsoulis, 1986a). A parametric study revealed that placing enough elements around the singularity as shown in Figure 4.3 made the results presented here virtually free from mesh influence.

The stream function formulation was also employed in order to visualize the flow field via streamlines. The Poisson equation:

$$\nabla^2 \psi = -\omega \tag{4.2}$$

was solved *a posteriori* for the stream function ψ by making use of the known vorticity ω at the nodes. The free surface of the extrudate was determined iteratively by constructing a streamline using the most recently computed velocity field as proposed by Nickell et al. (1974) and explained in section 2.7. The final swelling ratios of 19.2% for planar dies and 13.0% for capillary dies have also been found by Mitsoulis et al. (1984b), Coleman (1981) and Crochet and Keunings (1982b).

Figure 4.4 shows the final (deformed) finite element grid (GRID2) along with the flow field as visualized through velocity vectors, streamlines and isobars for the case of planar (slit) dies. The corresponding results for axisymmetric geometries (capillary dies) are shown in Figure 4.5. The velocity

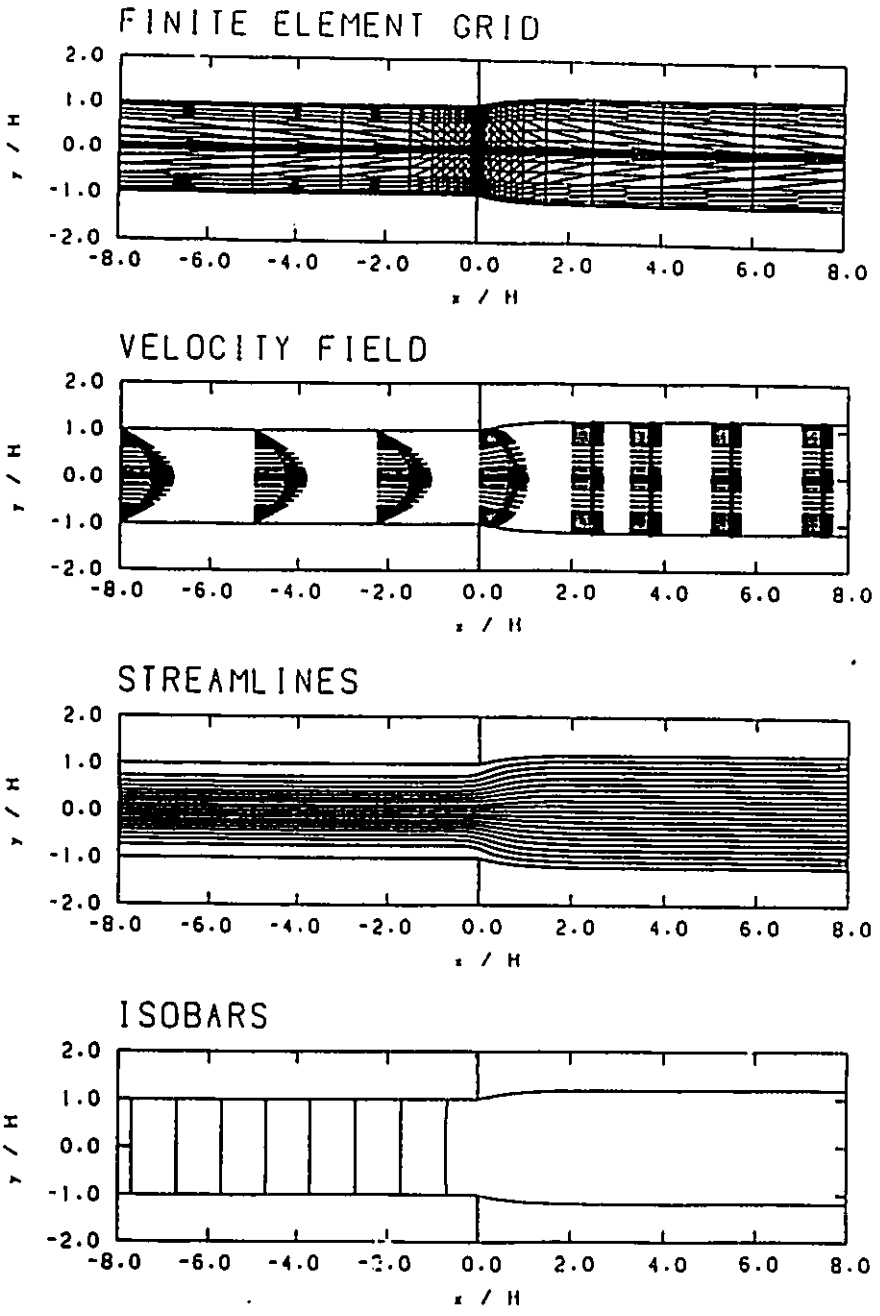

Figure 4.4: Results from the solution of a Newtonian fluid extruded through a slit die.

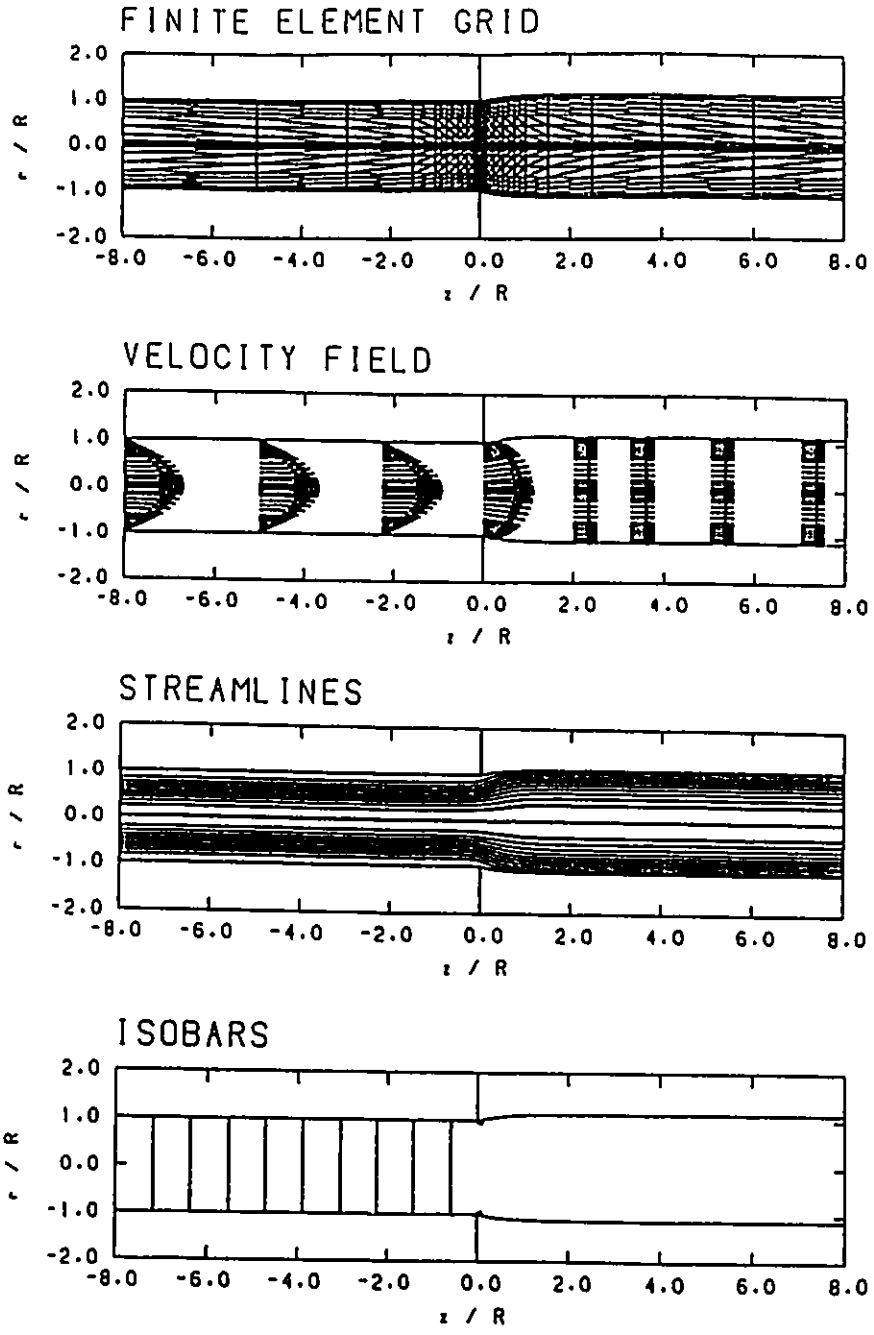

Figure 4.5: Results from the solution of a Newtonian fluid extruded through a capillary die.

field reveals that the Newtonian fluid retains its fully developed Poiseuille profile almost up to the die exit and then it rearranges and assumes a plug-flow flat profile within a length approximately equal to the die gap width of $2H$ (or equivalently die diameter D). Therefore, Newtonian fluids fully develop within very short distances.

The streamline pattern (obtained by normalizing the stream function to take the value of 0.0 at the wall/free surface and 1.0 at the center-line with increments of 0.1 in-between) shows the smooth rearrangement from the constrained Poiseuille flow within the die to the free flow of the extrudate outside the die. These results as presented in Figures 4.4 and 4.5 are also in excellent agreement with the results of Mitsoulis (1986a) and Crochet and Keunings (1980).

The center-line pressure at the die exit has definitely a non-zero value, although it is often assumed in theoretical analyses that the Poiseuille pressure gradients so extrapolate to zero pressure at $x = 0$. In fact, the value of the exit pressure ΔP_{ex} gives rise to the exit correction n_{ex} which can be expressed as :

$$n_{ex} = \frac{\Delta P_{ex}}{2\tau_w} = \frac{\Delta P - \Delta P_{sl}}{2\tau_w} \tag{4.3}$$

where ΔP is the overall pressure drop between the pressure at the inlet and the ambient pressure and ΔP_{sl} is the Poiseuille pressure drop in the slit without considering the extrudate. The Newtonian value of the exit correc-

tion was found to be 0.153 for planar dies and 0.248 for capillary dies, fully in agreement with Mitsoulis (1986a) and Reddy and Tanner (1978).

4.3 Exit Flow of Bingham Fluids

The numerical simulations were performed for Bingham fluids for both planar and axisymmetric geometries (slit and capillary dies, respectively). Previous results for this case have appeared in the literature (Papanastasiou, 1987, Ellwood et al., 1990) and a comparison is thus possible, especially for extrudate swell calculations. Our results extend further to calculations of excess pressure losses and a more accurate depiction of yielded/unyielded regions.

Calculations were carried out for modified Bingham fluids with the intention to determine the yielded/unyielded regions, extrudate swelling and exit correction. Runs were performed with the Papanastasiou model with $m = 200$ and different τ_y values. Following Papanastasiou (1987), we have pursued the calculations for $0 \leq \tau_y^* < \Delta P^*$ (or respectively, $0 \leq Bi < \infty$), where the dimensionless pressure gradient ΔP^* is equal to 3 for planar and 4 for axisymmetric geometries in the upstream channel. A comparison with Figure 3 of Ellwood et al. (1990) for the free surface profile in planar flow is given in Figure 4.6 for $\tau_y^* = 0.1$ ($Bi = 0.21$). The agreement between the two works is very good.

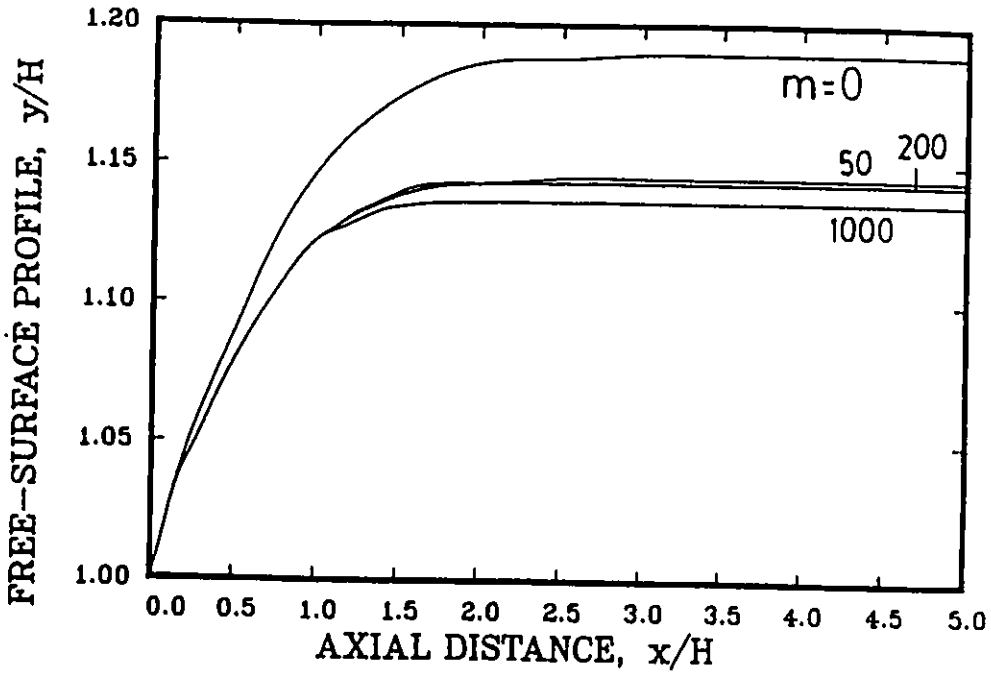

Figure 4.6: Free surface profile of a Bingham fluid extruded from a slit die ($\tau_y^* = 0.1, Bi = 0.21$). Comparison between results of Ellwood et al. (1990) ($m = 0, 50, 1000$) and this work ($m = 200$).

The extrudate swell (or contraction in this case) as a function of τ_y^* is given in Figure 4.7 and as a function of Bi in Figure 4.8 for both geometries (slits and capillaries). It is seen that increasing the yield stress reduces the Newtonian value of swelling from the well-established values of 19% for planar and 13% for axisymmetric dies (Mitsoulis et al., 1984b) to 0% as expected for extrusion of solids (plug-flow profile throughout the flow field, hence no rearrangement near the exit from parabolic to plug-like profile). The results of Papanastasiou (1987) for planar geometries are also shown in Figure 4.7. It is interesting to note that our results reveal a slight contraction below 1 for a certain range of yield stress and an asymptotic approach towards 1 at the end of the τ_y^* range. This contraction reaches about 5% for planar and 2% for axisymmetric dies. Extensive numerical experiments (different grids, lower tolerance for the norm-of-the-error, increase of m-parameter in the constitutive equation from 200 to 1000) showed that these contractions were always present.

The minimum in the swelling as the Bi number increases may be at first sight quite puzzling since one would expect a monotonic decrease to no swelling. To explain the appearance of the minimum it is instructive to consider the two regions, a plug flow region (unyielded) occupying the core and the surrounding fluid regions (yielded) between the core and the wall. This is equivalent to having two fluids with different viscosities, a very

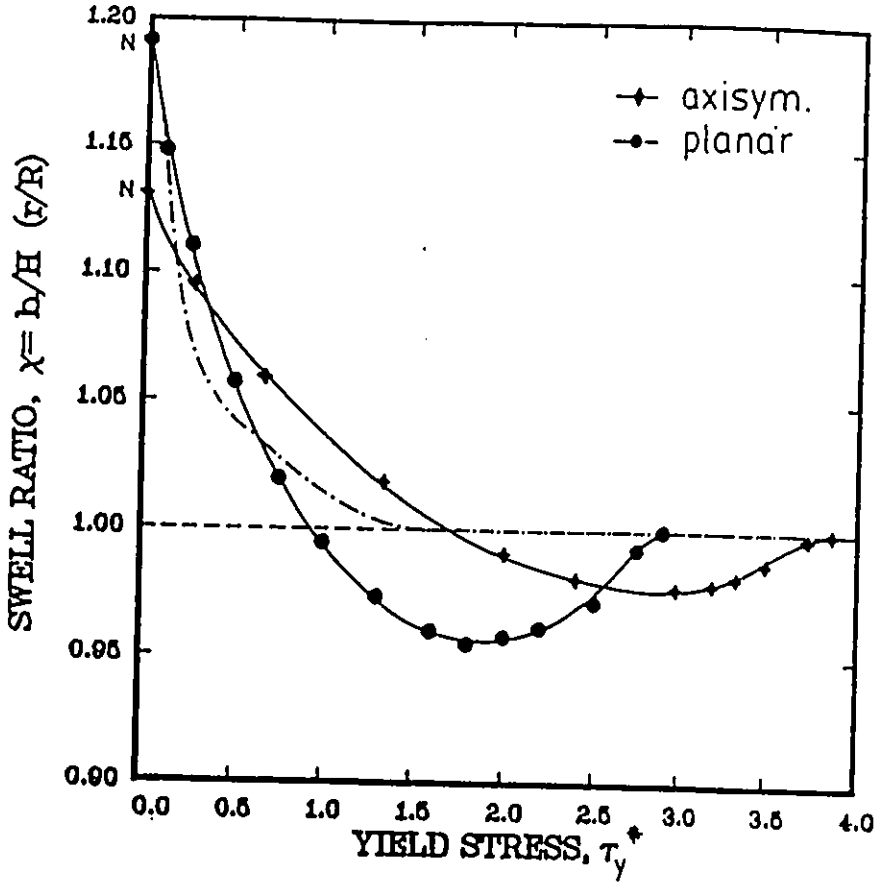

Figure 4.7: Extrudate swell vs. dimensionless yield stress τ_y^* for Bingham fluids extruded through planar and circular dies (N corresponds to Newtonian result for τ_y^*=0). The dotted line corresponds to planar results of Papanastasiou (1987).

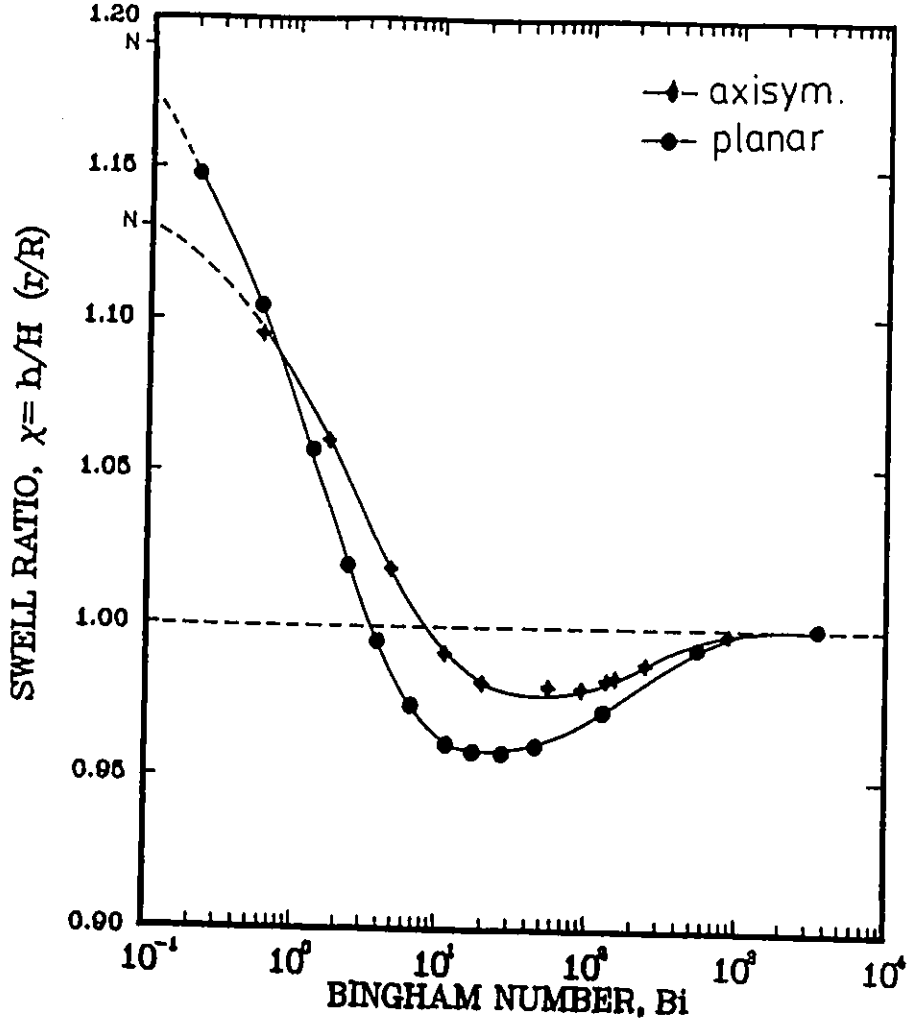

Figure 4.8: Extrudate swell vs. Bi for Bingham fluids extruded through planar and circular dies (N corresponds to Newtonian result for Bi =0).

high-viscosity core and a low-viscosity outer layer. As shown by Tanner (1980) in his inelastic theory of extrudate swell and by Mitsoulis (1986b) in extrudate swell studies for double-layer flows, a less viscous outer layer results in a reduced swelling that can go below 1, depending on the viscosity ratio but *also* on the feed ratio (relative height of the core with respect to the cross-section of the die). It has been established by Mitsoulis (1986b) that outer layers near the wall shrink rather than swell. When the core occupies progressively more of the cross-section of the die (say 50% *or* 70% *or* 90%), it has been shown that for the same viscosity ratio there is *less* reduction in the swelling (Mitsoulis, 1986b). In the present case, as Bi is increased and the plug flow core occupies more of the flow domain, as this plug emerges the surrounding thin layers of fluid shrink and are simply accelerated to the (higher) velocity of the core, giving a swell ratio less than unity. Thus, as Bi is increased, the swell ratio *always* approaches unity from below.

This behaviour is in agreement with statements presented by Beverly and Tanner (1989), who argue that at high yield stress values (or correspondingly very low shear rates) *"the only feasible kinematic pattern is that the unyielded core continues straight through near the axis and all velocity rearrangements take place near the die wall. In this case, it is clear that no swelling can take place and, from mass conservation, a slight reduction in diameter must result"*. However, their insufficiently dense grid could not capture this phe-

nomenon. Our highly dense grids capture these changes very well as will be shown in what follows.

The corresponding progressive growth of solid (unyielded) regions in the flow field is shown in Figure 4.9 (planar case) and Figure 4.10 (axisymmetric case) for increasing values of τ_y^* or Bi. The shaded areas correspond to unyielded regions (solid). The fully-developed conditions at entry give rise to horizontal lines for the envelope of the solid region.

The case of $\tau_y^* = 1.6$, $\Delta P^* = 3$, has also been shown by Papanastasiou (1987) in his Figure 12a and is reproduced here in Figure 4.11 together with our results. A point to be noticed is the difference in the yielded/unyielded regions with his previous results. There, the unyielded (shaded) region extended all the way along the centerline from entry to exit. As was pointed out by Beverly and Tanner (1989), at low τ_y^* values where the fully-developed profile gives a height of unyielded/yielded regions much less than the die gap (or radius), this cannot be the case because the rearrangement near the exit will cause gradients and the material will yield. Papanastasiou's results were obtained by applying an arbitrary criterion for yielding, i.e. that the second invariant of half the rate-of-strain tensor $\bar{\bar{D}} = \frac{1}{2}\bar{\bar{\dot{\gamma}}}$ exceed the value of 0.001. This also caused the determination of an incorrect entry height for the unyielded region which is in disagreement with the analytical solution for this τ_y^* value. Here, we have used the criterion that yielding occurs when the

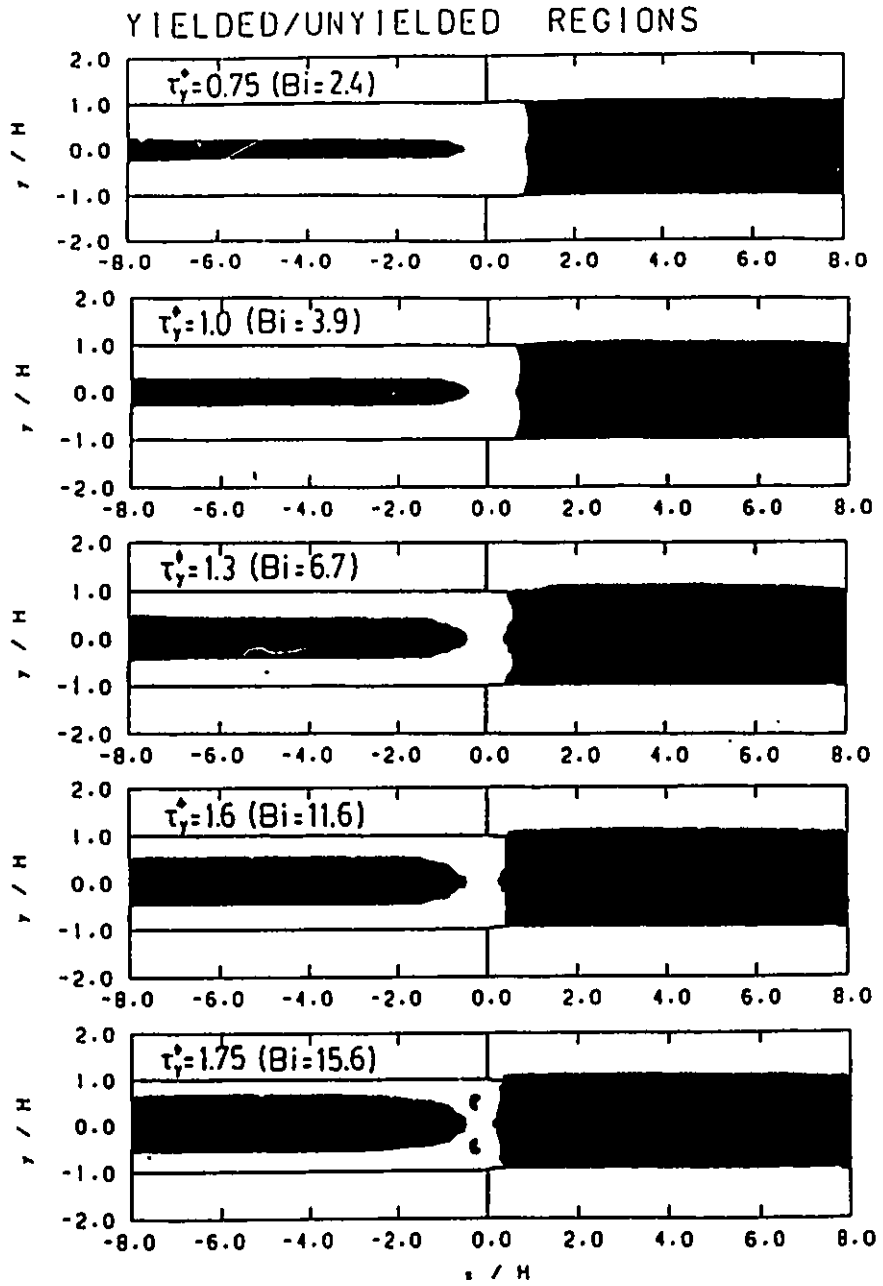

Figure 4.9: Progressive growth of the unyielded zone (shaded) in planar extrusion flow of Bingham fluids ($\Delta P^* = 3$).

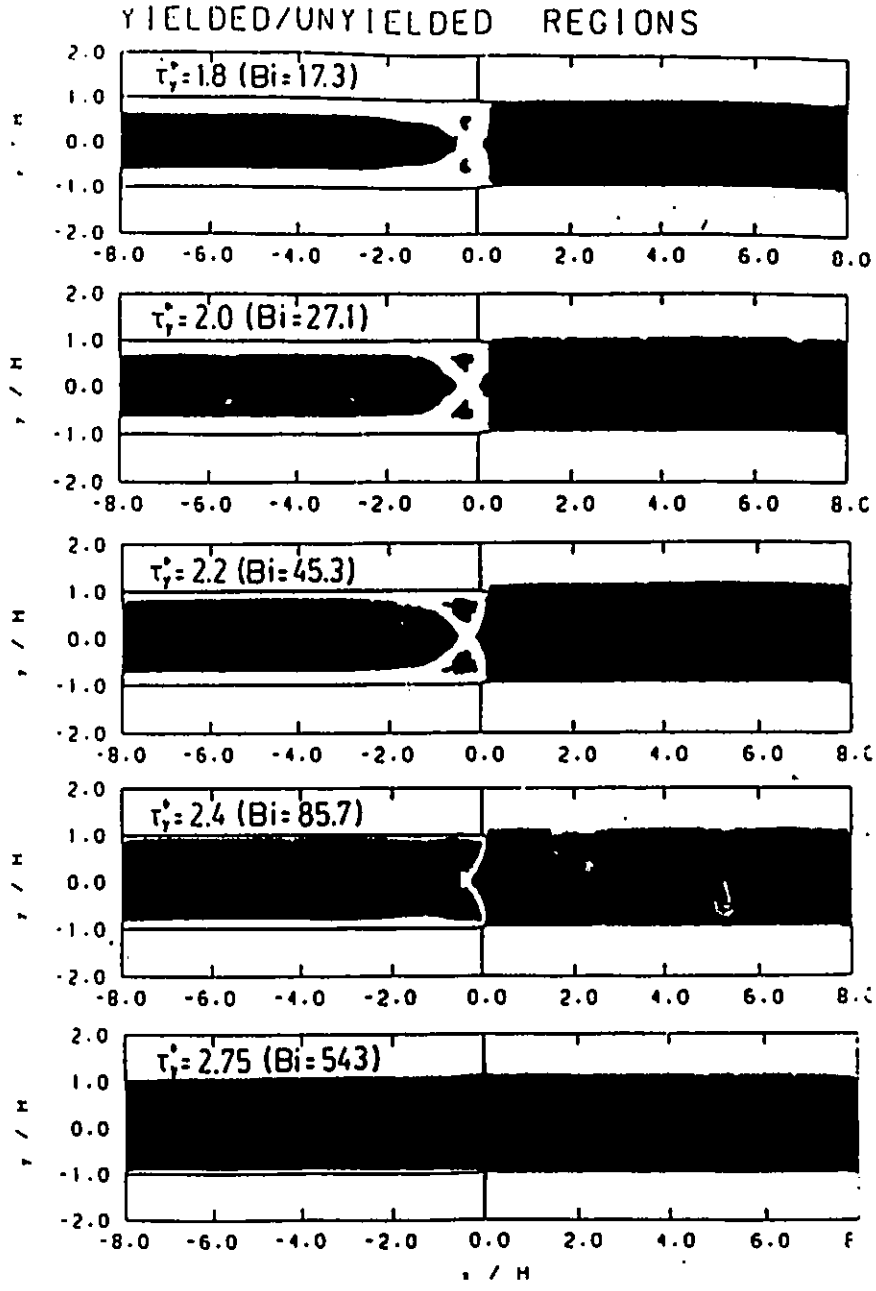

Figure 4.9 (cont'd)

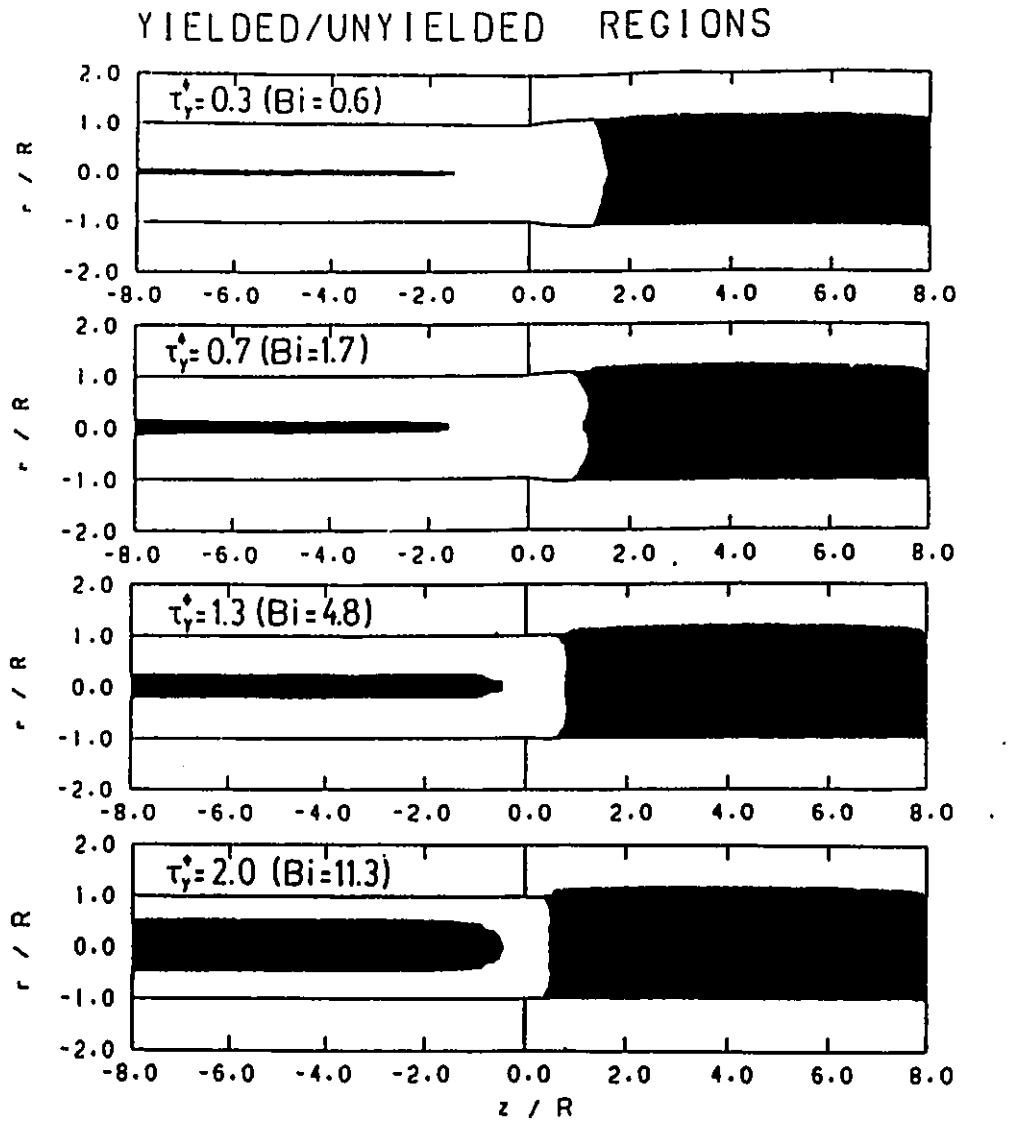

Figure 4.10: Progressive growth of the unyielded zone (shaded) in axisymmetric extrusion flow of Bingham fluids ($\Delta P^* = 4$).

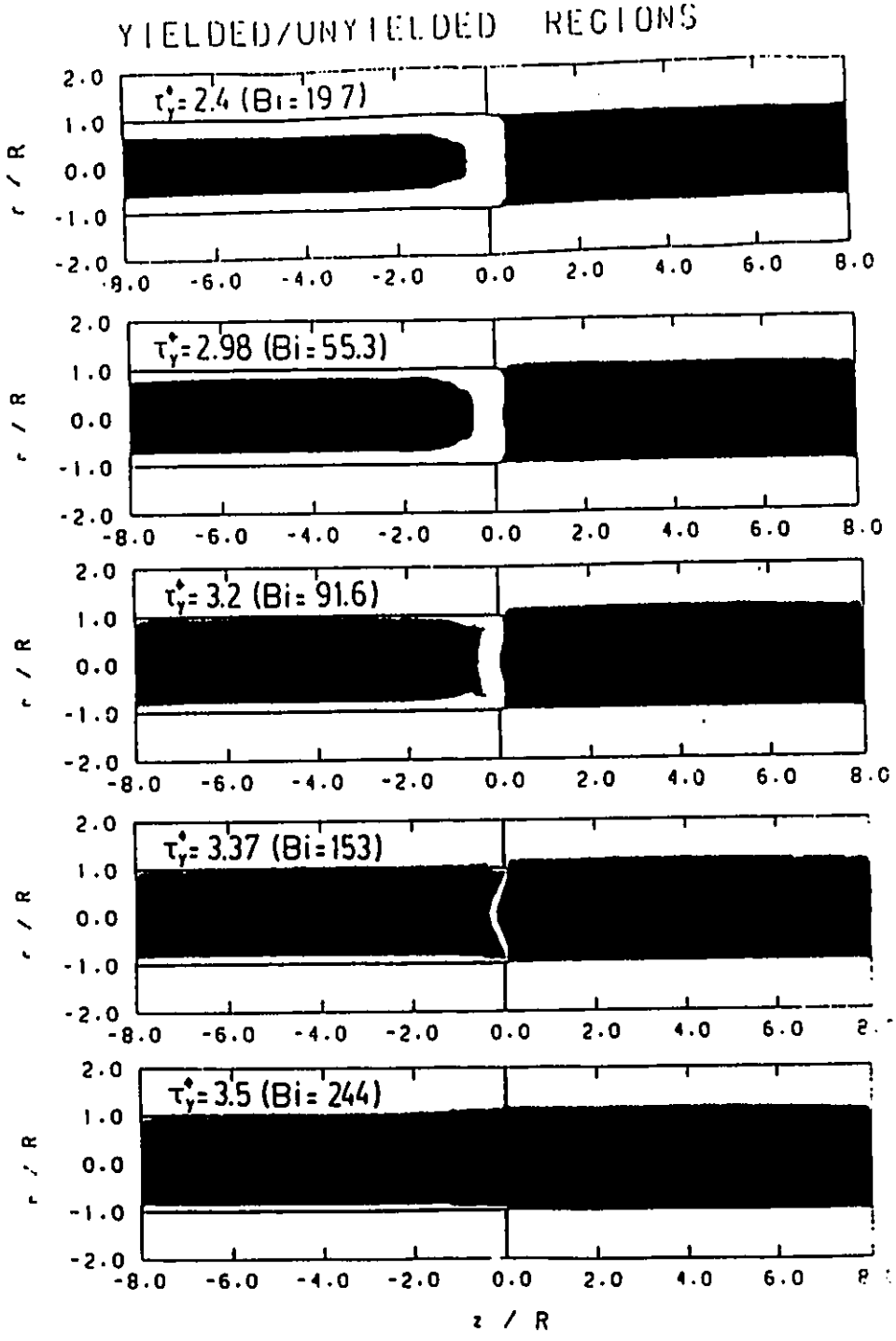

Figure 4.10 (Cont'd)

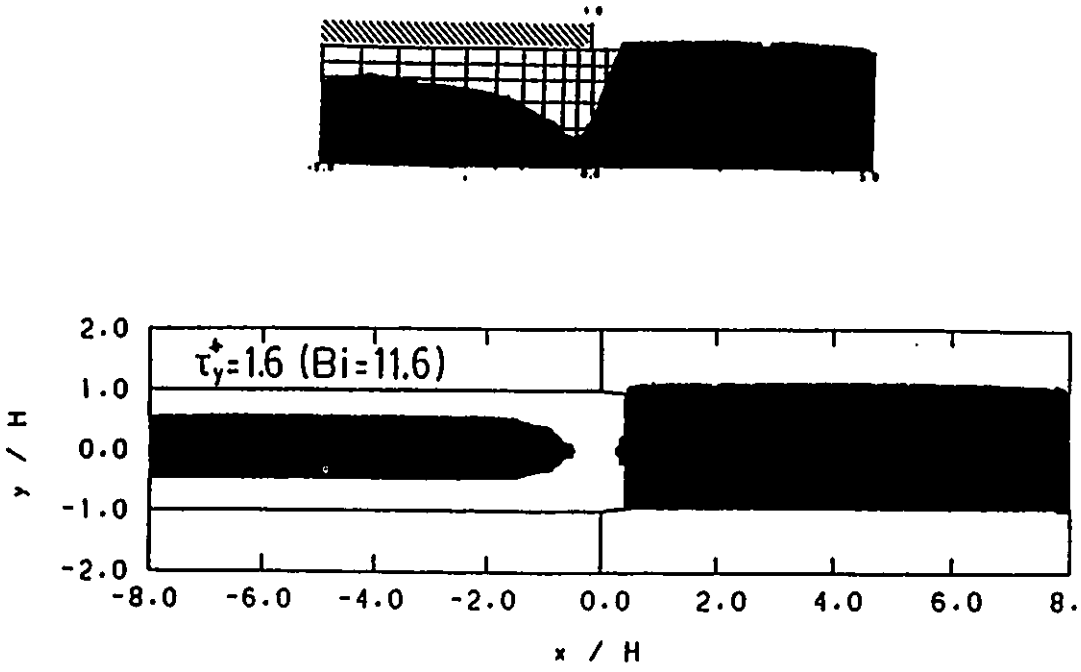

Figure 4.11: Comparison between the results of Papanastasiou (1987) (upper half) and present work (lower half) for extrusion of a Bingham plastic through a slit die at $\tau_y^* = 1.6$ ($Bi = 11.6$).

magnitude $|\tau|$ of the extra-stress tensor $\bar{\bar{\tau}}$ exceeds the value τ_y of the yield stress, a number which is not arbitrary and also not very small or close to zero. Our results are then in agreement with those of Beverly and Tanner (1989), showing that yielding occurs near and after the die exit for small τ_y^* or Bi values. The yielded region becomes smaller as τ_y^* (or Bi) increases and disappears only for high enough values of τ_y^*, where most of the material behaves as solid in the die (see Figures 4.9 and 4.10). In a physical situation and for a given Bingham material, we expect the process to be reversed from the one shown, i.e. at very low extrusion rates (or shear rates) the material will be mostly unyielded; as the throughput increases and the shear rates get higher, the material behaves more like a fluid having reduced solid regions, until finally it flows inside the die as a Newtonian fluid and only in the extrudate, where the gradients are zero, it behaves like a solid. This behaviour was shown by Beverly and Tanner (1989) for increasing shear rates $\dot{\gamma}$ in the range $1 \leq \dot{\gamma} \leq 100s^{-1}$ (or equivalently $4.4 \geq Bi \geq 0.44$) for a certain viscoplastic material.

The overall pressure drop ΔP in the system obtained from each run can be used to evaluate the exit correction n_{ex} defined by Equation (4.1). The results for the two geometries are plotted in Figure 4.12 as a function of τ_y^* and in Figure 4.13 as a function of Bi. It is interesting to see that for small values of τ_y^* or Bi, there is a slight increase of n_{ex}, but afterwards the extra

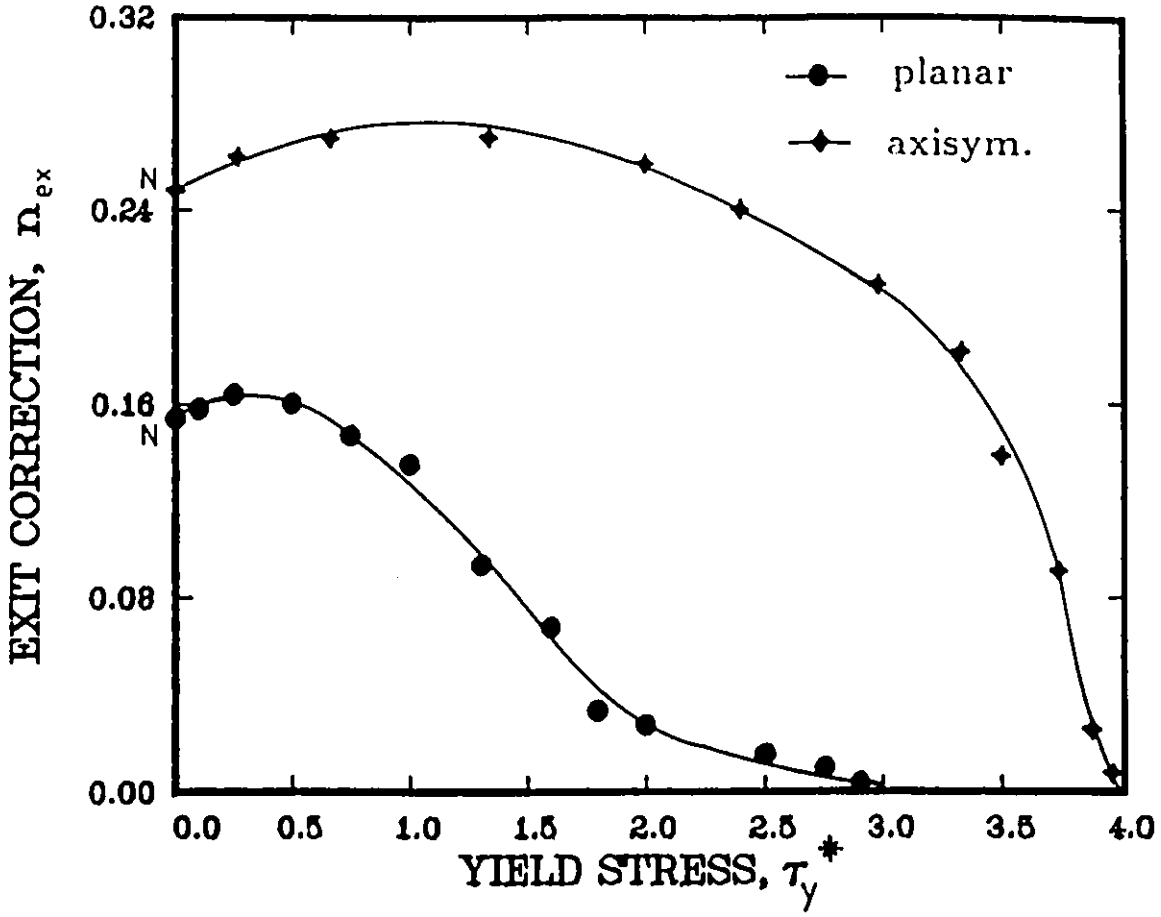

Figure 4.12: Exit correction vs. dimensionless yield stress τ_y^* for Bingham fluids extruded from capillary and slit dies (N corresponds to Newtonian result for $\tau_y^* = 0$).

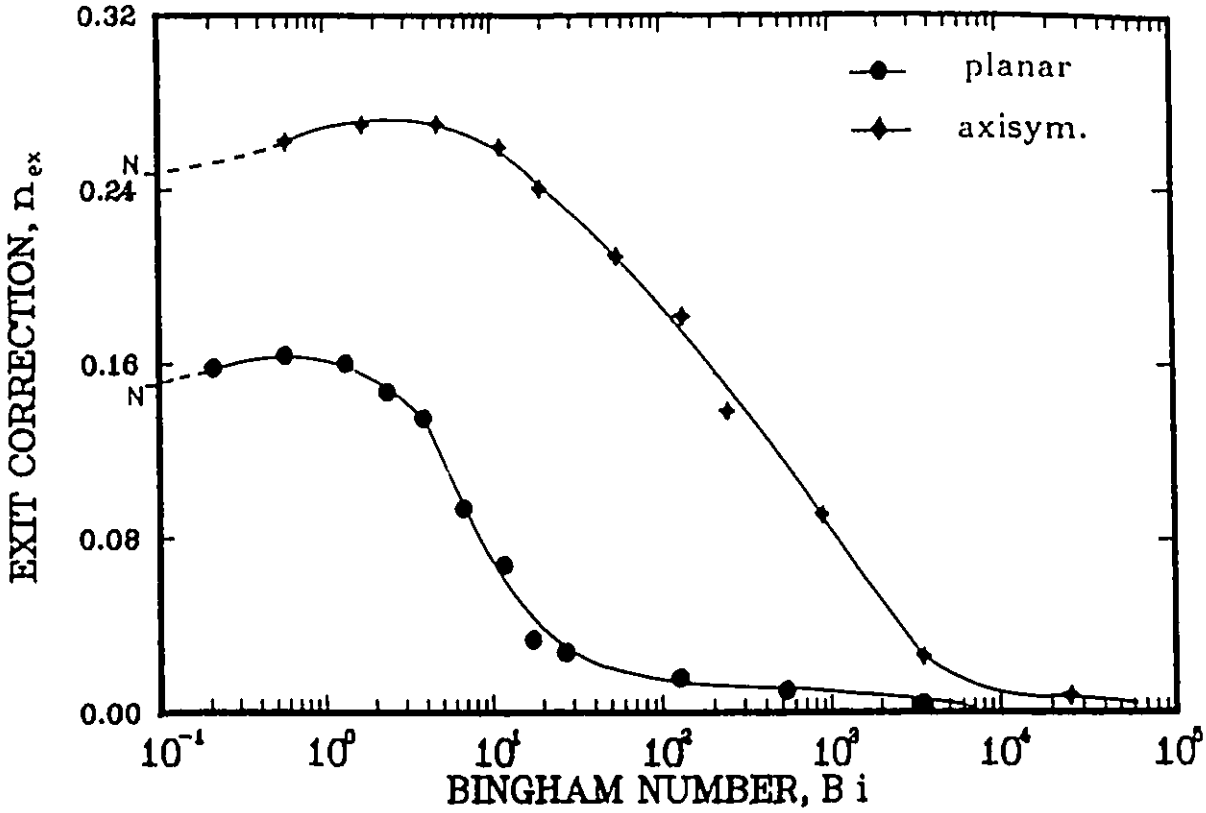

Figure 4.13: Exit correction vs. Bi for Bingham fluids extruded from capillary and slit dies (N corresponds to Newtonian result for $Bi = 0$).

pressure losses decrease to finally reach zero values as $Bi \rightarrow \infty$, as expected since a plug-like profile would generate no extra pressure losses. This is also the case for power-law fluids as the power-law index n approaches zero (Mitsoulis et al., 1984a). However, the overshoot for low values of Bi is unexpected and reminds us of the reduction of the Newtonian extrudate swell for low values of the Weissenberg number when using the Maxwell model (Tanner, 1985).

The sum of entry and exit pressure losses gives rise to the end (or Bagley) correction, as explained in Section 3.2.1 (Equations 3.10 and 3.11). The results for Bingham fluids as a function of τ_y^* are given in Figure 4.14 and as a function of Bi in Figure 4.15. Note the virtually linear relationship with τ_y^* and sigmoidal behaviour with Bi. The linear relationship follows the equations:

$$(planar) \qquad n_B = 0.476\tau_y^* + 0.535 \qquad (4.4)$$

$$(axisymmetric) \qquad n_B = 0.587\tau_y^* + 0.827 \qquad (4.5)$$

Thus, Bingham fluids exhibit an increase in the end (Bagley) correction proportional to the yield stress, which is responsible for substantially increasing the excess pressure losses in extrusion through dies. The numerical values of

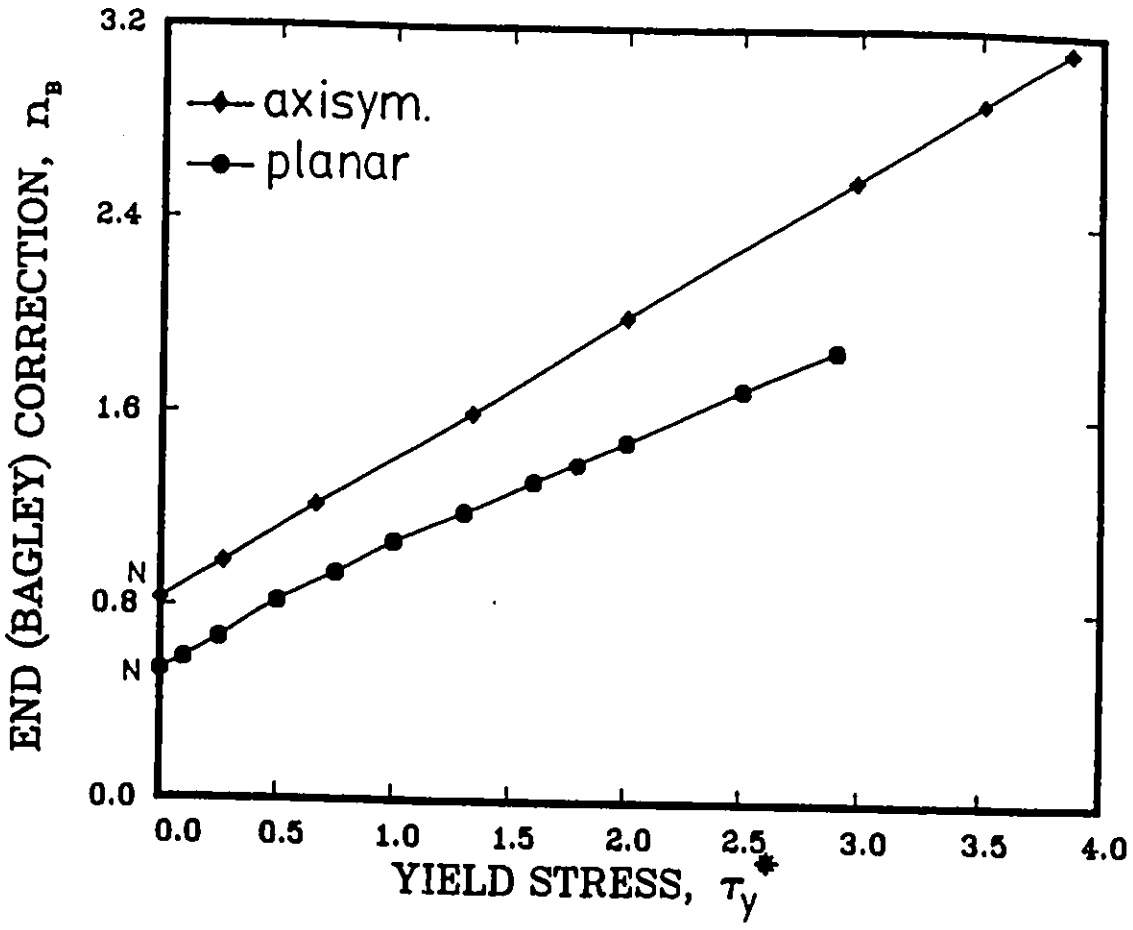

Figure 4.14: End (Bagley) correction vs. dimensionless yield stress τ_y^* in extrusion of Bingham fluids (N corresponds to Newtonian result for $\tau_y^* = 0$).

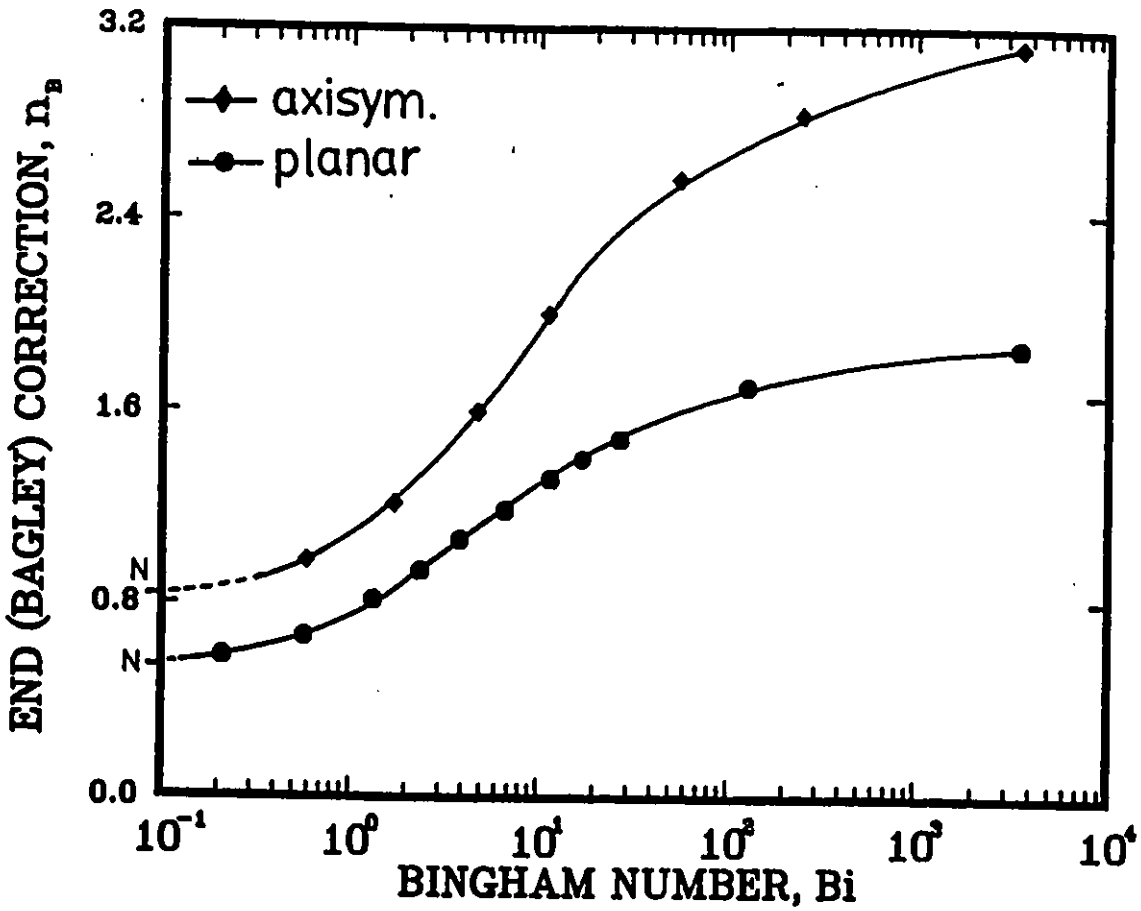

Figure 4.15: End (Bagley) correction vs. Bi in extrusion of Bingham fluids (N corresponds to Newtonian result for $Bi = 0$).

all results are given in Appendix B in form of tables.

4.4 Concluding Remarks

This chapter has presented a finite element analysis of Bingham viscoplastic materials flowing through slit and capillary extrusion dies. The constitutive equation used incorporated Papanastasiou's modification to the Bingham model, which is valid for both yielded and unyielded zones. The present analysis accurately captures the extent and shape of yielded/unyielded regions and for the first time it shows the progressive growth of solid regions in die exit flows from total fluid (Newtonian case) to total solid, as the dimensionless Bingham number increases approaching infinity. New contributions include:

(a) accurate determination of extrudate swell, which shows a contraction below 1 for a certain range of Bi numbers and has been totally missed by previous researchers;

(b) accurate determination of yielded/unyielded regions and discovery of errors by a previous investigation (Papanastasiou, 1987);

(c) determination of excess pressure losses over and above the Newtonian values (exit correction), necessary to push Bingham plastics through extrusion dies. The latter results show a maximum for a certain range of

Bingham numbers and then they approach asymptotically zero, as expected for extrusion of solids. Entrance and exit pressure losses have been combined to calculate the end (Bagley) correction for Bingham plastics. This has been found to be appreciable, reaching about 3.7 (planar case) to 3.8 (axisymmetric case) times higher values than their Newtonian counterparts for the case of high Bi values.

Chapter 5

Combined Entry and Exit Flow of a Viscoplastic Material: Comparison with Experiments

This chapter presents a finite element simulation of an experimental study carried out for a viscoelastic material exhibiting yield stress, i.e. a visco-elastico-plastic material. The experiments have been performed in a capillary die for different flow rates. The analysis takes into account the full flow domain, i.e. both entry flow from the reservoir into the capillary die and exit flow of the extrudate into the atmosphere. The material is modelled as a Herschel-Bulkley fluid incorporating Papanastasiou's modification to hold

uniformly in yielded/unyielded regions. Non-isothermal effects are taken into account by solving the energy equation. The results are compared with previous numerical simulations and experimental data for extrudate swell, extrudate surface temperature rises and pressure drops.

5.1 Introduction

Carter and Warren (1987) conducted extensive experiments to characterize a series of propellant doughs used for propulsion in many guns and some rockets, in an effort to study extrudate swell effects. The materials are viscoelastic and have a yield point, hence their characterization as **visco-elastico-plastic**; they tend to be fibrous and are inhomogeneous. Propellant doughs are composed of nitrocellulose plasticized with nitroglycerin using varying amounts of solvent blends which act as stabilizers. From these results, Beverly and Tanner (1989) modelled a particular propellant dough with a composition code 35/45, i.e. a dough with 35% wt. nitroglycerin in a solvent of acetone/ethanol with a ratio 45/55 by weight containing 55 pph wt. of nitrocellulose. Carter and Warren (1987) have fitted shear stress vs. shear rate data and found that a Herschel-Bulkley model (section 2.3.5) gives an adequate fit. The one-dimensional model is given by:

$$\tau = \tau_y + k\dot{\gamma}^n \tag{5.1}$$

Table 5.1: Propellant dough (35/45) flow curve parameters.

Extrusion Temperature $T_o(°C)$	Yield Stress τ_y (kPa)	Consistency Index k $(kPa.s^n)$	Power-Law Index n $(-)$
20.0	39.0	17.9	0.440
35.0	47.5	4.33	0.466
50.0	50.0	1.27	0.533

where τ_y is the yield stress, k is the consistency index and n is the power-law index. The values of the parameters for 3 different temperatures are given in Table 5.1 and plotted as a function of temperature in Figure 5.1. The following data is also available:

Specific heat, C_p	1.0 $J/g.K$
Thermal conductivity, k_T	0.0034 $J/cm.s.K$
Density, ρ	0.84 g/cm^3

The experimental curve for shear stress vs. apparent shear rate is shown in

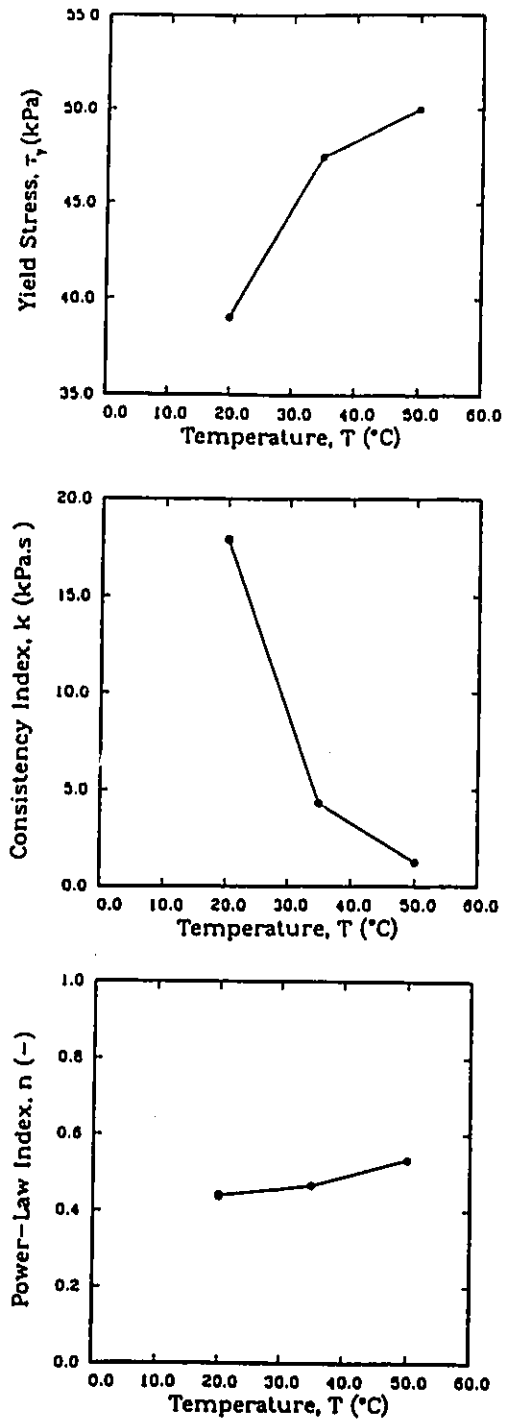

Figure 5.1: Propellant dough 35/45 material parameters as a function of temperature (Carter and Warren, 1987).

Figure 5.2. The apparent shear rate is defined as

$$\dot{\gamma}_a = \frac{4Q}{\pi R^3} \tag{5.2}$$

where Q is the flow rate (cm^3/s) and R is the tube radius (=0.1 cm in the experiments).

Beverly and Tanner (1989) have modelled this behaviour with a modified Phan-Thien/Tanner (MPTT) viscoelastic model incorporating yield stress. The fit of this model to the experimental data is also shown in Figure 5.2 along with the fit obtained from using the Herschel-Bulkley model with the data given in Table 5.1 for $20°C$. It is seen that neither model can fit well the experimental curve at high shear rates. Beverly and Tanner (1989) proceeded with the simulations of this particular propellant dough in order to determine the experimentally found extrudate swell. Their analysis is non-isothermal and also visco-elastico-plastic. However, despite the sophistication of their model, the results were found to be in agreement with the experiments only for low to moderate apparent shear rates ($\dot{\gamma}_a < 100\ s^{-1}$) as shown in Figure 5.3. For higher $\dot{\gamma}_a$ values, there is a maximum value of extrudate swell found experimentally around $\dot{\gamma}_a = 100\ s^{-1}$, after which there is a reduction in the swelling, while the numerical simulations showed a monotonic increase with $\dot{\gamma}_a$. Another drawback of their work was the insufficiently dense finite element grid used in the computations, which may have given wrong yielded/unyielded regions.

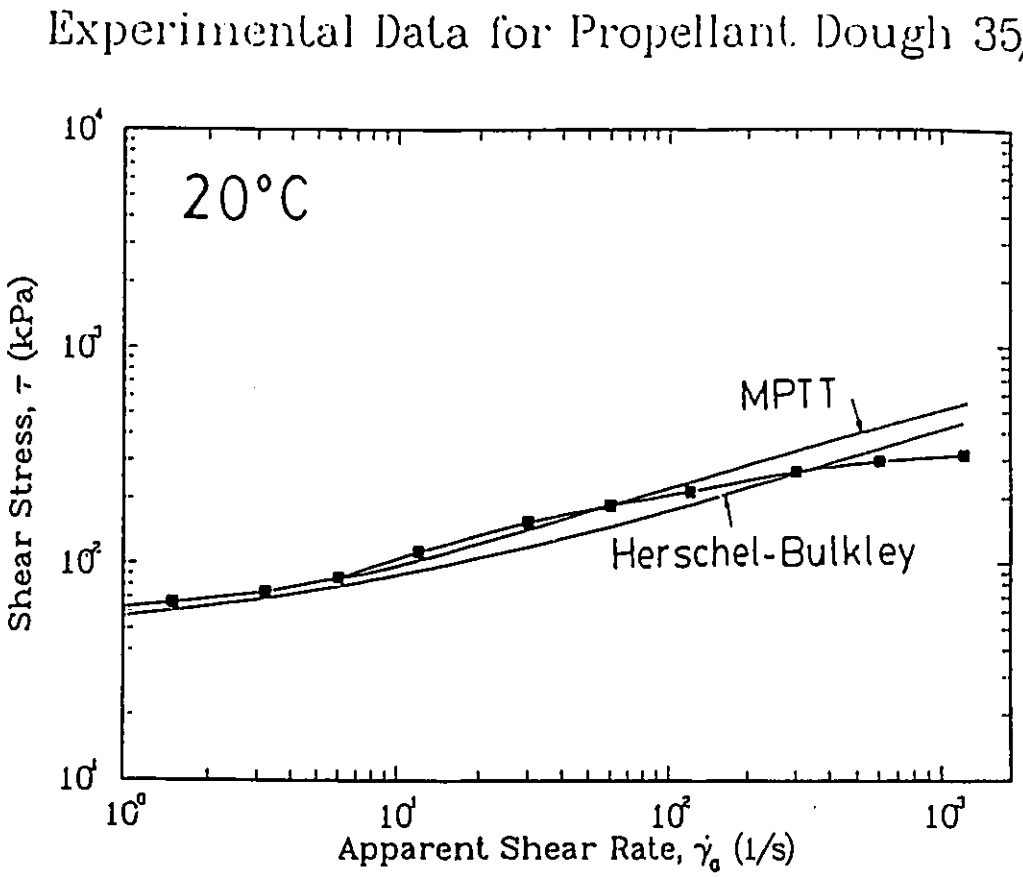

Figure 5.2: Experimental shear data (symbols) for a viscoplastic material and their best fit by different models (MPTT data from Beverly and Tanner, 1989).

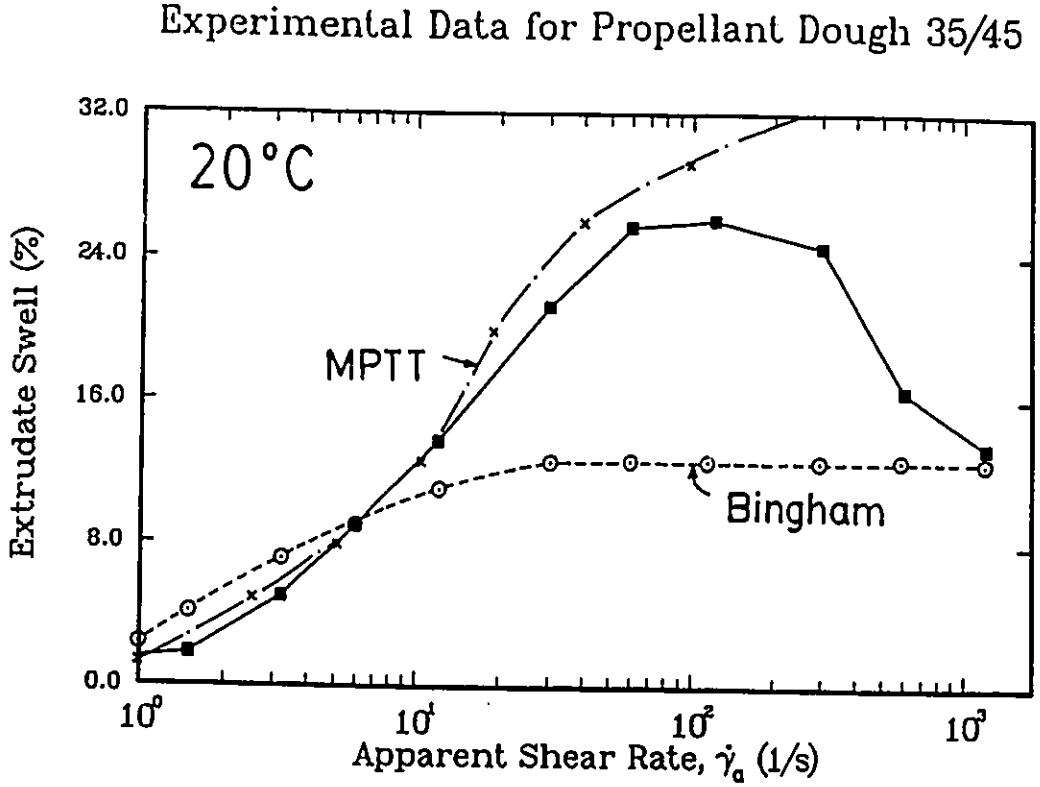

Figure 5.3: Comparison between experimental data (solid symbols) of extrudate swell for a viscoplastic material and predictions by different models (MPTT data from Beverly and Tanner, 1989).

It is the purpose of this chapter to use our experience with Bingham fluid computations to re-examine the problem and try to find out the reasons for the extrudate swell behaviour of this material. Our analysis will be based on different models and will include also a non-isothermal analysis.

5.2 Isothermal Flow—Bingham Model

We begin the analysis by assuming a Bingham model

$$\tau = \tau_y + \mu\dot{\gamma} \tag{5.3}$$

where τ_y = 39 kPa and μ = 70 kPa.s, as given by Beverly and Tanner's (1989) best fit to the data. With these values one can find immediately the dimensionless yield stress τ_y^* or Bingham number Bi for each apparent shear rate of the experiment. The results are given in Table 5.2. Without any calculations, one can find from the dimensionless graphs of Figures 4.7 and 4.8 the corresponding swelling ratios. The results are plotted in Figure 5.3, and the agreement is shown to be surprisingly good at low and high apparent shear rates. However, for intermediate $\dot{\gamma}_a$ values there are discrepancies reaching a maximum at $\dot{\gamma}_a = 100\ s^{-1}$ of up to 48%. The corresponding flow fields showing the distribution of yielded/unyielded regions are presented in Figure 5.4 and are compared with the ones given by Beverly and Tanner (1989). There are, of course, discrepancies as expected because of (a) differ-

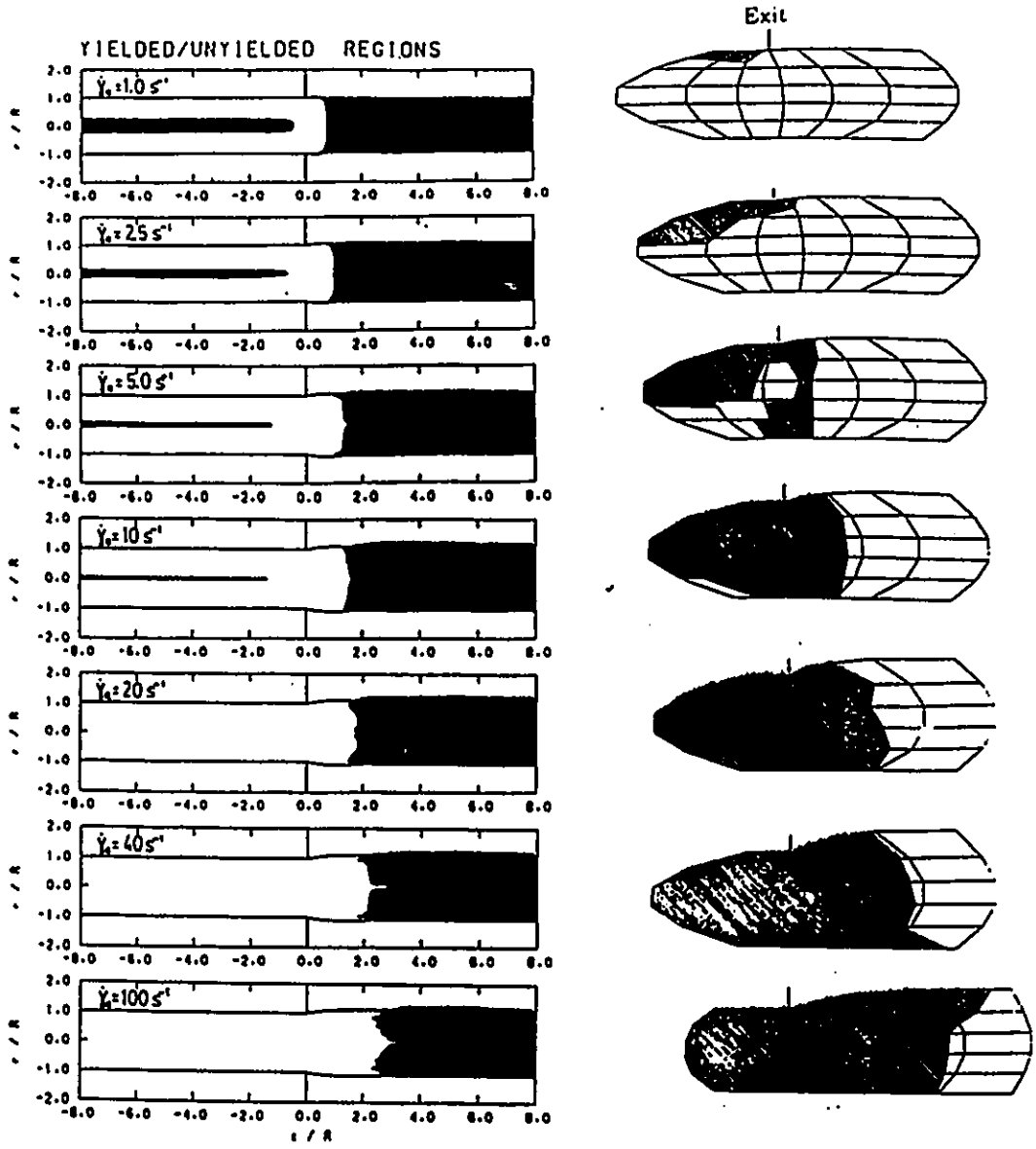

Figure 5.4: Comparison between present work (left) and Beverly and Tanner's (1989) for the yielded/unyielded regions in extrusion flow of a viscoplastic material. Note shading is reversed in the two works and the previous work shows only the upper half of the domain.

$\dot{\gamma}_a(s^{-1})$	τ_y^*	Bi	$Sw\%$
1.0	1.28	4.46	2.5
1.5	1.00	2.97	4.0
3.2	0.57	1.39	7.0
6.0	0.33	0.74	9.0
12.0	0.17	0.37	11.0
30.0	0.07	0.15	12.8
60.0	0.037	0.075	12.8
120.0	0.018	0.037	12.8
300.0	0.0074	0.015	12.8
600.0	0.0037	0.0074	12.9
1200.0	0.0019	0.0037	13.0

Table 5.2: Swell ratios for different apparent shear rates predicted by Bingham model for propellant dough 35/45 ($\tau_y = 39\ kPa, \mu = 70\ kPa.s$).

ent model, (b) different yield criterion, (c) insufficiently dense grids used in the previous work.

5.3 Non-Isothermal Analysis— Herschel-Bulkley Model

A full non-isothermal analysis was carried out for the design of Figure 5.5 comprising entry flow from the extruder barrel (reservoir) into a long capillary die and exit flow into the atmosphere. In the experiments, the die radius R is 0.1 cm, the die length L is 10 cm (L/R=100) and the reservoir radius R_{res} is 0.9525 cm ($R_{res}/R \approx 10$). In the experimental study the extrudate's surface temperature was measured 2.5 cm after the die exit.

For the present analysis we have considered a reservoir depth of $R_{res}/R = 10$ with entry at -10R upstream from the die entrance. Such dimensions are sufficient for imposition of fully-developed velocity profile and isothermal temperatures at entry, while the pressure drop in such a reservoir is negligible compared with the pressure losses in the long die. The exit section of the extrudate has been set at +25R downstream from the die exit so that the temperature rise can be monitored there and compared with the experimental findings.

The finite element grid used is shown in Figure 5.6. It consists of 852

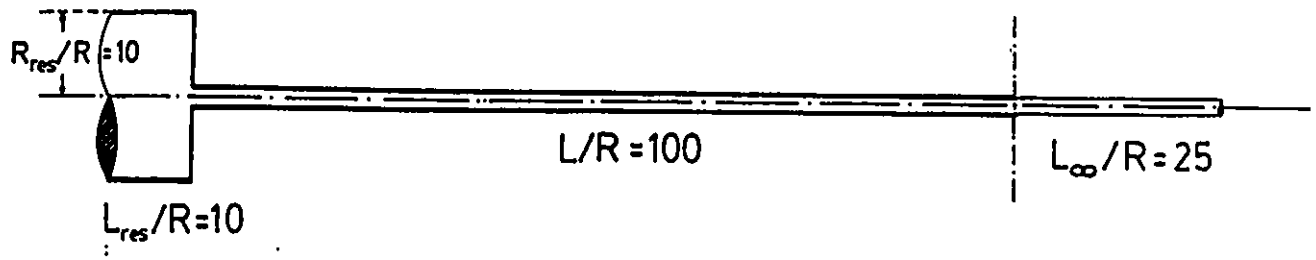

Figure 5.5: Schematic diagram of the flow domain used in the FEM non-isothermal computations for flow of propellant dough 35/45 through an extrusion die.

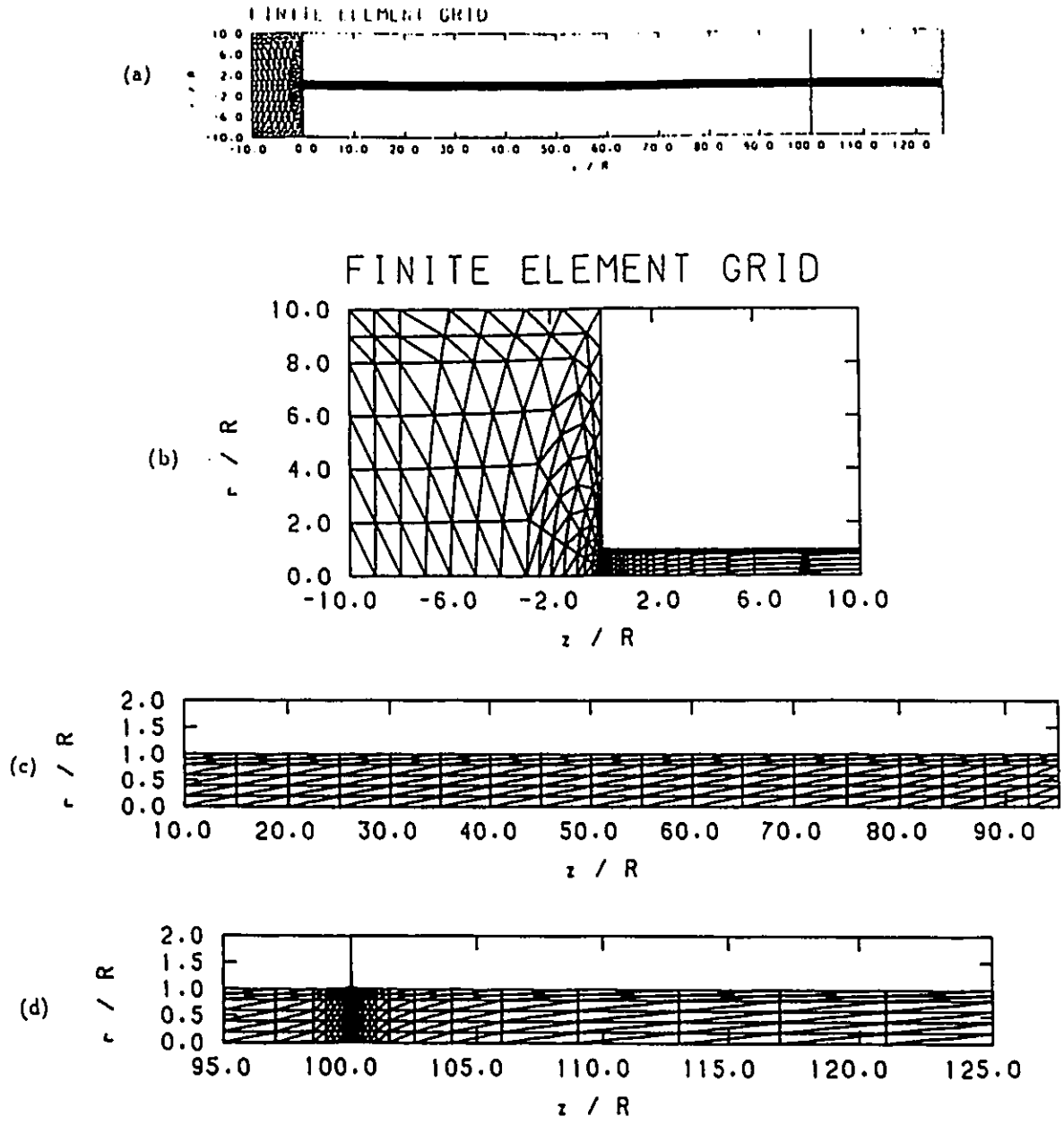

Figure 5.6: (a) Overall view of finite element grid used in the computations.(b) Detailed grid in the entry region, (c) detailed grid in the die region, (d) detailed grid in the exit region.

elements, 1859 nodes and 3834 unknown d.o.f. (13 nodes across, 143 nodes along). Care has been taken to have the same grid density near the die entry and exit as done previously in the analyses of entry and exit flows. The adequacy of the grid was verified against the Newtonian solution for entry and exit flows and the Newtonian extrudate swell. Note that such a grid requires computer memory close to the limit of 8 MBytes available in the University of Ottawa's AMDAHL-5880 mainframe computer. The Newtonian solution with free surface requires about 75 CPU secs (4 iterations needed).

For the viscoplastic material 35/45, runs were performed for 10 apparent shear rates corresponding to the ones carried out experimentally by Carter and Warren (1987). In each case, the fully developed power-law profile corresponding to the current $\dot{\gamma}_a$ was given as entry boundary condition. For the non-isothermal analysis, the boundary conditions were isothermal walls kept at $20°C$, the temperature of the experiments, while the material was assumed to enter at $20°C$ as well. Because of the relatively large reservoir and the very slow flow inside it, the flow is indeed isothermal there, and these entry boundary conditions are very well justified. On the extrudate free surface, zero heat flux was assumed, which is standard practice in extrusion of highly viscous materials (Tanner, 1985). Similar boundary conditions were used in the numerical simulations by Beverly and Tanner (1989), but they imposed

them at the entry to the die, since no reservoir was included in their analysis.

The results from the simulations are tabulated in Table 5.3. In graphical form, we begin with the depiction of yielded/unyielded region at entry (Figure 5.7) and exit (Figure 5.8) as the flow rate (or equivalently apparent shear rate $\dot{\gamma}_a$) increases. For low $\dot{\gamma}_a$ values, the unyielded region occupies most of the reservoir and the center of the die, while at the exit it comes very close to the die lips. As $\dot{\gamma}_a$ increases, yielding increases to form totally fluid regions everywhere except in the extrudate, where a plug velocity profile results in unyielded zones. These, however, tend to move farther and farther from the die lips. These results are in qualitative agreement with the previous ones presented in Figure 5.4.

The maximum temperature increases along the flow domain for increasing apparent shear rates as shown in Figure 5.9. The corresponding results for the centerline temperatures are shown in Figure 5.10. For low $\dot{\gamma}_a$ values, the flow is nearly isothermal (no discernible temperature rises due to viscous dissipation). However, for the highest shear rates, the viscous-dissipated energy causes high temperature rises and also differences between maximum and centerline temperatures.

The temperature rise at the extrudate free surface 2.5 cm from the die exit is plotted against $\dot{\gamma}_a$ in Figure 5.11, together with the experimentally

$\dot{\gamma}_a(s^{-1})$	Bi	$\Delta T(°C)$	$\Delta P(MPa)$	$Sw(\%)$
1.5	510.6	0.01	14.3	-1.38
3.2	156.6	0.02	16.4	-1.35
6.0	58.70	0.05	18.7	-1.15
12.0	20.00	0.1	22.0	-1.00
30.0	4.800	0.4	28.1	-0.43
60.0	1.600	1.1	34.3	0.11
120.0	0.550	2.9	41.8	0.79
300.0	0.130	9.1	51.1	2.79
600.0	0.045	16.9	48.5	1.84
1200.0	0.015	23.7	47.2	-1.65

Table 5.3: Simulation results for propellant dough 35/45.

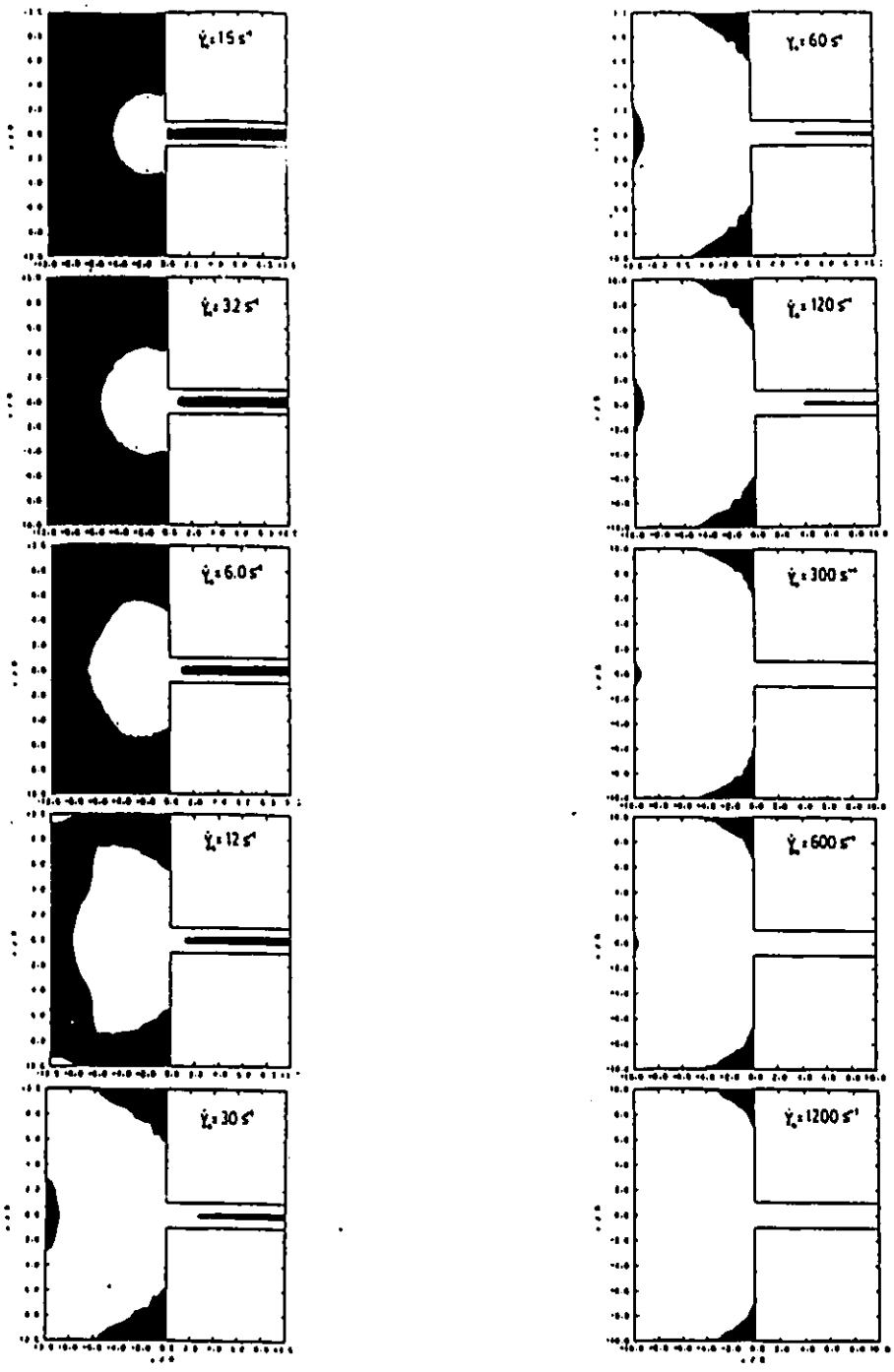

Figure 5.7: Progressive disappearance of the unyielded zone (shaded) as the apparent shear rate increases in entry flow of propellant dough 35/45.

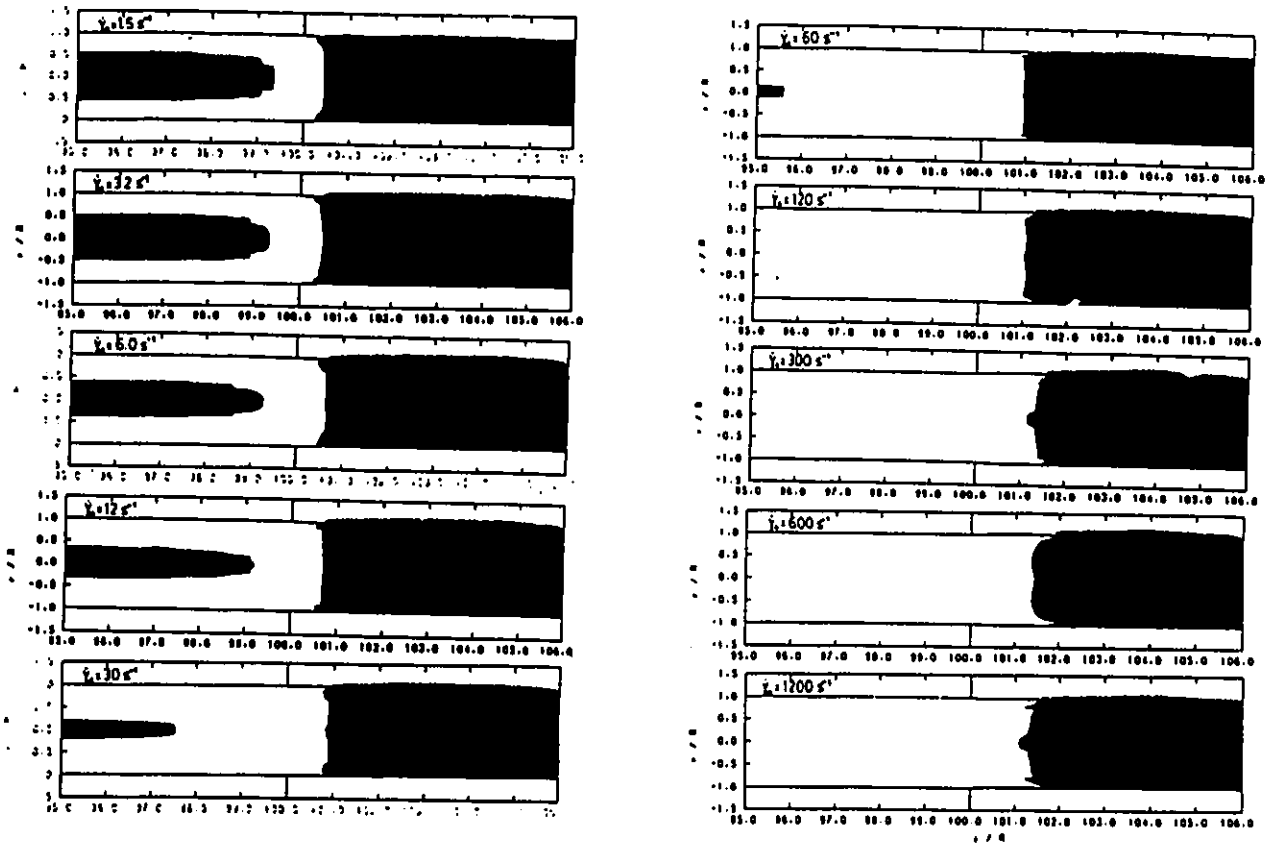

Figure 5.8: Progressive disappearance of the unyielded zone (shaded) as the apparent shear rate increases in exit flow of propellant dough 35/45.

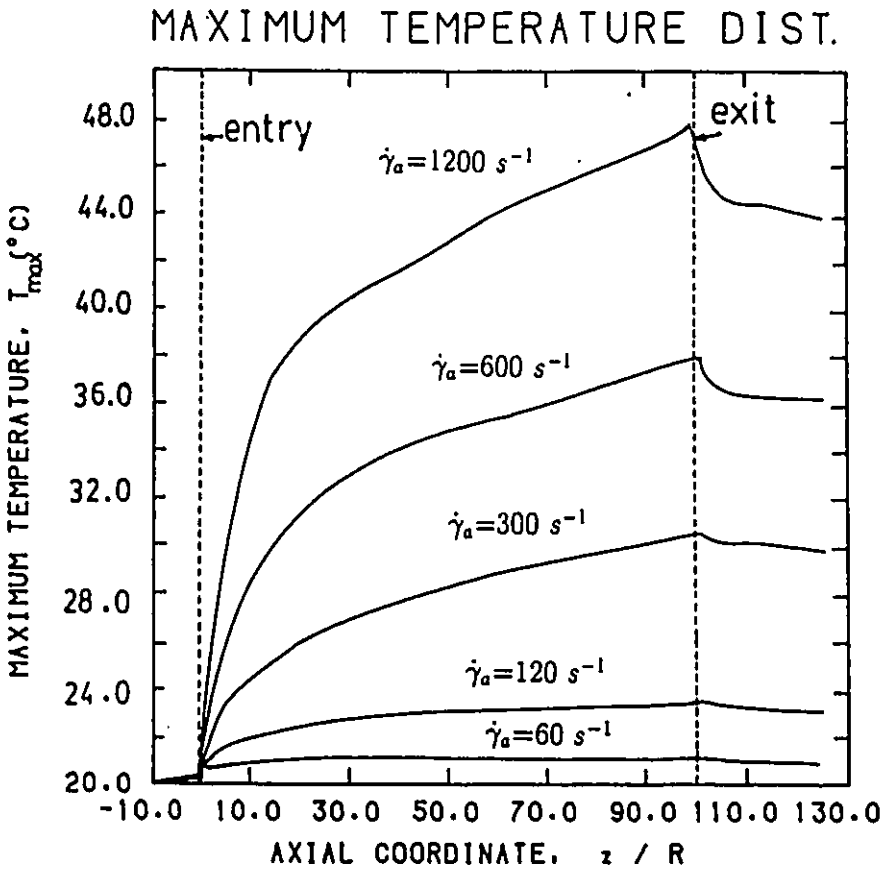

Figure 5.9: Maximum temperature rises along the flow domain for different apparent shear rates in extrusion of propellant dough 35/45.

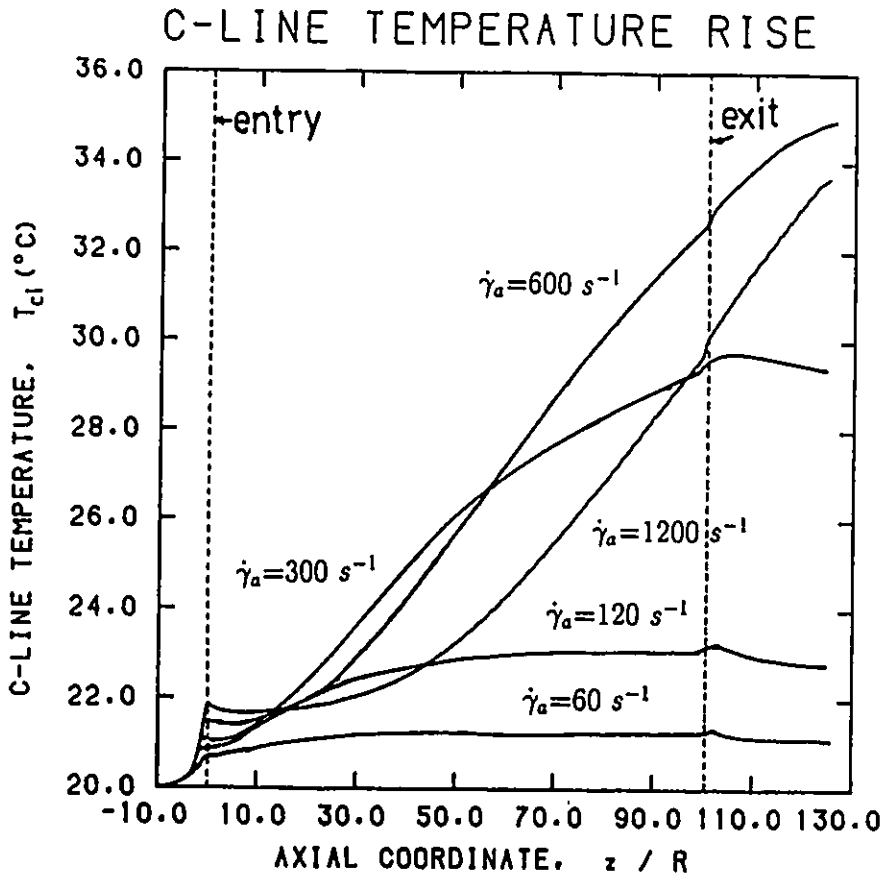

Figure 5.10: Centerline temperature rises along the flow domain for different apparent shear rates in extrusion of propellant dough 35/45.

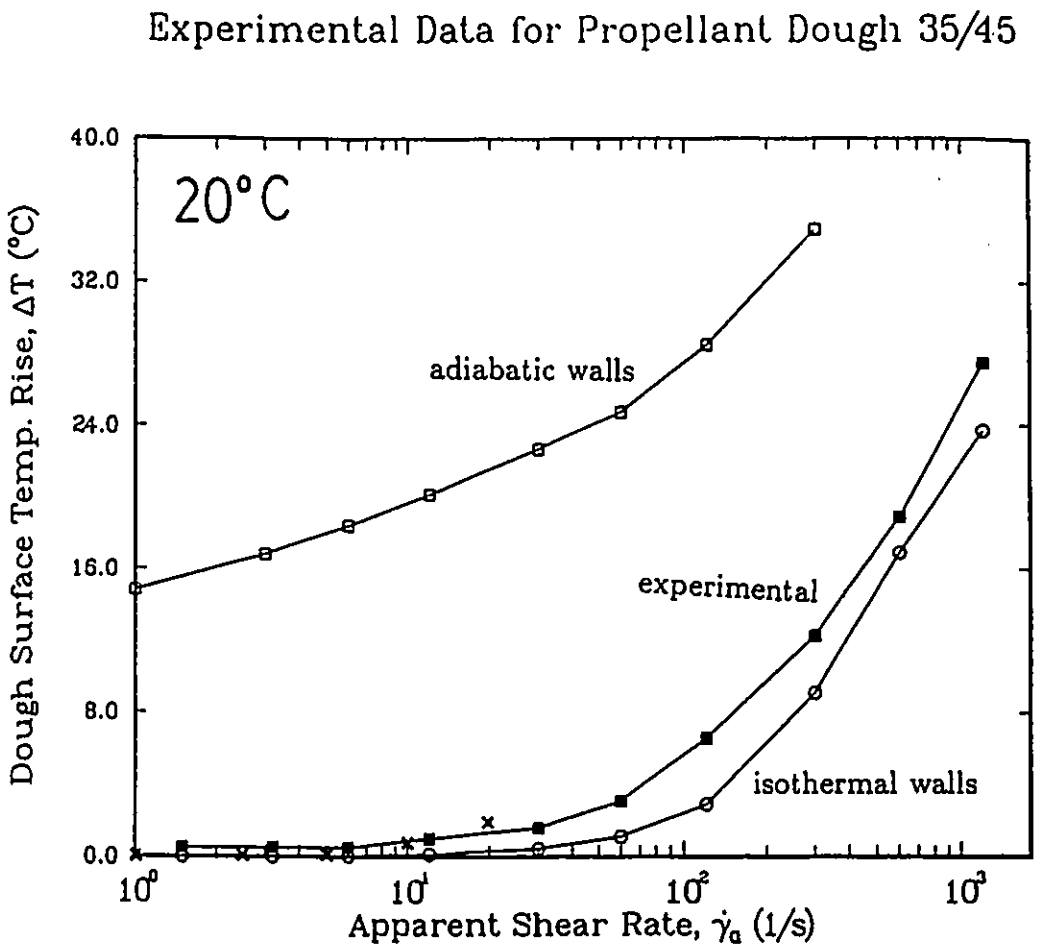

Figure 5.11: Comparison between experimental data (solid symbols, Carter and Warren, 1987) and numerical simulation (open symbols, this work) for extrudate surface temperature rise 2.5 cm after the die exit for propellant dough 35/45 modelled as a viscoplastic Herschel-Bulkley fluid. The results by Beverly and Tanner (1989) are also shown (x symbols).

found values and the previous results by Beverly and Tanner (1989). It is seen that the numerical simulations assuming **isothermal walls** underestimate the experimental values by as much as $3.5°C$ at the highest apparent shear rate $\dot{\gamma}_a = 1200\ s^{-1}$. On the other hand, assuming **adiabatic walls** highly overestimates the experimental values. In reality, the correct boundary condition at the walls is between isothermal and adiabatic (Heng, 1987), but closer to isothermal walls in this case since the die was thermally controlled at $20°C$. With this in mind, it becomes obvious that the assumption of isothermal walls in the present simulations is justified giving reasonable results.

The temperature and velocity profiles at the die exit have been given by Carter and Warren (1987) for $\dot{\gamma}_a = 1200\ s^{-1}$. Their calculations were made by the Finite Difference Method (FDM) for the die length. The present results are shown for comparison in Figure 5.12. The agreement is seen to be reasonably close, taking into account the different methods (no free surface calculation in FDM) and the fact that their analysis is strictly one-dimensional (no v_r-velocity component). The biggest differences occur in the temperature profile at the exit where Carter and Warren (1987) assume a thermal balance at the wall which gives a value of about $52°C$, whereas the present analysis assumes isothermal boundary conditions with the walls kept at $20°C$. Finally at entry there are small differences because Carter

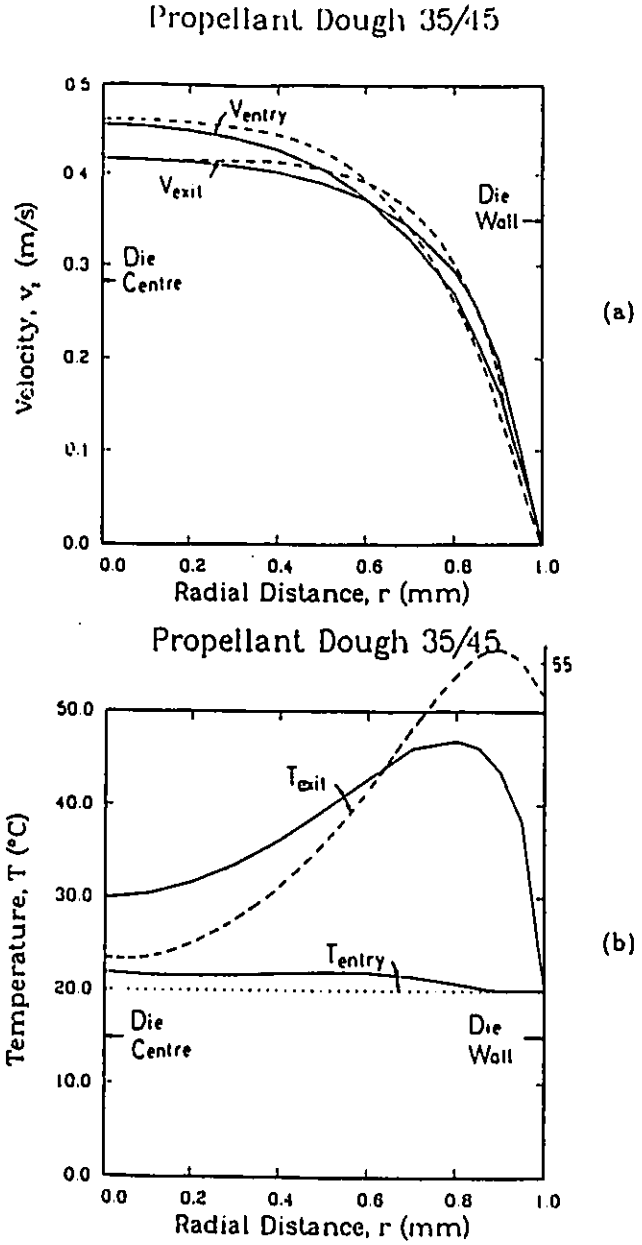

Figure 5.12: Calculated (a) velocity and (b) temperature profiles for propellant dough 35/45 at apparent shear rate 1200 s^{-1}. Comparison between present work (solid lines) and previous work (dashed lines, Carter and Warren, 1987).

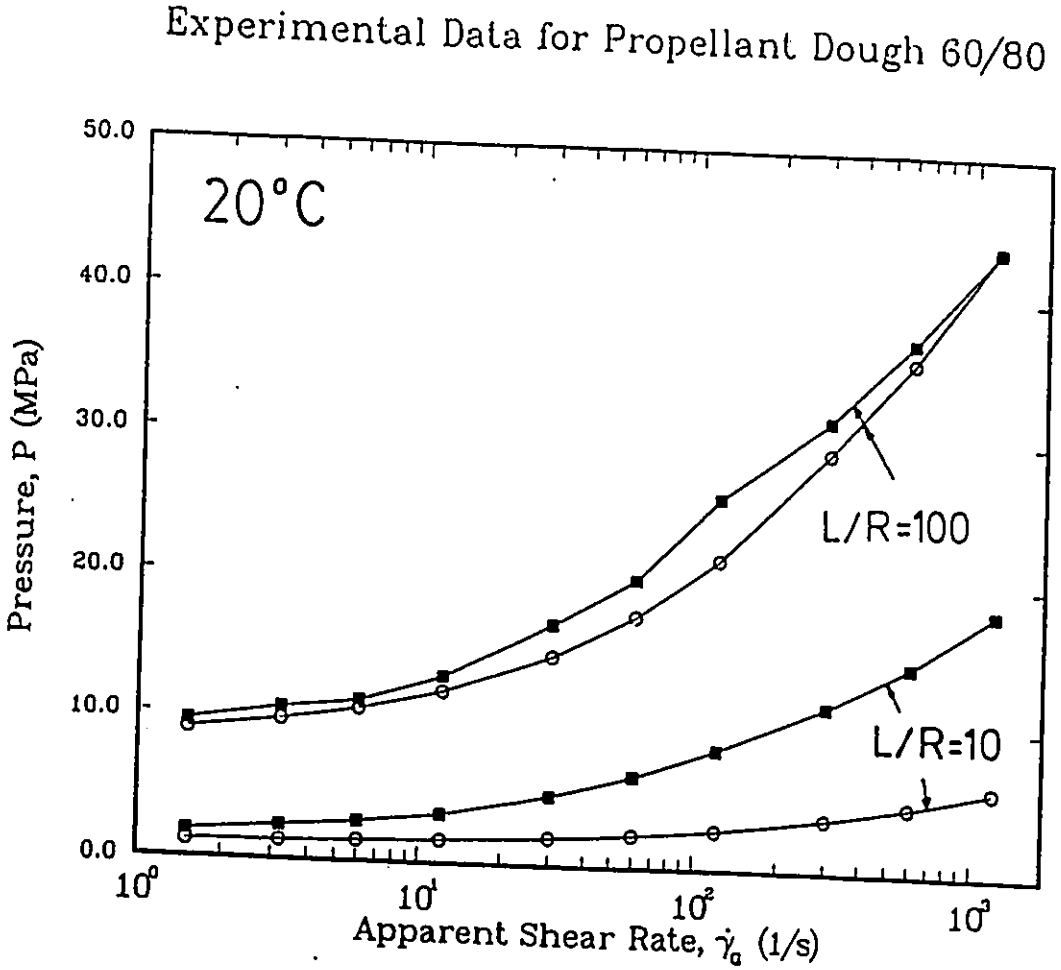

Figure 5.13: Comparison between experimental data (solid symbols, Carter and Warren, 1987) and numerical simulations (open symbols, this work) for pressure of propellant dough 60/80 modelled as a viscoplastic Herschel-Bulkley fluid.

and Warren (1987) have not taken into account the reservoir before the die entry.

Another quantity of interest and for comparison with experimental values is the pressure drop in the system and hence the calculation of end (Bagley) correction, n_B. Carter and Warren (1987) give n_B values for all cases, as well as raw data for pressure for the case of another propeliant dough characterized as 60/80. Using the material parameter data for 60/80 given by Carter and Warren (1987), the simulations were repeated and the results for pressure drop in the system for different $\dot{\gamma}_a$ values are shown in Figure 5.13 for two different die lengths, the longest die ($L/R = 100$) and the shortest die ($L/R = 10$). It is interesting to note that the numerical simulation results show a good agreement with the experimental findings for the longest die and very poor agreement for the shortest die especially for the high $\dot{\gamma}_a$ values. However, this is not surprising if we bear in mind that the propellant doughs used in the experiments were really visco-**elastico**-plastic, and one of the greatest manifestations of viscoelasticity is the ability of the material to **relax** its stresses, when given enough time. In the longest die (L/R=100), this is indeed the case, the material totally relaxes and behaves as an inelastic fluid in shear flow. Thus, an inelastic model such as the Herschel-Bulkley model, is adequate to correctly predict pressure drops due to shear flow in the long die. However, this is not the case for the shortest die ($L/R = 10$),

where the material has not relaxed, and extra pressure drops are required to push it through and overcome its high stress levels. In this case, an inelastic model is inadequate to account for viscoelasticity and it always gives underestimates of the pressure drops required, hence the discrepancies between simulations and experiments.

The experimental determination of the end (Bagley) correction is carried out by constructing the Bagley plot as shown in Figure 5.14. According to the theory (Bagley, 1957), the cut-off value read from a plot of ΔP vs. L/R for $\Delta P = 0$ gives the extra length required for the excess pressure losses, which is shown to be equal to n_B. From such Bagley plots, Carter and Warren (1987) have found the experimental values of n_B.

In the case of propellant dough 35/45, the results from the simulations are used to construct the Bagley plot shown in Figure 5.15. The values of n_B read off from the graph are used to determine the Bagley correction for different apparent shear rates and are compared to the experimental findings in Figure 5.16. As expected, there are big discrepancies due to the visco-elastic nature of the material as explained above. However, the pressure drops found by the simulations for the longest die ($L/R = 100$) should correspond to the experimentally found ones, according to the above-mentioned arguments.

The last comparisons with the experimental findings concern the extrudate swell results. In this respect also the results are rather disappointing.

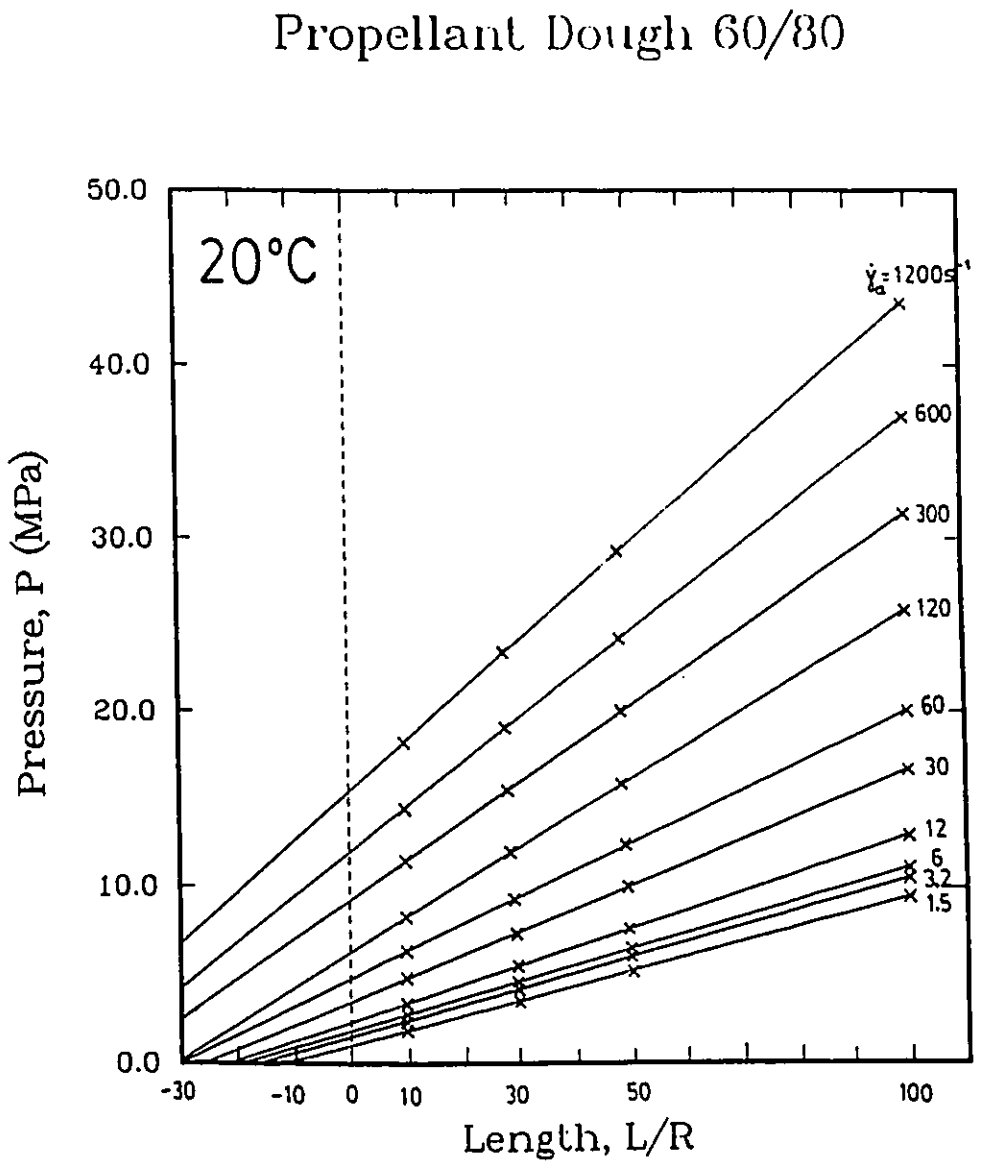

Figure 5.14: Bagley plot for propellant dough 60/80 according to Carter and Warren (1987).

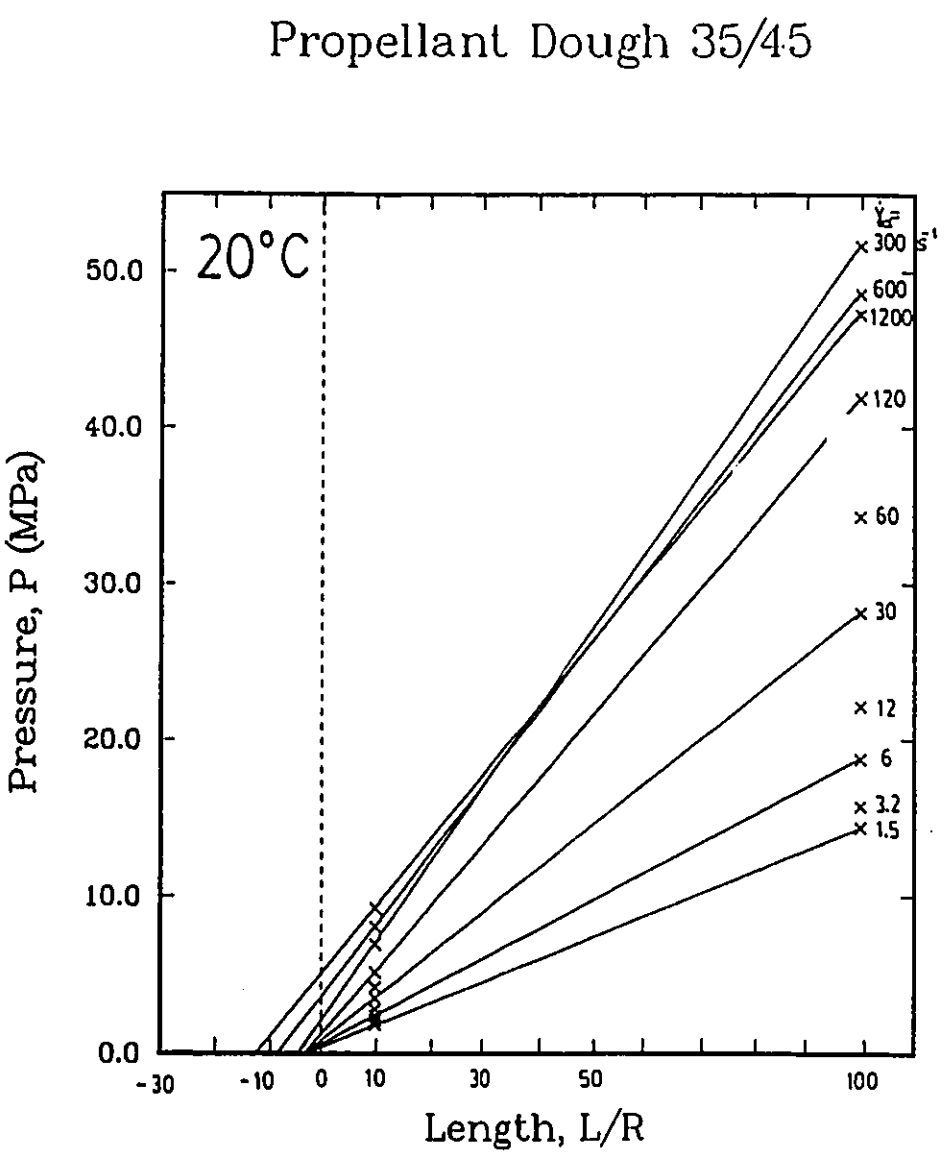

Figure 5.15: Bagley plot for propellant dough 35/45 using the pressure results from the numerical simulations.

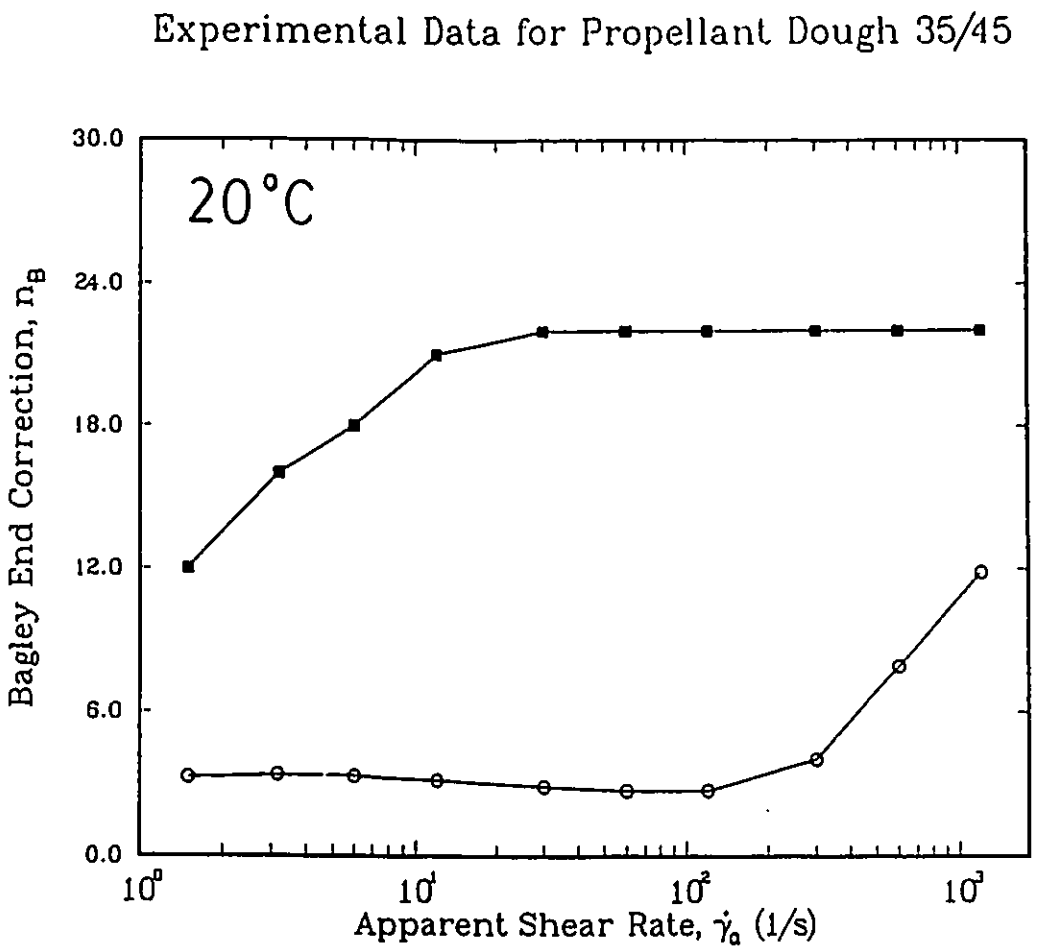

Figure 5.16: Comparison between experimental data (solid symbols, Carter and Warren, 1987) and numerical simulations (open symbols, this work) for Bagley correction of propellant dough 35/45 modelled as a viscoplastic Herschel-Bulkley fluid.

The values hardly exceed 2% and hover around 0% or no swelling, as shown in Figure 5.17. As explained earlier, this is hardly surprising because of the viscoelasticity of the material, which is responsible for the increased swelling. The purely inelastic Herschel-Bulkley model obviously cannot capture these phenomena associated with lack of shear flow outside the die. However, the interesting trend of increasing swelling and its decrease for higher $\dot{\gamma}_a$ values is captured by the simulations, unlike Beverly and Tanner's (1987) results which showed a continued increase. This decrease in swelling behaviour is apparently due to thermal effects which become dominant for the highest flow rates, decreasing the viscosity and hence increasing the Bi number in the flow.

5.4 Concluding Remarks

In this chapter an effort has been made to simulate some experimental data obtained for a visco-elastico-plastic material that obeys in shear flow the Herschel-Bulkley model. A full non-isothermal analysis has been carried out for a flow domain closely approximating the physical system of the experiments. The results have shown that good agreement can be obtained for quantities associated with shearing flow, such as temperature rises due to viscous dissipation and pressure drops for long dies. However, in cases

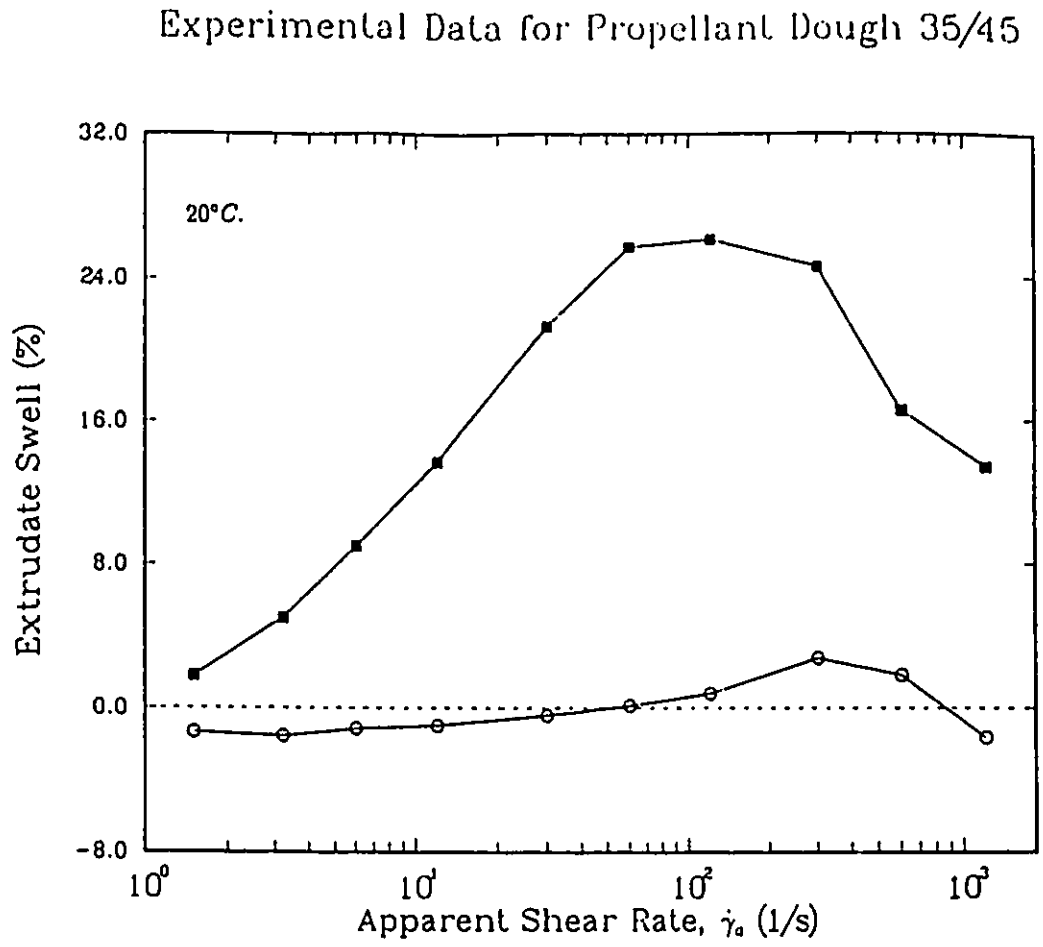

Figure 5.17: Comparison between experimental data (solid symbols, Carter and Warren, 1987) and numerical simulation (open symbols, this work) for extrudate swell of propellant dough 35/45 modelled as a viscoplastic Herschel-Bulkley fluid.

where the **elastic** character of the material dominates, such as extrudate swell and Bagley correction, the inelastic Herschel-Bulkley model in unable to predict such phenomena, giving almost no swelling and very small Bagley corrections. This shows the limitations of such inelastic models to accurately predict phenomena associated with the material's viscoelastic character.

Chapter 6

Conclusions and Recommendations

The present work has dealt with the numerical simulation of viscoplastic materials exhibiting a yield stress. A series of flows have been analyzed with the Finite Element Method (FEM). The models used are the Newtonian fluid, Bingham plastic and Herschel-Bulkley fluid, the last two incorporating Papanastasiou's modification to make them uniformly valid for both yielded and unyielded regions. The extent and shape of these regions have been found using the criterion that yielding occurs when the magnitude of the stress tensor exceeds the yield stress. This criterion was found to be more appropriate than previous criteria used in the literature which employed an

arbitrarily small value of the magnitude of the rate-of-strain tensor.

Problems that have been solved are:

1. Fully-developed, pressure-driven (Poiseuille) flow between parallel plates and in tubes.
2. Entry flows through 4:1 abrupt planar and axisymmetric contractions.
3. Exit flows through slit and capillary dies and determination of extrudate swell.
4. Combined entry and exit flow from a capillary die under non-isothermal conditions in a bid to simulate experimental results for a viscoelastic material exhibiting yield stress.

The major contributions of the present work are:

- A thorough and accurate determination of yielded/unyielded regions in entry and exit flows, showing the progressive growth of solid region as a dimensionless yield stress (τ_y^*) or Bingham number (Bi) increases. Earlier attempts in the literature were only partial and often misleading with inadequate and/or erroneous depictions.
- An accurate determination of the extrudate swell for Bingham plastics, which shows the important (and previously missed) phenomenon of contraction below 1 for a certain range of τ_y^* or Bi, and then an asymptotic approach towards 1 from below. This surprising phenomenon was properly explained

using kinematic considerations.

- An accurate determination of the excess pressure losses for Bingham plastics in entry and exit flows over and above the Newtonian values, thus giving rise to entrance, exit and end (Bagley) corrections necessary to predict pressure drops in flows through dies. The results showed a monotonic increase with τ_y^* or Bi, giving linear relationships with τ_y^* and sigmoidal relationships with Bi. For the highest values of Bi (as the unyielded regions dominate), the end correction can reach 3.7 (planar case) to 3.8 (axisymmetric case) higher values than their Newtonian counterparts (Bi=0).

The numerical simulation of a visco-elastico-plastic material with the Herschel-Bulkley model revealed that the model can give good predictions whenever shearing effects dominate. Thus it can predict reasonably well pressure drops and temperature rises due to viscous heating in shear flows from long dies (L/R=100). However, it predicts virtually no extrudate swell (around 2%), whereas experimental values can be as high as 26%. The inability of purely viscoplastic models to account for any viscoelasticity at all is a serious drawback and calls for the development and implementation of such visco-elastico-plastic models.

The main recommendation for future work is basically the need for a visco-elastico-plastic simulation that correctly accounts both for viscoelasticity and yield stress. Recent success with the K-BKZ integral-type, vis-

coelastic model in simulating strong viscoelastic behaviour of polymer melts (Luo and Mitsoulis, 1990), makes such a model a good candidate, after the proper modifications have been implemented to account for the presence of a yield stress.

From the numerical point of view, it was found that the Picard scheme used in the present work, although robust, easy to implement and straightforward in execution, it was painfully slow to converge. Future work should include some acceleration scheme or better still, the Newton-Raphson method with its quadratic convergence rate and wealth of information that can be extracted from the Jacobian matrix with regard to stability analysis (Papanastasiou, 1987).

Bibliography

[1] Agur, E.E. and J. Vlachopoulos, *"Numerical Simulation of a Single-Screw Plasticating Extruder"*, Polym. Eng. Sci., 2, 1084-1094 (1982).

[2] Argon, A.S.,*"Constitutive Equations in Plasticity"*, MIT Press, Cambridge, MA (1975).

[3] Astarita, G., *"Letter to the Editor: The Engineering Reality of the Yield Stress"*, J. Rheol., 34, 275-277 (1990).

[4] Bagley, E.B., *"End Corrections in the Capillary Flow of Polyethylene"*, J.Appl.Phys., 28, 624-626 (1957).

[5] Ballenger, T.F. and J.L. White, *"The Development of the Velocity Field in Polymer Melts in a Reservoir Approaching a Capillary Die"*, J. Appl. Polym. Sci., 15, 1949-1962 (1971).

[6] Barnes, H.A. and K. Walters, *"The Yield Stress Myth"*, Rheol. Acta, 24, 323-326 (1985).

[7] Ben-Sabar, E. and B. Caswell, *"A Stable Finite Element Simulation of Convective Transport"*, Int. J. Num. Meth. Eng., **14**, 545-565 (1979).

[8] Beris, A.N., J.A. Tsamopoulos, R.C. Armstrong, and R.A. Brown, *"Creeping Motion of a Sphere through a Bingham Plastic"*, J. Fluid Mech., **158**, 219-244 (1985).

[9] Beverly, C.R. and R.I. Tanner *"Numerical Analysis of Extrudate Swell in Viscoelastic Materials with Yield Stress"*, J. Rheol., **33**, 989-1009 (1989).

[10] Bingham, E.C., *"Fluidity and Plasticity"*, McGraw-Hill, New York (1922).

[11] Bird, R.B., W.E. Stewart, and E.N. Lightfoot, *"Transport Phenomena"*, Wiley, New York (1960).

[12] Bird, R.B., R.C. Armstrong, O. Hassager, *"Dynamics of Polymeric Liquids"*, Vol. 1, Wiley, New York (1977).

[13] Bird, R.B., G.C. Dai, and B.J. Yarusso, *"The Rheology and Flow of Viscoplastic Materials"*, Rev. Chem. Eng., **1**, 1-70 (1983).

[14] Boger, D.V., *"A Highly Elastic Constant-Viscosity Fluid"*, J. Non-Newt. Fluid Mech., **3**, 87-91 (1977).

[15] Boger, D.V., R. Gupta, and R.I. Tanner, *"The End Correction for Power-law Fluids in the Capillary Rheometer"*, J. Non-Newt. Fluid Mech., **4**, 239-248 (1978).

[16] Boger, D.V., *"Circular Entry Flows of Inelastic and Viscoelastic Fluids"*, Advances in Transport Processes, Vol. II, Eds. A.S. Mujumdar and R.A. Mashelkar, Halsted Press, Wiley Eastern Ltd., New Delhi, 43-104 (1982).

[17] Carter R.E. and R.C. Warren, *"Extrusion Stresses, Die Swell, and Viscous Heating Effects in Double-Base Propellants"*, J. Rheol., **31**, 151-173 (1987).

[18] Casson, N., *"Rheology of Disperse Systems"*, Ed. C. C. Mill, Pergamon Press, New York (1959).

[19] Coleman, C.J., *"A Finite Element Routine for Analyzing Non-Newtonian Flows. Part I: Basic Method and Preliminary Results"*, J. Non-Newt. Fluid Mech., **7**, 289-301 (1980).

[20] Coleman, C.J., *"A Finite Element Routine for Analyzing Non-Newtonian Flows. Part II: The Extrusion of a Maxwell Fluid"*, J. Non-Newt. Fluid Mech., **8**, 261-270 (1981).

[21] Crochet, M.J. and R. Keunings, *"Die Swell of a Maxwell Fluid: Numerical Prediction"*, J. Non-Newt. Fluid Mech., 7, 199-212 (1980).

[22] Crochet, M.J. and R. Keunings, *"On Numerical Die Swel l Calculation"*, J. Non-Newt. Fluid Mech., **10**, 85-94 (1982a).

[23] Crochet, M.J. and R. Keunings, *"Finite Element Analysis of Die Swell of a Highly Elastic Fluid"*, J. Non-Newt. Fluid Mech., **10**, 339-356 (1982b).

[24] Dzuy, N.O. and D.V. Boger, *"Direct Yield Stress Measurement with the Vane Method"*, J. Rheol., **29**, 335-347 (1985).

[25] Ellwood, K.R.J., G.C. Georgiou, T.C. Papanastasiou, and J.O. Wilkes, *"Laminar Jets of Bingham-Plastic Liquids"*, J. Rheol., 34, 787-812 (1990).

[26] Fredrickson, A.G., *"Principles and Applications of Rheology"*, Prentice Hall, Englewood Cliffs, NJ (1964).

[27] Gartling, D.K., *"The Numerical Simulation of Plastic Fluids"*, Num. Meth. Lam. Turb. Flow (Eds. C. Taylor, J.A. Johnson, and W.R. Smith) , Proc. 3rd Int. Conf., Seattle, Pineridge Press, Swansea, UK, 669-679 (1983).

[28] Gartling, D.K., *"One Dimensional Finite Element Solutions for a Maxwell Fluid"*, J. Non-Newt. Fluid Mech., **17**, 203-231 (1985).

[29] Gartling, D.K. and N. Phan-Thien, *"A Numerical Simulation of a Plastic Fluid in a Parallel-Plate Plastometer"*, J. Non-Newt. Fluid Mech., 14, 347-360 (1984).

[30] Gerald, C.F. and P.O. Wheatley, *"Applied Numerical Analysis"*, 4th edition, Addison-Wesley, New York (1989).

[31] Han, C.D. and M. Charles, *"Entrance- and Exit-Correction in Capillary Flow of Molten Polymers"*, Trans. Soc. Rheol., **15**, 371-384 (1971).

[32] Han, C.D., *"Rheology in Polymer Processing"*, Academic Press, New York (1976).

[33] Hannachi, A., *"Computer-Aided Analysis and Design of Multilayer Polymer Melt Flows"*, Comprehensive Report, Dept. Chem. Eng., Univ. of Ottawa, Ont. (1990).

[34] Harnett, J.P. and R. Y. Z. Hu, *"The Yield Stress-An Engineering Reality"*, J. Rheol., **33**, 671-679 (1989).

[35] Heng, F.L., *"Computer-Aided Analysis and Design for Extrusion Dies"*, M.A.Sc. Thesis, Dept. Chem. Eng., Univ. of Ottawa, Ont. (1987).

[36] Herschel, W.H. and R. Bulkley, *"Konsistenzmessungen von Gummi-Benzollosungen"*, Kolloid Z., **39**, 291-300 (1926).

[37] Hieber, C.A., *"Entrance Pressure Losses for Power-Law Fluid at Small Reynolds Number"*, Rheol. Acta, **26**, 92-95 (1987).

[38] Hood, P., *"Frontal Solution Program for Unsymmetric Matrices"*, Int. J. Num. Meth. Eng., **10**, 379-399 (1976).

[39] Huebner, K.H. and E.A. Thornton, *"The Finite Element Method for Engineers"*, Wiley, New York (1982).

[40] Keentok, M., J.F. Milthorpe, and E.J. O'Donovan, *"On the Shearing Zone around Rotating Vanes in Plastic Liquids: Theory and Experiment"*, J. Non-Newt. Fluid Mech., **17**, 23-35 (1985).

[41] Kistler, S.F. and L.E. Scriven, *"Coating Flow Theory by Finite Element and Asymptotic Analysis of the Navier-Stokes System"*, Int. J. Num. Meth. Fluids, **4**, 207-229 (1984).

[42] Kwag, C. and J. Vlachopoulos *"An Assessment of Cogswell's Method for Measurement of Extensional Viscosity"*, Poly. Eng. Sci. Vol 31 **14**, 1015-1021 (1991).

[43] Lipscomb, G.G. and M.M. Denn, *"Flow of Bingham Fluids in Complex Geometries"*, J. Non-Newt. Fluid Mech., **14**, 337-346 (1984).

[44] Luo, X-L. and E. Mitsoulis, *"A Numerical Study of the Effect of Elongational Viscosity on Vortex Growth in Contraction Flows of Polyethlene Melts"*, J.Rheol., bf 34, 309-342 (1990).

[45] Malvern, L.E., *"An Introduction to the Mechanics of the Continuous Medium "*, Prentice Hall, Englewood, NJ (1969).

[46] Metzner, A.B., *"Rheology of Suspensions in Polymeric Liquids"*, J. Rheol., **29**, 739-772 (1985).

[47] Middleman, S. and J. Gavis, *"Expansion and Contraction of Capillary Jets of Newtonian Liquids"*, Phys. Fluids, **4**, 355-359 (1961).

[48] Mitsoulis, E., *"Finite Element Analysis of Two-Dimensional Polymer Melt Flows"*, Ph.D. Thesis, Dept. Chem. Eng., McMaster Univ., Hamilton, Ont. (1984).

[49] Mitsoulis, E., *"The Numerical Simulation of Boger Fluids: A Viscometric Approximation Approach"*, Polym. Eng. Sci., **26**, 1552-1562 (1986a).

[50] Mitsoulis, E.,*"Extrudate Swell in Double-Layer Flows"*, J. Rheol., **30(S)**, S23-S44 (1986b).

[51] Mitsoulis, E.,*"A Heuristic Approach to Modeling Viscoelasticity in Polymer Processing"*, Proc. ANTEC'88, Soc.Plast.Eng., Atlanta, GA, Vol. **34**, 140-144 (1988).

[52] Mitsoulis, E., *"Numerical Simulation of Viscoelastic Fluids"*, In Encyclopedia of Fluid Mechanics, Vol. **9**, Polymer Flow Engineering (Ed. N.P. Cheremisinoff), Gulf Publ. Co., Houston, 649-704 (1990).

[53] Mitsoulis, E. J. Vlachopoulos, and F.A., Mirza, *"MACVIP - A Finite Element Program for Creeping Viscoelastic Flows"*, Internal Report, Faculty of Eng., McMaster Univ. Hamilton, Ont. (1983).

[54] Mitsoulis, E., J. Vlachopoulos, and F.A. Mirza, *"Numerical Simulation of Entry and Exit Flows in Slit Dies"*, Polym. Eng. Sci., 24, 707-715 (1984a).

[55] Mitsoulis, E., J. Vlachopoulos, and F.A. Mirza, *"Simulation of Extrudate Swell from Long Slit and Capillary Dies"*, Polym. Proc. Eng., **2**, 153-177 (1984b).

[56] Nguyen, H. and D.V. Boger, *"The Kinematics and Stability of Die Entry Flows"*, J. Non-Newt. Fluid Mech., 5, 353-368 (1979).

[57] Nickell, R.E., R.I. Tanner, and B. Caswell *"The Solution of Viscous Incompressible Jet and Free-Surface Flows Using Finite Element Method"*, J. Fluid Mech., **65**, 189-206 (1974).

[58] O'Donovan, E.J. and R.I. Tanner, *"Numerical Study of the Bingham Squeeze Film Problem"*, J. Non-Newt. Fluid Mech., **15**, 75-83 (1984).

[59] Papanastasiou, T.C., *"Flow of Materials with Yield"*, J. Rheol., **31**, 385-404 (1987).

[60] Pearson, J.R.A., *"Mechanics of Polymer Processing"*, Elsevier, New York (1985).

[61] Reddy, K.R. and R.I. Tanner, *"Finite Element Solution of Viscous Jet Flows with Surface Tension"*, Comput. Fluids, **6**, 83-91 (1978).

[62] Ryan, M.E. and A. Dutta, *"A Finite Difference Simulation of Extrudate Swell"*, Proc. 2nd World Congr. Chem. Eng., Montreal, Vol. VI, 277-281 (1981).

[63] Scott, P.S., F. Mirza, and J. Vlachopoulos, *"Finite-Element Simulation of Laminar Viscoplastic Flows with Regions of Recirculation"*, J. Rheol., **32**, 387-400 (1988).

[64] Tanner, R.I., *"Die-Swell Reconsidered: Some Numerical Solutions Using a Finite Element Program"*, Appl. Polym. Symp., **20**, 201-208 (1973).

[65] Tanner, R.I., *"A New Inelastic Theory of Die-Swell,"* J. Non-Newt. Fluid Mech., **6**, 289-302 (1980).

[66] Tanner, R.I. and J.F. Milthorpe, *"Numerical Simulation of the Flow of Fluids with Yield Stress"*, Num. Meth. Lam. Turb. Flow, (Eds. C.

Taylor, J.A. Johnson, and W.R Smith), Proc. 3rd Int. Conf., Seattle, Pineridge Press, Swansea, UK, 680-690 (1983).

[67] Tanner, R.I., *"Engineering Rheology"*, Clarendon Press, Oxford, UK (1985).

[68] Taylor, C. and T.G. Hughes, *"Finite Element Programming of the Navier-Stokes Equations"*, Pineridge Press, Swansea, UK (1981).

[69] Vlachopoulos, J., *"Should You Use Finite Difference of Finite Element Method"*, Proc. 35th ANTEC, Soc. Plast. Eng., Montreal, Quebec, Vol. **23**, 519-520 (1977).

[70] Vlachopoulos, J., *"Extrudate Swell in Polymers"*, Rev. Def. Beh. Mat., **3**, 219-248 (1981).

[71] White, J.L. and A. Kondo, *"Flow Patterns in Polyethylene and Polystyrene Melts during Extrusion through a Die Entry Region: Measurements and Interpretation"*, J. Non-Newt. Fluid Mech., **3**, 41-64 (1977/1978).

[72] White, J.L., Y. Wang, A. I. Isayev, N. Nakajima, F. C. Weissert, and K. Min, *"Modeling of Shear Viscosity Behavior and Extrusion Through Dies for Rubber Compounds"*, Rubber Chem. Technol., **60**, 337-358 (1986).

[73] White, S.A., A.D. Gotsis, and D.G. Baird. "*Review of the Entry Flow Problem: Experimental and Numerical*". J. Non-Newt. Fluid Mech., 24. 121-161 (1987).

Appendix A

Convergence Study of the Numerical Scheme

The iterative scheme used in the computations was **direct substitution**, also called **Picard method** (Gerald and Wheatley, 1989). This takes the form:

$$[K(x)]\{X\} = \{F\} \tag{A.1}$$

where $\{x\}$ is the vector of unknowns, $[K(x)]$ is the non-linear global stiffness matrix and $\{F\}$ is the global load vector. The initial estimate $\{X_o\}$ comes from the solution of the Newtonian problem ($\tau_y = 0$). The new solution is obtained by direct substitution of the previous solution in the $[K]$ matrix to provide an update. Although robust, easy to implement and with a wide

range of convergence, its convergence rate is linear as shown in Figure A.1. where the norm of the error vector $\| e \|$ is plotted vs. number of iterations for the case of Poiseuille flow between parallel plates (section 3.1.1) and in a tube (section 3.1.2). It is seen that it takes around 20 iterations to reach a norm below 10^{-3} for this case of dimensionless numbers ($\tau_y^* = 1.6$, $Bi = 11.6$ for the planar case and $\tau_y^* = 1.87$, $Bi = 9.5$ for the axisymmetric case). The number of iterations increases with τ_y^* or Bi and it takes about 60 iterations to reach the same norm for the highest values of τ_y^* or Bi. Convergence can be accelerated by a zeroth-order continuation method, i.e. using the results of a previous dimensionless parameter to obtain results for a higher value of this parameter (e.g. increase the yield stress τ_y or decrease the flow rate).

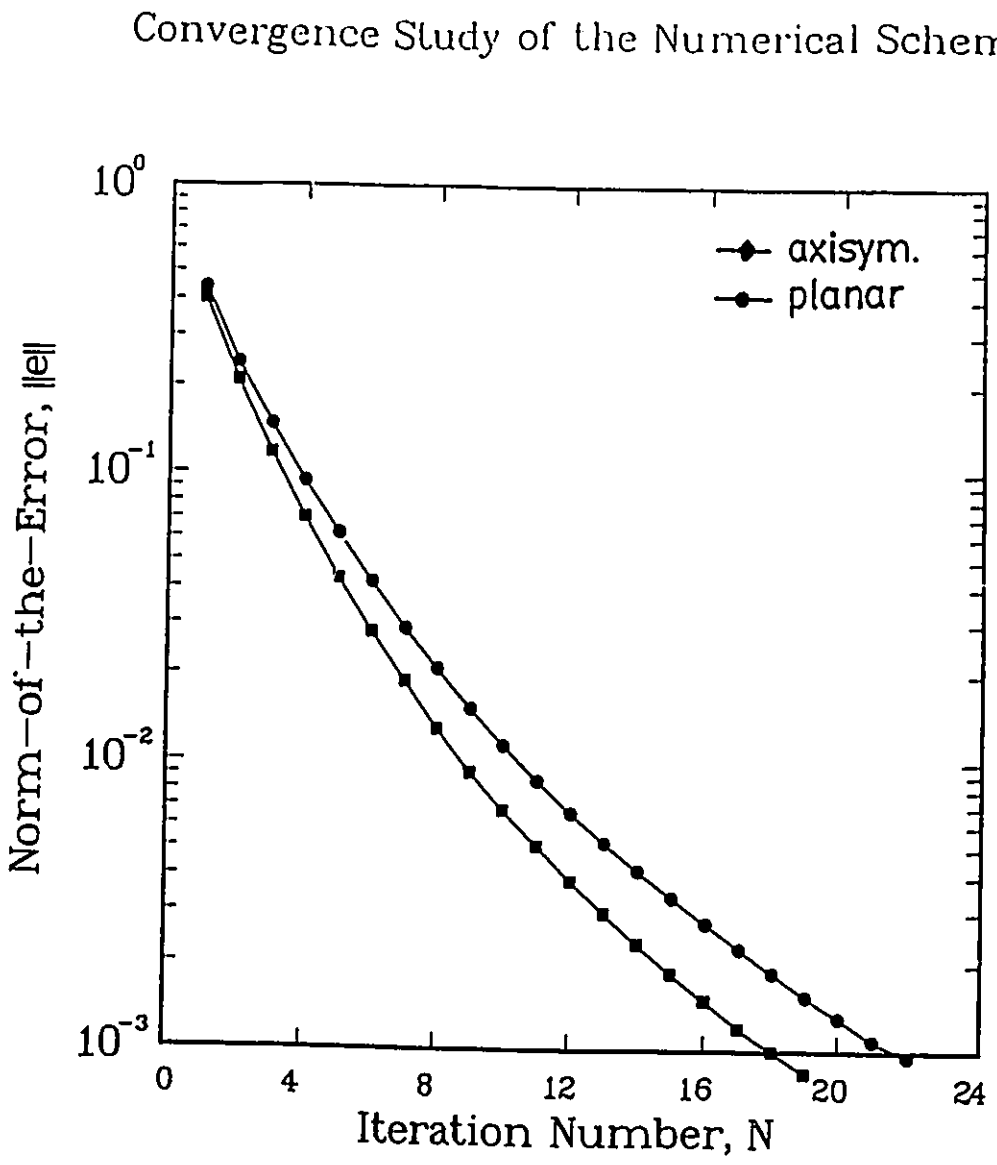

Figure A.1: Convergence study of Picard method for Poiseuille flow of a Bingham plastic between parallel plates ($\tau_y^* = 1.6,\ Bi = 11.6$) and in a tube ($\tau_y^* = 1.87,\ Bi = 9.5$).

Appendix B

Numerical Results for Entry and Exit Flows of Bingham Plastics

The numerical values of all results for the entry flow (Chapter 3) and exit flow (Chapter 4) are tabulated in Table B.1 as a function of τ_y^* and Bi for planar geometries. Corresponding results for axisymmetric geometries are given in Table B.2.

Table B.1: Results from the simulations for entry flow of Bingham plastics through a 4:1 planar contraction and exit flow through a slit die.

τ_y^*	Bi	n_{en}	n_{ex}	n_B	$Sw\%$
0.0	0.0	0.380710	0.15425	0.53496	1.191234
0.1	0.21	0.424078	0.15815	0.58223	1.471670
0.25	0.57	0.504122	0.16460	0.52058	1.104582
0.5	1.33	0.659550	0.16031	0.81985	1.057146
0.75	2.37	0.791876	0.14710	0.93898	1.019546
1.0	3.86	0.933203	0.13512	1.06473	0.994571
1.3	6.65	1.096640	0.09375	1.19039	0.973529
1.6	11.6	1.253930	0.06790	1.32180	0.960855
1.75	15.6	1.344490	0.03433	1.37882	0.958459
2.0	27.1	1.460120	0.03191	1.49191	0.957978
2.5	127.0	1.688900	0.01595	1.70485	0.971893
2.75	543.0	1.721000	0.01025	1.73125	0.992972
2.9	3518.5	1.869000	0.00410	1.87311	1.007374

Table B.2: Results from the simulations for entry flow of Bingham plastics through a 4:1 axisymmetric contraction and exit flow through a capillary die.

τ_y^*	Bi	n_{en}	n_{ex}	n_B	$Sw\%$
0.0	0.0	0.579078	0.2480	0.82707	1.130738
0.267	0.59	0.720244	0.2620	0.98224	1.095337
0.667	1.71	0.949652	0.2700	1.21965	1.060287
1.333	4.77	1.328100	0.2701	1.59820	1.018647
2.000	11.3	1.732938	0.2603	1.99322	0.990783
2.400	19.7	2.072312	0.2158	2.28810	0.981187
2.980	55.6	2.351232	0.2093	2.56053	0.980000
3.330	134.3	2.65000	0.1818	2.83180	0.982320
3.373	152.7	2.654002	0.1625	2.81651	0.983344
3.500	243.8	2.816114	0.1385	2.95452	0.987727
3.733	878.7	3.021620	0.0911	3.11270	0.997813
3.860	3557.8	3.113000	0.0260	3.13931	1.009822